UNIVERSITY OF BERGEN
DEPARTMENT OF PHYSICS AND TECHNOLOGY

MASTER THESIS
OPTICS AND ATOMIC PHYSICS

Use of market ready light dosimeters for patients with erythropoietic protoporphyria disorder

Svein NEDREBØ jr.

supervised by
Børge HAMRE, *Dept. of Physics and Technology, UiB*
and
Atle BRUN, *Dept. of Clinical Science, UiB*

Acknowledgements

I would like to acknowledge the preceding people and company for their support and help with my thesis:

> My supervisors, **Børge Hamre** and **Atle Brun**, for the guidance, help and feedback you have provided for me in my work with this thesis. I greatly appreciate the opportunity I have been given with this thesis, to help other people.

> **SunSense** and **Åsulv Tønnesland** at SunSense for the two prototypes I was provided to test, and for the help and tech-support you have provided.

> **Yi-Chun Chen**, in the Optics group, for reading through my thesis and providing valuable feedback.

A special thanks to *Kaja*, for all your love you give and the joy you are, my friends at *Nano* and *Lektor*, for all the good times we have shared in the last five years, and to my *parents*, *family* and *friends* back home, for their support and encouragement. I could not have gotten this far without any of you.

I

Abstract

Erythropoietic protoporphyria (EPP) disorder causes severe pain in the skin when patients are overexposed to light, particularly blue light. These patients can only stay exposed to sunlight for a short amount of time, and since there are few ways to protect against visible light, their life quality is considerably reduced. Estimation of accumulated dose is traditionally done by comparing exposed time to an individual maximum time; only found by accident after overexposure. No dosimeter is currently in use, and no correlation between weather quantities, like UV index, have previously been investigated. Phillips makes a wrist wearable device - ActiWatch Spectrum Plus - for measuring activity and exposure to light using photodiodes in the visual spectrum. The SunSprite company makes SunSprite; a clip-on device meant to improve sleep and mood by measuring time spent in light stronger than 10000 lx. It communicates to an app, where more data is displayed. The SunSense company are currently developing the SunSense RGB; also clip-on device with photodiodes in the visual spectrum, and with dosage calculator in an app that communicates with the devices. In this thesis we classify these three devices, and investigates if they can be used by EPP patients to measure light doses. Further on, we investigate if a dose-rate index for EPP patients have any correlation with UV index, or other radiation quantities that are easily available as forecast. We find that the SunSprite does not provide any way of displaying useful information for EPP patients. ActiWatch Spectrum Plus is proven to be unreliable as an irradiance sensor, due to the sensor being in a hole with no diffuser on top. The prototype from SunSense has a sensor that could be used by EPP patients, and is fairly stable with regards to responsivity. It is found that the device could benefit from a better cosine response; either through raising the sensor closer to the diffuser, or via another diffuser. We also define two EPP light indices that can be helpful for EPP patients, PLi and optimized PLi. The correlation between these two indices and the UV index is found to be poor, but the correlation with the illuminance is good, perhaps making it possible to use one channel lux-meters to monitor EPP light doses. The daily accumulated dose does not correlate with the maximum UV index, but correlation with the average UV index between 13:00 and 15:00 was found, suggesting that some weather forecasts can be used to plan the day.

Contents

V

List of Figures

VII

VIII

IX

X

1 Introduction

1.1 Light and life
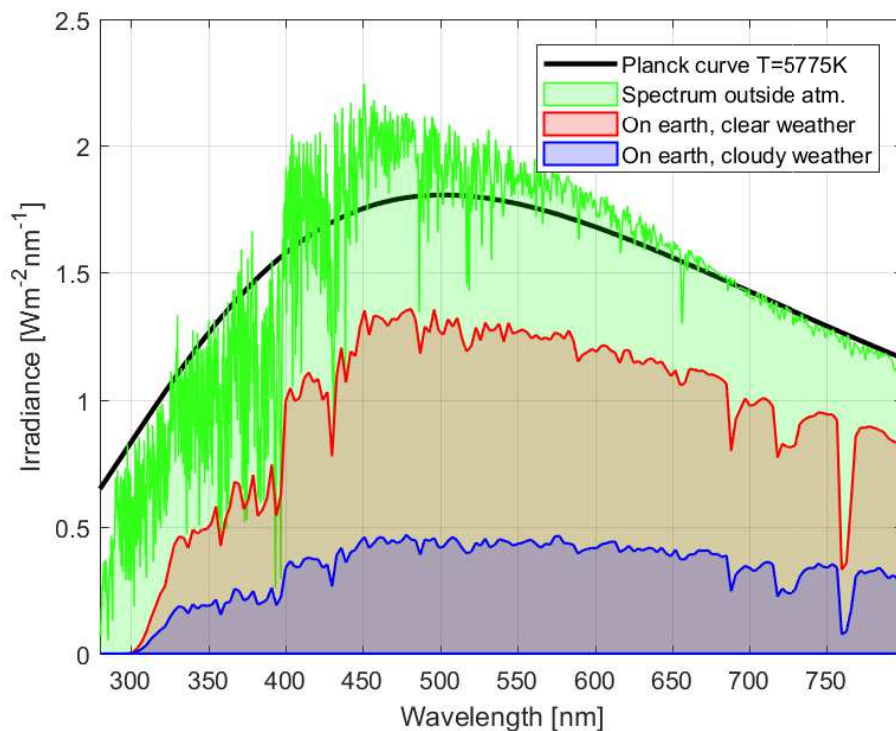
Figure 1: Some irradiance spectra. Planck curve representing Sun (black line), solar spectrum outside atmosphere, solar zenith angle of 0° (green), and two simulated spectra at sea level, at 40° solar zenith angle; clear and cloudy weather (simulations by AccuRT).

Light surrounds us all, and is the very reason for life on Earth. The oxygen we breath and depend upon originate from photosynthesis in plants; that use visual light to break carbondioxide and water into oxygen. Most of the light we are exposed to originates from above; the Sun. Visible light (400-700 nm) is particularly important for humans, and organisms in general. The hormone melatonin is produced in the eye of humans (and animals, bacteria, etc.), and regulates sleep and wake pattern [Kimberly and R., 2009]. Production of melatonin is suppressed when the eye is exposed to blue light (460-480 nm) [Brainard et al., 2001]. UV-B also is important for the body, as vitamin D is produced in skin under the influence of UV-B rays.

Life on Earth usually utilises light in the visual spectrum, as can be seen from the examples above. There could be several reasons. One is that the spectrum has a maximum in visual part when plotted as a function of wavelength, see Figure 1. Visual light also penetrates water well, compared with wavelengths < 400 nm and > 700 nm. This is also the part of the spectrum human eyes have evolved to detect. Looking at the world in normal sunlight with eyes adapted to light in the microwave region (1 mm to 1 m), would require a very sensitive eye; or the world would be a dark place.

Intensity of light varies a lot. In terms of closest order of magnitude, the lux (illuminance) varies from less than 10^{-1} lx at night and 10^2 lx in normal houses and on overcast days, up to over 10^5 lx on bright days. Figure 2 shows how much illuminance changes its order in different placings.
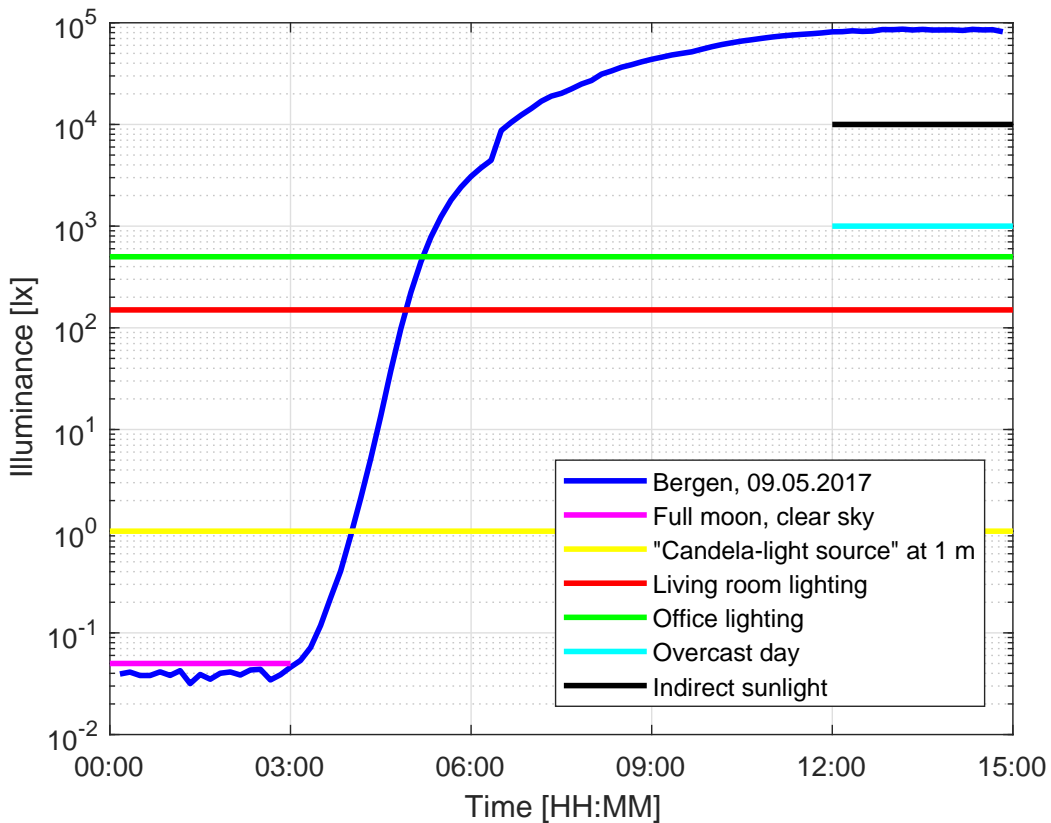
Figure 2: Logarithmic plot of lux values in Bergen 9th of May, 2016 (blue line, measurements by Ramses 80E2 radiometer), and a few other locations: Night illuminated by full moon [Kyba et al., 2017], a candle shining 1 cd observed at 1 m, other lines are values from NOAO.

Light and life is also in the focus of studies in recent years. Different light

dosimeters have been used to assess how light exposure influence circadian timing [Akacem et al., 2016; Figueiro et al., 2011] and mood [Park et al., 2007]. The affect of blue-blocking glasses on patients with mania have been examined by Henriksen et al. [2014, 2016].

1.2 Porphyria disorders

Porphyrins are a set of intermediate molecules in the haem biosynthesis. For normal, healthy humans, most of the porphyrins are synthesised to haem; used to transport oxygen to cells (haemoglobin). *Porphyria disorders* is a group of eight disorders with origin in the haem biosynthesis (see Figure 3), due to malfunction in one of the associated enzymes. Malfunction in different enzymes gives different disorders, with different symptoms. The synthesis of haem is strictly regulated [Besur et al., 2014]. Because wanted amount haem is not produced, the entire synthesis is up-regulated (sped up); causing an even larger bottle-neck effect on the intermediate enzyme with deficiency, and more porphyrin is leaked out of the cycle.

The eight porphyria disorders can be divided in two groups, according to what symptoms they cause: acute porphyria and cutaneous porphyria [Puy et al., 2010]. Two porphyrias cause both acute symptoms and cutaneous symptoms Acute symptoms affects the nervous system and can cause for example nausea, change in blood pressure, and can even affect motoric innervation or cause seizures. Cutaneous phorphyrias have symptoms relates to skin damage, caused by photosensitazion.

The photosensitivity of cutaneous porphyrias are caused by the excess porphyrins accumulating in the skin.

1.3 Erythropoietic Protoporphyria

Erytropoietic protoporphyria (EPP) is one of the cutaneous porphyria diseases. It is a rare photo-sensitivity disorder, and symptoms are caused by increased amounts of the molecule protoporhyrin IX (PPIX) in the skin [Meerman, 2000]. PPIX is the last intermediate molecule in the synthesis of haem [Aijoka et al., 2016], see Figure 3. The cause of EPP is a malfunction in the enzyme ferrochelatase (FECH) [Bonkowsky et al., 1975; Thapar and Bonkovsky, 2008]. FECH is the enzyme catalysing the insertion of iron into PPIX to make haem. A malfunction in FECH, making it operate as low as a 13% capacity [Bonkowsky et al., 1975], causes release of PPIX to blood, which via the blood cells accumulate in skin cells [Brun and Sandberg, 1991]. In humans with functioning FECH, a small amount of PPIX leaks out to the blood. The malfunction in FECH for EPP patients causes a bottle-neck-like
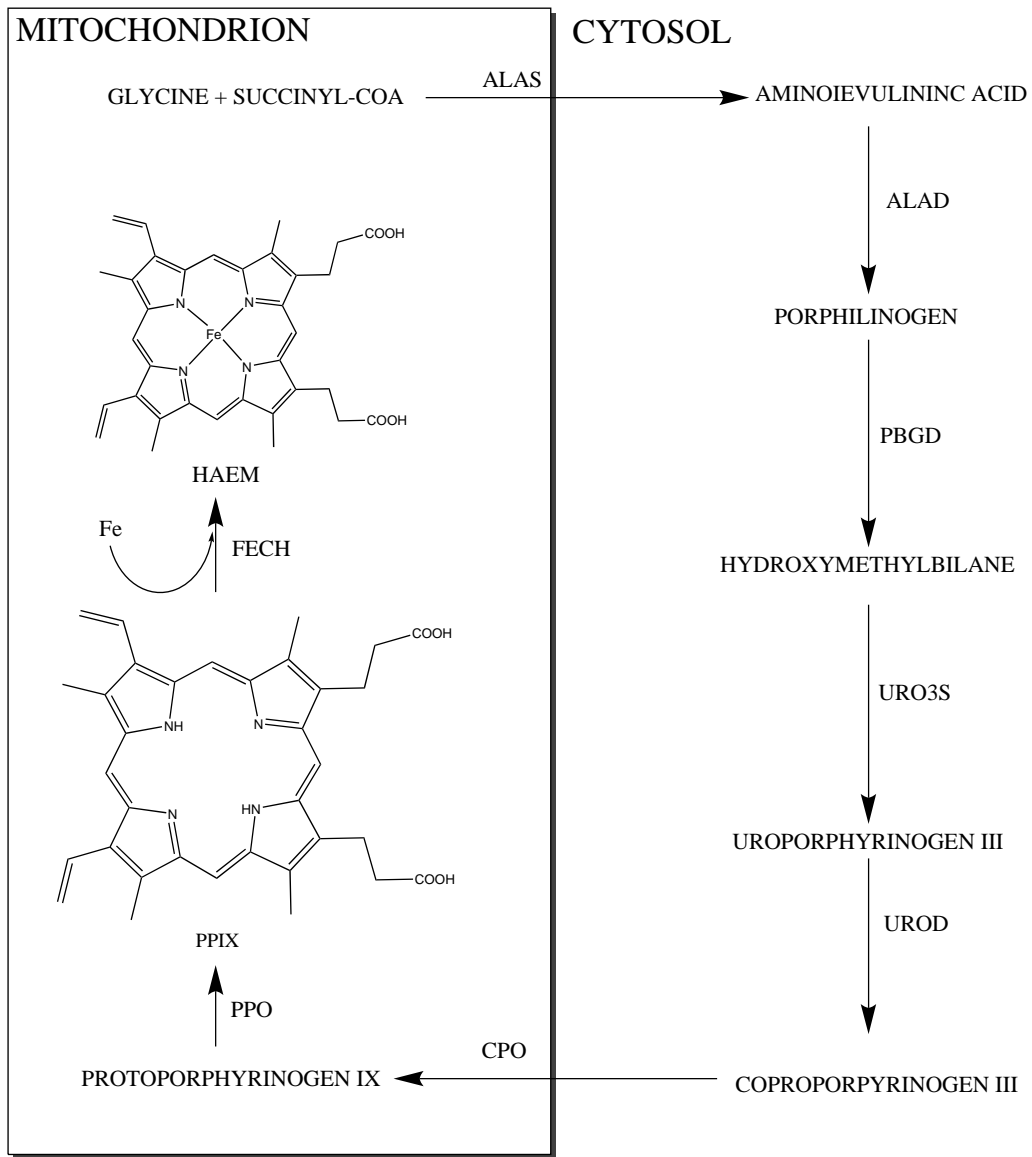
Figure 3: The haem bio-synthesis pathway. Inspired by Aijoka et al. [2016, fig. 1]

effect, and much more PPIX is generated in the haem biosynthesis of the red blood cells and is thereafter released into the circulation and transferred to skin cells and cells in other organs of the body. PPIX is easily exited by light with wavelength around 400 nm [Magnus et al., 1961; Mahmoud et al., 2008; Nielsen et al., 2005; Wahlin et al., 2011], and releases free radicals [Meerman, 2000].

The disease is uncommon, and is often overlooked by doctors. Its occurrence is reported between 1 : 75000 and 1 : 200000 [Elder et al., 2013; Lecha et al., 2009; Marko et al., 2007; Minder et al., 2009; Puy et al., 2010]. Symptoms of EPP are usually acute photo-sensitivity, that may cause blisters or reddening of the skin [Minder et al., 2009; Thapar and Bonkovsky, 2008; Thunell et al., 2000]. When diagnosed, the only cause of action is increase of protection through clothes, sunblock, spray tan, or simply by staying inside. This will, however, affect life quality [Thapar and Bonkovsky, 2008].

Patients can describe symptoms as burning areas and intense pain (not visible symptoms), or they can show symptoms as blistering and reddened areas of the exposed body parts. The symptoms arises after exposure to sun, and patient can usually handle up to 30 minutes of direct sun before symptoms arises. This number varies from patient to patient.

EPP patients learn from experience how long they can stay exposed around midday on a clear summer day without developing skin pain. This is usually in the scale of minutes [de Bataille et al., 2016]. The maximum exposure time serves as a reference for how long they can stay outside. Due to the extreme pain associated with symptoms, maximum tolerance is only measured by accident, when patients unintentionally gets overexposed. This experience does usually not come until their teens.

1.3.1 What can be done

As mentioned in Section 1, the intensity of light varies with a magnitude over 10^7. It is not all light that is problematic for EPP patients. Indoor lighting is fine, but sunlight through the windows can have a much higher irradiance and in this way a problem. Protection from the sunlight is therefore essential for EPP patients, in order to avoid symptoms. There are several methods and products EPP patients can utilize, however most of the methods involve blocking of relevant part of the solar spectrum (blue and UV-A). A report from 2006 [Holme et al., 2006] reports little to be done to help them, and does not mention any use of dose estimating, other than keeping track of time, and guessing on the weather.

For blocking and avoiding the blue and UV-A light, an efficient method is to stay inside. This would, however, lower the quality of life considerably. When outside, EPP patients use occlusive clothing, hoods and hats, gloves, sunglasses and sunblock. When inside, lesser precautions are needed because of the lower intensity, but sunlight can still enter the room through windows. For protection, yellow/orange filters absorbing blue light can be applied to the windows of the house and/or car.

A study by de Bataille et al. [2016] shows that 40 % of the patients in the

study had an improved tolerance to after repeated exposure. This suggests that exposure to sunlight could be beneficial regarding the tolerance, but also carries all the known benefits of sunlight (like vitamin D synthesis). The study of Swedish EPP patients by Wahlin et al. [2011] reports that 84 % of the about 50 participants had insufficient vitamin D concentration. Another study, of 48 Dutch EPP patients, shows that 46 % of the investigated patients had vitamin D deficiency, and suggests treatment [Spelt et al., 2010].

β-carotene supplements is widely used by EPP patients. Excess β-carotene is stored in the fat in the body, and also occurs in epidermis. This causes a yellow-colouring of the skin. The yellowing is caused by the absorption spectrum of β-carotene, which is in the blue region. Excess β-carotene is therefore a pigment-supplement. A review by Todd [1994] includes several references to different studies showing a positive effect of β-carotene on tolerance, but a more recent meta-study by Minder et al. [2009] finds 16 studies on total of 377 patients studying the effects of β-carotene on EPP patients. Minder et al. reports that even though 18% of the cases reported no effect, the only placebo-trial reported no significant effect on β-carotene on EPP patients tolerance.

There are also patients using UV-B phototherapy [Collins and Ferguson, 1995]. This is mainly to induce tanning (pigment formation), thus reducing the amount of light reaching PPIX. The natural pigment is termed melanin and is formed in the skin cells called melanocytes in the lower layer of the skin (stratum basale), and also in other pigmented areas of the body. UV-B phototherapy helps to produce pigments, because UV radiation on the melanocyte cells stimulate production of melanin.

A relatively new way to induce melanin formation, is treatment with afamelatonide [Langendonk et al., 2015; Minder, 2010]. Afamelatonide is a drug used to stimulate α-melanocyte, thus inducing pigment formation.

When surgeries are performed, the patient is illuminated by a strong light. This has been known to cause complications for EPP patients during liver transplantation. Studies suggest that yellow filters can be used, and surgeries can safely be performed [Wahlin et al., 2008].

Because overexposure of light causes extreme pain to EPP patients, they usually overprotect themselves. This overprotection leads to an additional and unnecessary reduction in quality of life.

1.4   Devices

Because EPP patients react to light in the visual spectrum, we set out to find devices that could be used to measure the accumulated dose.

Two devices were found that could be used to give such a dose estimate:

The SunSprite and Phillips ActiWatch Spectrum Plus. The much simpler SunSprite measures exposure of visible light (Lux), and its goal is to help one get the daily dose of sunlight one need [SunSprite, 2017]. It can be attached almost on any clothes, thanks to a magnet on a rubber band. Phillips' ActiWatch is a more complex activity device. It is worn like a watch, and measures light exposure using three photo diodes: one for red, one for green and one for blue. Phillips also provides software for extracting the data, and further analysis. The ActiWatch is meant as a daily activity monitor, with light sensors for extra information. An early model in the ActiWatch series - ActiWatch Spectrum - have been investigated by Figueiro et al. [2012]; Price et al. [2012]. Prize et al. tests the ActiWatch Spectrum, and though not stated clearly, so does probably Figuerio. They conclude a big issue on the ActiWatch Spectrum due to the placement of the photodiodes: in a well with no diffuser. The ActiWatch Spectrum Plus has a similar construction, but the diodes are placed much closer together, and the well is circular and much smaller.

Another device, though not on the market today, have been tested: SunSense RGB, by SunSense. SunSense makes two devices available today; One and Pro. SunSense One measures UV index, and is used to measure dose of UV light. SunSense Pro can also measure visual light, and can communicate with the SunSense app via bluetooth. The app gathers data from SunSense RGB to estimate dose and current conditions, as well weather forecast data to estimate precautions and forecasts. The devise tested is a prototype, based on SunSense Pro: SunSense RGB. Like the SunSense Pro it has both UV-sensors and visual sensors, and can communicate via bluetooth. SunSense RGB is developed to be useful for EPP patients, and that is why it has been included.

1.5 Indices

Porphyria Light index (PLi) is defined in the same way the Ultraviolet Light index (UV index). This could be useful for giving the EPP patients an estimate for how dangerous it is for them to be outside, just like for UV index and sun burn. If there is some correlation between the UV index and PL index, this would be especially useful: The Norwegian Radiation Protection Agency (NRPA) daily reports the expected UV index [NRPA, 2016]. If by some simple transformation we could turn the UV index to PL index, the EPP patients would have an easy way of determining how they should behave in terms of protection.

1.6 Classification

The term *classification* is here used to describe any defining feature of the devices; how it responds to light at different wavelengths, how it responds to light incoming at different angles, number of active channels, construction etc. Classification is therefore the features of a device that makes it desirable, and will be especially important for the devices that hopefully can be used by EPP patients.

The CIE (International Commission on Illumination) aims to set the standard in light research, and has issued a technical report on illuminance and luminance meters; CIE 069-1987. It provides guidelines and standards on how to classify devices meant to measure luminance/illuminance.

To obtain information on the instruments, a combination of laboratory measurements and data provided from manufacturer will be used. Classification of instrument will be done in laboratory settings, under controlled conditions.

1.7 Motivation and aim of the thesis

As shown, light is important for humans, and sunlight is hard to avoid in daily activities. Patients with EPP disorder have very limited tolerance to light in the UV and visible spectrum, and life quality is therefore heavily influenced.

There are no current methods for EPP patients to estimate their accumulated dose, or well documented way to plan their day from forecasts. The only way to estimate how long or how much longer they can stay exposed is to guess from experience. To better the living quality, this thesis investigates if there are options for light dose measurements available today that could be beneficial for EPP patients. Many devices on the market today measure certain parts of the light spectrum, and they could perhaps be used to estimate a dose or dosage rate (energy). Easily obtainable weather information, like UV index, will also be investigated for any correlation with similar indices for EPP patients (PL index and optimized PL index).

Aim of thesis

The thesis aims to answer the following issues related to EPP patients and their quality of life:

- To classify the market available light-measuring devices Phillips Acti-Watch Spectrum Plus and SunSprite. To classify the prototype of the SunSense RGB. From the classifications, arguments will be made as

to if the devices can safely be used to accurately estimate a dose proportional to the amount of energy absorbed by PPIX in EPP patients skin.

- Can readily available weather data, like the UV index, be used to predict a dosage-rate index (PL and optimized PL index) related to energy absorbed by PPIX in EPP patients?

- To compare indices/values, like Lux, UV index, PL index and optimized PL index, and find any correlations between these, that could be beneficial for EPP patients. Indices/values will be calculated from data gathered by radiometers in Bergen over a period of half a year. The indices/values from measured data will be compared/supported by calculations from simulations by the radiation transfer simulation tool, AccuRT.

1.8 Outline

Section two goes further in detail at theory used for calculations and discussion in the thesis.

Section three presents the instruments that will be used in this thesis: Ramses instruments (by Mess- und Datentechnik GmbH) will be used for comparison; as a reference. The devices that are validated are also given an introduction (Phillips ActiWatch Spectrum Plus, SunSprite and SunSense RGB).

Section four presents methods used to obtain data; whether it is in the laboratory or in the field. The section also includes how simulations have been done.

Section five will show results gather in the field, laboratory and via simulations. Comparisons and discussing will also be conducted in this section. The section is structured in subsections, and each subsection investigates a certain aspect of the results.

Section six will include the conclusions of the thesis. Conclusions will be presented with references to the results/discussion that validates it.

Section seven will make suggestions to further work to be done.

Lastly are the references used for the thesis, a short dictionary summarizing any abbreviations used and what they mean. The appendix that follows includes additional information that might be interesting for the reader.

2 Theory

2.1 Radiometry

Radiometry is the science of measuring light. This thesis uses two different quantities for light measurement,

- Radiance

- Irradiance

[1] Radiance is the flux of energy (light), through a solid angle through a surface. It has dimension of power per area per solid angle per wavelength ($\text{Wm}^{-2}\text{sr}^{-1}\text{nm}^{-1}$). Letting P be the radiant energy per time and $\cos(\theta)dA$ be the projected area, the radiance L into/from a solid angle $d\Omega$ is defined by:

$$L = \frac{d^3 P}{d\Omega dA d\lambda \cos(\theta)} \tag{1}$$

Irradiance is the flux of energy (light), through a surface. It has a dimension of power per area per wavelength ($\text{Wm}^{-2}\text{nm}^{-1}$). Irradiance is divided in different types: scalar and cosine irradiance, and both are defined from radiance. Scalar irradiance is defined by integrating radiance over a hemisphere of directions:

$$\begin{aligned} F_s &= \int_{2\pi} L(\Omega) d\Omega \\ &= \int_0^{2\pi} \int_0^{\frac{\pi}{2}} L(\theta, \phi) \sin(\theta) d\theta d\phi \end{aligned} \tag{2}$$

while cosine irradiance is defined by integrating the cosine of the solid angle;

$$\begin{aligned} F_c &= \int_{2\pi} L(\Omega) \cos(\theta) d\Omega \\ &= \int_0^{2\pi} \int_0^{\frac{\pi}{2}} L(\theta, \phi) \cos(\theta) \sin(\theta) d\theta d\phi \end{aligned} \tag{3}$$

Note that the hemisphere integration is carried out over can be oriented both "up" and "down" (consider it the north and south part of the Earth, sliced at the equator). This will affect what irradiance you are calculating: Either

---

[1]For a complete explanation of radiance and irradiance, see textbooks like *Fundamentals of Atmospheric Radiation - An introduction with 400 problems*, by C.F. Bohren and E.E. Clothiaux.

irradiance to/from the top, or to/from the bottom. The symbol F will be used further on in the thesis, and whether it is scalar og cosine irradiance will be specified in text.

Cosine irradiance is used for definition of UV index (see Section 2.1.1), and also for indices explained in Section 2.1.3, and is therefore the main focus in measurements for the thesis. Radiance is used for calculating irradiance when the lower part of the horizon is blocked, because of the dependency on polar angle. Radiance is also conserved in optical systems of no absorption, and is used for illustrations with varying irradiance in optical set-ups.

2.1.1 Ultraviolet light index

The ultraviolet light index, UV index or simply UVi, is an index meant to give scale to the general public to indicate the amount of ultralight radiation they are exposed to. It has been standardized by CIE [CIE S013/E2003; ISO/CIE 17166/1999]. The scale is widely used, and the Norwegian Radiation Protection Authority (NRPA) provides a daily foresights and measurements for the index, available to the public [NRPA, 2016].

The UV index, UVi, is calculated by:

$$UVi = \frac{40}{\text{Wm}^{-2}} \int_0^\infty A_{UV}(\lambda) \cdot F(\lambda) d\lambda \qquad (4)$$

where F is the solar irradiance, and the erythema action spectrum, A_{UV}, is defined in Equation 5 [CIE S013/E2003; ISO/CIE 17166/1999; Webb et al., 2011]. See Figure 4 for a plot of the action function.

$$A_{UV}(\lambda) = \begin{cases} 1, & 250 \leq \lambda \leq 298 \\ 10^{0.094(298-\lambda)}, & 298 \leq \lambda \leq 328 \\ 10^{0.015(139-\lambda)}, & 350 \leq \lambda \leq 420 \end{cases} \qquad (5)$$

Calculating the UVi using the integral and constant in Equation 4 serves as a neat way to handle the UV radiation. The factor 40 in front of the integral in Equation 4 makes the UV index usually come between 0 and 15, and for extreme situations above. The higher the UV index, the higher the precaution required. A table of different UV index intervals and the advised reaction is also obtainable, from sources as the NRPA's website [NRPA, 2016].

2.1.2 UV dose

UV dose can be calculated by integrating the UV index over time [ISO/CIE 17166/1999]. A normal integration interval is one day, denoted by Daily UV
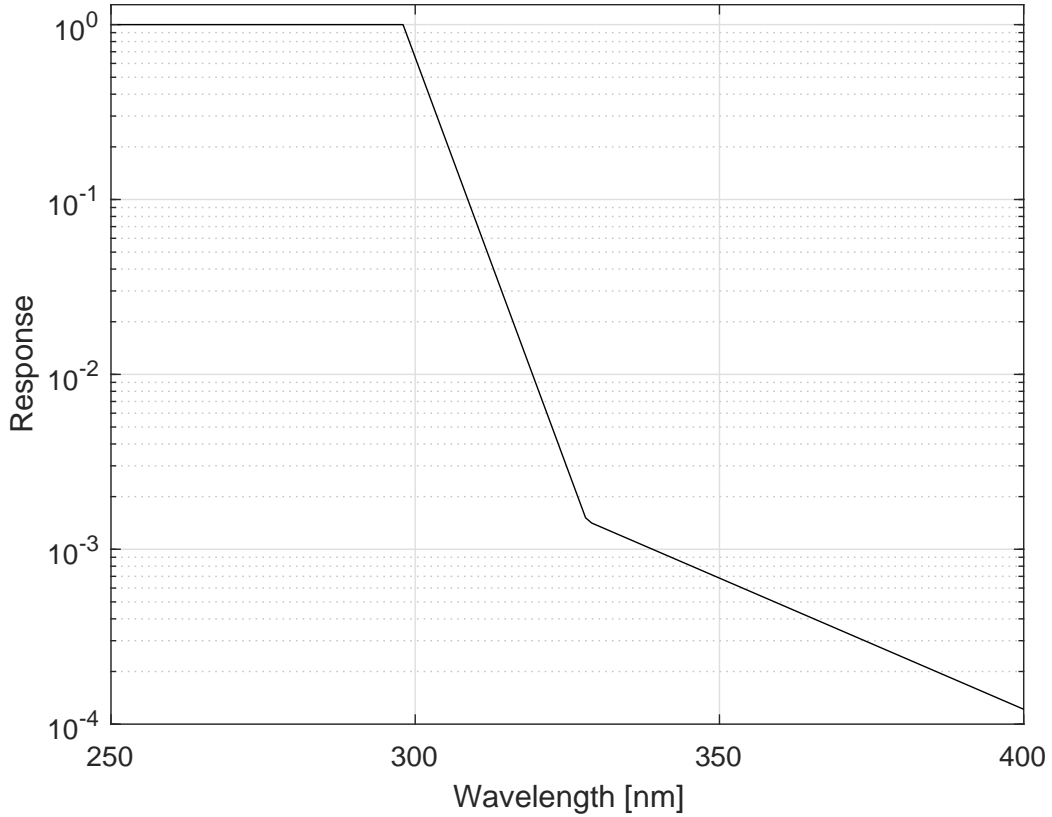
Figure 4: Logarithmic plot of the action spectrum of ultraviolet radiation.

Dose (DUVD). More precisely, the DUVD is calculated by Equation 6.

$$DUVD = \int_{day} \int_0^\infty A_{UV}(\lambda) F(\lambda, t) d\lambda dt \qquad (6)$$

The unit of UV dose is MED; minimal erythema dose. 1 MED is defined to be the minimal dose needed to induce damage on the average person (depends on protection, pigments, skin colour and others).

2.1.3 Porphyria light index

The Porphyria Light index, PLi, is an index meant to serve the same purpose as the UVi, but directed toward the EPP patients. This is done by finding a suitable action function for PPIX as a photosynthesizer in the skin of EPP patients. If the patients have access to this index, they will have a more accurate way of determining their ways of protection, compared to just look up at the sky and guess.

The idea of the PLi is the same as the UV index: Multiplying a wavelength dependent *action function*, $A(\lambda)$ with the solar irradiance, $F(\lambda)$, and integrating over all wavelengths heralds a number proportional to the index. This gives our relation to an index I_i:

$$k_i \int_0^\infty A_i(\lambda)F(\lambda)d\lambda = I_i \tag{7}$$

The subscript on $A_i(\lambda)$ and k_i is there to indicate the constant k is only constant for one response function. In this thesis we have used two different action spectrum for calculating two similar but different indices.

An absorption spectrum for PPIX was provided from Wahlin et al. [2011]. They had dissolved PPIX in dimethyl sulphoxide, and measured the absorbance in the range of 300 nm to 800 nm in lab conditions, using a spectrophotometer.

Nielsen et al. [2005, Figure 1] demonstrates that the penetration of light into skin largely depends on wavelength. As the figure shows, there is a shift in the spectrum further down in the skin. Very little blue light penetrates, therefore shifting the spectrum towards longer wavelengths. Another action spectrum was obtained, taking into account that PPIX is not found free, but in blood or skin cells. The same shift in absorption spectrum, as presented by Nielsen et al., is found by Srikanthan et al., but this time in laboratory. They investigated a sample with red blood cells enriched with PPIX. Using a blackbody light source, and a number of different filters, they sent very narrow wavelength intervals of light on the sample, exciting the PPIX. Using the intensity of light, transmittance of the filters and the different temperatures, the action spectrum was obtained.

The first action spectrum - the absorption spectrum of PPIX - is refereed to as "PL action function", the latter "Optimized PL action function". Both are plotted in Figure 5. Note how the optimized PL action spectrum is more sensitive to green and red light than PL action spectrum, therefore having more in common with the luminous efficiency function (see Figure 6) used for calculating illuminance.

When choosing the constant of proportion, k_i, it is chosen so that the index I_i becomes 100 when the irradiance spectrum, $F(\lambda)$, is the irradiance spectrum just outside the Earth's atmosphere. The normalizing was chosen as this because the indices will be between 0 and 100 under normal conditions, therefore following in the footsteps of UVi without being to similar. The choice of normalizing it to the solar spectrum outside the atmosphere is merely a choice of reference point. The two action spectra is plotted in Figure 5, both normalised to give an index of 100 outside Earth's atmosphere.

13
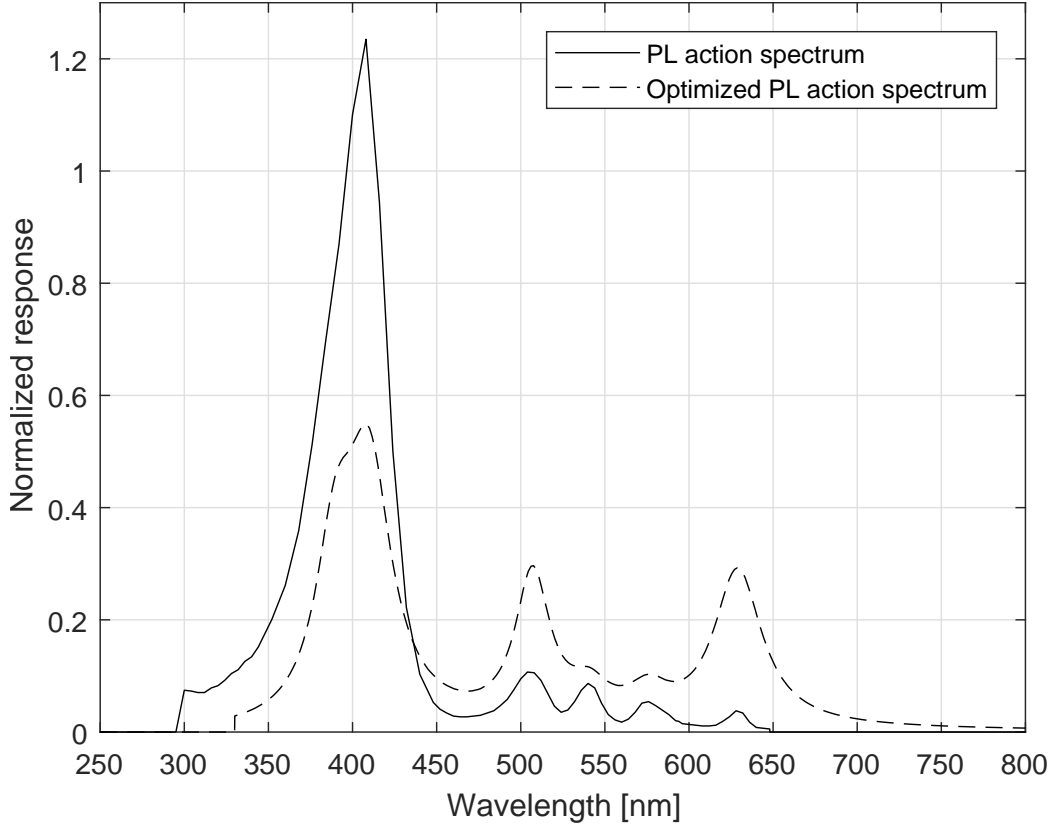
Figure 5: Plot of the two action spectra for porphyria light. The spectra are normalised so that the PL index and optimized PL index is 100 outside Earth's atmosphere

No matter what constant of proportion is chosen, the index I_i should be corrected in such a way that it is relate-able and easy to use.

One question that arises: is there a way for EPP patients to utilize tables of UV indices, like NRPA's, to easily estimate the PL index? This question is the topic of Section 5.8.

2.1.4 PL dose

EPP patients have to keep a close eye on how much light they are exposed to. Inspired by DUVD, discussed in Section 2.1.2, a similar daily dose is defined for light absorbed by PPIX. The accumulated daily porphyria light dose, DPLD, is defined in Equation 8.

$$DPLD = \int_{day} k_{pli} \int_0^\infty A_{PL}(\lambda) \cdot F(\lambda, t) d\lambda dt \tag{8}$$

14

At the end of Section 1.3 it is explained how EPP patients use a maximum tolerance time to estimate their maximal daily tolerance (DPLD$_{max}$) and how much they have been subjected to so far (APLD). Using the symbol t$_{max}$ for this tolerance time, the maximum dosage, DPLD$_{max}$ is calculated by integrating over t$_{max}$ in Equation 8. Note that this requires some knowledge with regards to the irradiance spectra, F(λ, t) of the time in question.

If EPP patients had an accurate way of measuring the PL index, they could estimate the accumulated PL dose, APLD (Equation 9).

$$
\begin{aligned}
APLD &= \int_{t_0}^{t} k_{pli} \int_0^{\infty} A_{PL}(\lambda) \cdot F(\lambda, t) d\lambda dt \\
&= \int_{t_0}^{t} PLi(t) dt
\end{aligned}
\tag{9}
$$

Using the maximum dosage DPLD$_{max}$, and measurements of accumulated dose so far APLD, patients gain a tool for estimating how much of the tolerance they have exhausted; APLD/DPLD$_{max}$. If the ratio is getting closer to 1, the patients should start thinking about taking extra precautions, or perhaps stepping inside for the day. This is analogous to UV dose, were 1 MED would induce symptoms (see Section 2.1.2).

As described in Section 2.1.3, the PL index is made to be 100 outside Earth's atmosphere, and is thus expected to be between 0 and 100 for most instances at earth's surface. A PL index of 50 is equivalent to a dosage rate of 50 PL units per second. Integrating over an hour, the PL dose is 180 000 PL units per hour. There are large variation in EPP patient's tolerance time. This is not only dependent on light conditions, but vary from person to person. Under the most extreme conditions, some of the EPP patients can only stay outside for 10 to 15 minutes (see Section 1.3), and for them the maximum dose would be 45 000.

2.2   Photometry

The eye does not respond equally well to all wavelengths, even within the visible spectrum. The study of light perceived by the eye is called *photometry*. Photometry has its own quantities and units, usually related to a radiometric quantity through multiplication by a weighting function, and a constant.

The weighing function in photometry is called luminous efficiency function, and there are mainly two different functions in use: the photopic and the scotopic. The photopic was the first one approved [CIE 1924], and describes the human eyes response to visible light under daylight conditions. Later on, the scotopic luminous efficiency function was made to account for

the eyes response to light under dark/night conditions. See Crawford [1949].
For our purpose, the most recent photopic one is chosen, as the devices measuring luminosity usually is supposed to work under daylight conditions. See Figure 6 for plots of the two luminous efficiency functions. Data for plots are obtained from Colour & Vision Research Laboratory [2017].
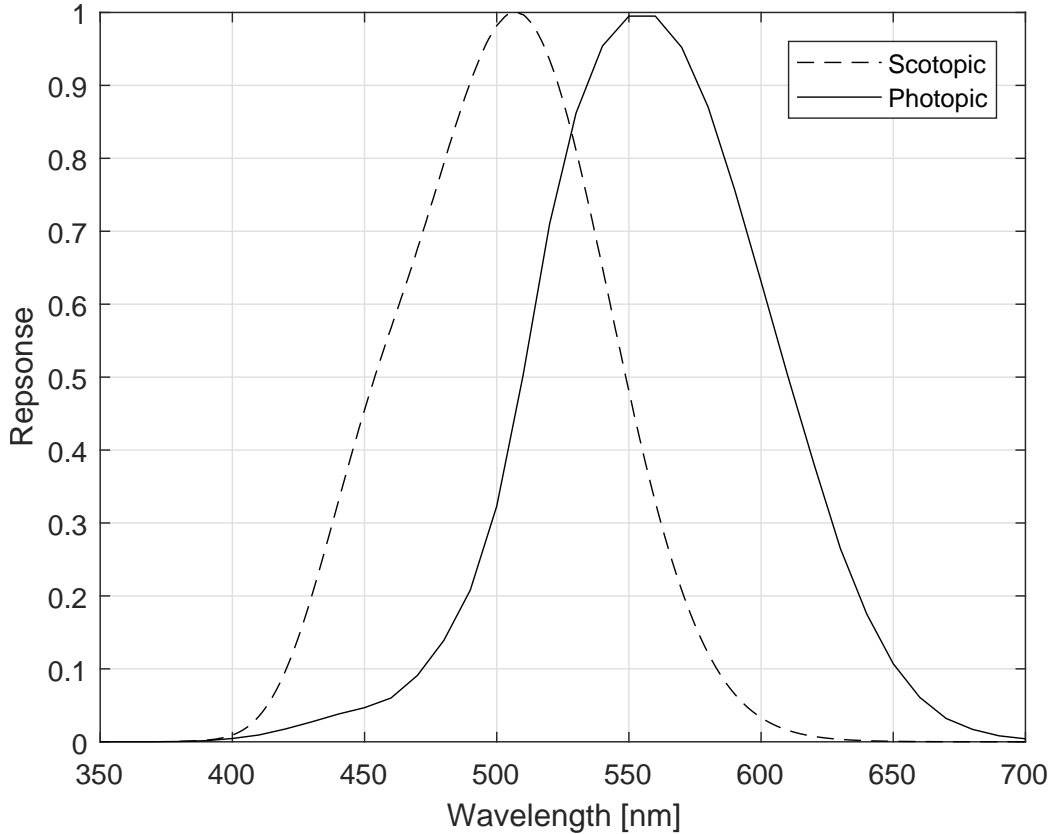
Figure 6: Plot of photopic [Stockman and Sharpe, 2000; Stockman et al., 2005] and scotopic [Crawford, 1949] luminous functions normalized to 1 at maximum.

2.2.1   Luminous intensity

Consider a light source, emitting in all directions. Luminous intensity is the measure of emitted power, weighted with the luminous efficiency function, per unit steradian. The unit of luminous intensity is the candela [cd], and has a formal definition [BIPD, 2017; CGPM, 1979]:

The candela is the luminous intensity, in a given direction, of a source that emits monochromatic radiation of frequency 540×10^{12} hertz and that has a radiant intensity in that direction of 1/683 watt per steradian.

2.2.2 Luminous flux

Luminous flux is used to describe the power perceived by the eye. It is analogous to radiant flux from radiometer. The unit of luminous flux is lumen [lm], and is related with candela through: 1 lm = 1 cd·sr.

2.2.3 Luminance

The photometric equivalence to radiance is luminance, with units of candela per square meter [cd/m^2]. Luminance is a measure of perceived energy by human eyes. To go from radiance to luminance, the radiance $L(\theta, \phi, \lambda)$ is weighted with a constant and the luminous efficiency function, $\bar{y}(\lambda)$, previously presented in Section 2.2. Radiance, L, and luminance, L_V, is related by:

$$L_V = 683 \int_0^\infty \bar{y}(\lambda) L(\theta, \phi, \lambda) d\lambda \tag{10}$$

2.2.4 Illuminance

Luminous flux incident on a surface is measured in lux, [lx]. This is called illuminance, and is a useful size to determine. Several of the devices investigated in this thesis provides data in lux.

Illuminance has the SI derived unit lux, [lx]. One lux is equal to one lumen per square area. Lumen is the unit for luminous flux; candela times steradian. Illuminance is used for the amount of power absorbed by the eye, and so the irradiance spectrum is weighted with a function to gain illuminance.

2.3 Radiative transfer equation

Light going through any medium is subject to attenuation. The loss of intensity due to absorption depends on both path length x and how well the medium absorbs light k. Attenuation due to absorption in a homogeneous medium follows Beer-Lambert's law:

$$L = L_0 e^{-kx} \tag{11}$$

with L being the outgoing radiance, and L_0 being incoming radiance. The constant k depends on the medium.

Scattering between light (photons) and particles are described by models such as Mie scattering and Rayleigh scattering. Rayleigh scattering describes scattering of light by particles smaller than the wavelength of the photon. Mie scattering model is used for scattering caused by heavier particles.
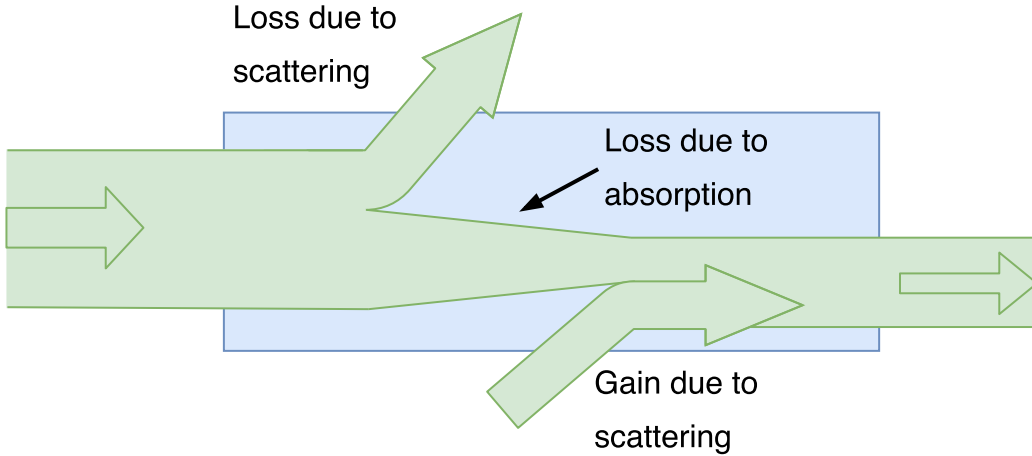
Figure 7: Sketch of absorption, gain and loss due to scattering of a beam (green) through a medium (blue).

The radiative transfer equation (RTE) describes the loss and gain of intensity in light as it travels through a medium. In addition to loss of intensity due to absorption and scattering out of the current direction, gain of energy can be from emission and scattering into the current direction. Figure 7 shows how scattering out and into the path and absorption affect the intensity of light. If the beam travels in direction $\hat{\Omega}$, and light scattered into the beam comes from direction $\hat{\Omega}'$, the RTE[2] in differential form can be presented as:

$$\frac{dL}{ds} = -\kappa L + \beta \int_{4\pi} p(\hat{\Omega}', \hat{\Omega}) L(\hat{\Omega}') d\omega' + Q \tag{12}$$

where the left side is change of irradiance with distance, and right side is loss due to attenuation and gain from scattering and other sources. The first term on the right side describes loss due to attenuation. κ consists of two terms: $\kappa = k + \beta$. k is the absorption coefficient from Equation 11, and β is the scattering to coefficient; analogous to k. The second term,

_____

[2]For a complete explanation of RTE - deviations and other forms -, see textbooks like *Fundamentals of Atmospheric Radiation - An introduction with 400 problems*, by C.F. Bohren and E.E. Clothiaux.

the integral, describes scattering out of the beam. $p(\hat{\Omega}', \hat{\Omega})$ is a probability function normalized to 1, describing the probability of a photon incoming at angle $\hat{\Omega}'$ to be scattered into path $\hat{\Omega}$. The last term, Q, describes gain of radiation due to other sources, such as Planck radiation from warm bodies. For light in the visual spectrum, the contributions to Q is light scattered into the beam directly from the beam from the sun.

2.4 Measuring light

Measuring light can be difficult. Light has several properties; intensity, direction, polarization and wavelength and frequency, to mention a few. Light also interacts with matter (scattering and absorption), making it change direction, intensity, wavelength/frequency and so fort. Even though we know a lot about light, it is difficult to measure.

When measuring light, one is usually looking for a spectrum. For sunlight, this spectrum is somewhat similar to a Planck curve, if rapid variations are smoothed out (Figure 1 shows a Planck curve and a the spectrum outside Earth's atmosphere). Absorption in Sun and Earth's atmospheres contributes to large changes in the spectrum at very narrow bands, and to detect these perfectly accurately the instruments would need sensors measuring a single wavelength at a time. This is not feasible in real life however, and current radiometers have a certain bandwidth the sensor channels register on. The channels responds best at a certain wavelength, but also register some light of other, surrounding wavelengths.

Another problem is how the light is gathered to the sensor. Light outside comes from all angles; direct sunlight, scattering by the atmosphere and sky, scattering from clouds, reflection of surfaces and other light sources. For a radiometer to measure cosine irradiance accurately, it would need to respond different to light incoming from different angles. Letting F_b be the irradiance of an incoming beam, i.e. irradiance integrated over a small solid angle, then the measured cosine irradiance should be as close to the ideal as possible:

$$F_c \approx F_{id} = F_b \cos(\theta) \tag{13}$$

Classification of cosine response on radiometers is necessary, and Michalsky et al. [1995]; Zibordi and Bulgarelli [2007] reports error in cosine irradiance. Because of the use of simpler radiometers - illuminance meters - in studies, the cosine response of those devices have also been examined [Figueiro et al., 2012; Price et al., 2012].
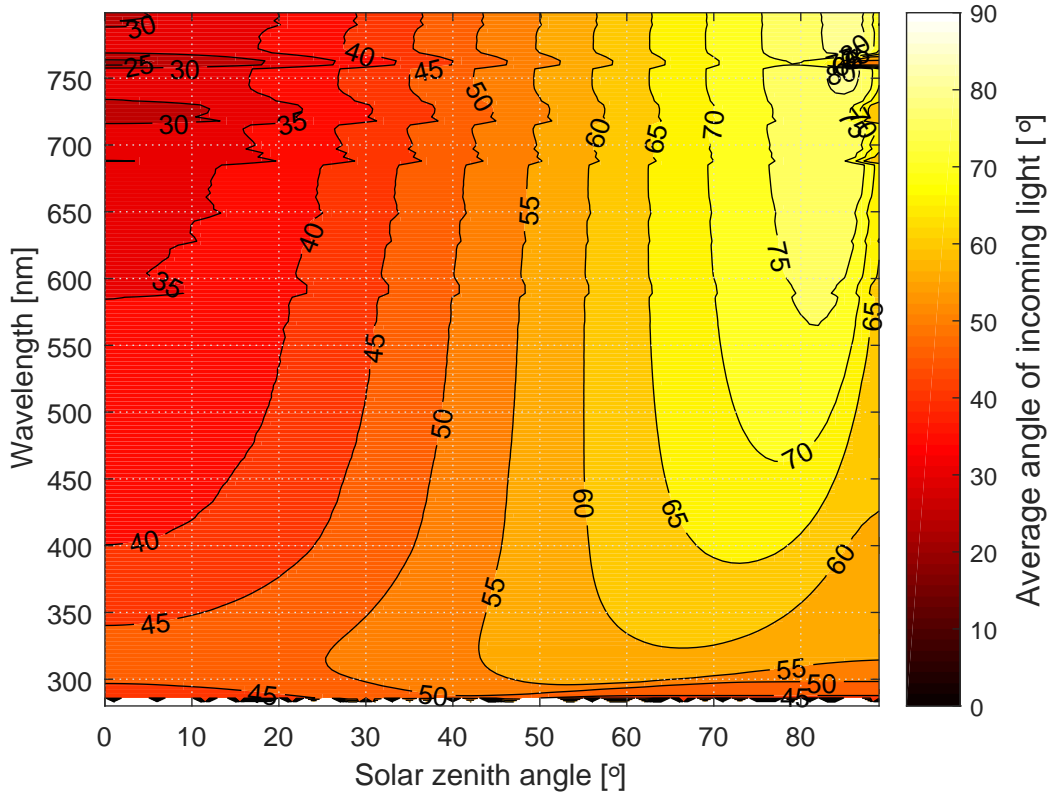
Figure 8: Average angle of incoming light, calculated from simulated spectrum on a clear day (no clouds, with aerosols), as a function of solar zenith angle (x-axis) and wavelength of the light (y-axis).

2.5   Average angle of incoming light

As discussed, light travelling through the atmosphere will be influenced by atmospheric molecules by both scattering and absorption. This causes light to hit an object from more angles than just the zenith angle. The average angle is the average zenith angle of all incoming light beams. This includes the solar beam itself. This angle is wavelength dependent, as light with different wavelengths get scattered/absorbed differently. Average angle is from a vertical axis perpendicular to horizontal plane, and is therefore comparable to zenith angle.

In this thesis, average angle of incoming light is calculated by dividing measurements of a cosine irradiance radiometer with a scalar irradiance radiometer. The scalar irradiance radiometer measures all light incoming at the detector equally well for all angles in its field of view. The cosine irradiance device measures light incoming perpendicular best (see Equation 13). The

response then gradually falls as a cosine function, till it measures 0 at 90°. The fraction will be between 0 and 1, and the angle is found by calculating the inverse cosine, see Equation 14. This representation of average zenith angle can be derived from

$$\theta_{avr} = \cos^{-1}(\frac{F_c}{F_s}) \tag{14}$$

This way to represent the average zenith angle can be derived from Gershun's law[3].

2.6 Classification of radiometers

2.6.1 Cosine response

The devices that will be tested are supposed to measure cosine irradiance. The cosine response, or angular response in some reports, is how the sensor measures light incoming at different angles. If θ is the angle from a vertical axis normal on a surface - polar angle - then an ideal cosine response should measure all incoming light at $\theta = 0$, and none at $\theta = \pm\frac{\pi}{2}$. An ideal cosine irradiance R_{id} is therefore:

$$R_{id} = \cos(\theta) \tag{15}$$

so the measured irradiance is:

$$F_{id} = R_{id} \cdot F_0 = F_0 \cos(\theta) \tag{16}$$

To achieve this, professional devices use *diffusers*. An ideal diffuser is a material that follows Lambert's law; the irradiance observed from an ideal diffuser is directly proportional to the cosine of the angle of incoming light beam. In other words; Equation 15.

Professional radiometers can get quite close to an ideal behaviour. See for instance Tveiteråsen [2013, Figure 4.13 and 4.14], with error less than 3% for all angles illuminated by isotropic light, when compared with an ideal cosine curve.

Classification of cosine response is important. For small polar angles it usually gives correct measurements. This is due to manufacturers calibrating the devices using normal incident light. For large angles, on the other hand, there's also the problem that measurements are very small compared to that of small angles. Due to this, noise and dark current in the device could make

---

[3]For the full derivation, see textbooks like *Fundamentals of Atmospheric Radiation - An introduction with 400 problems*, by C.F. Bohren and E.E. Clothiaux.

a relatively large contribution to the measurement, therefore giving large relative errors.

The relative error in cosine response is calculated by:

$$\epsilon(\theta, \phi) = (\frac{R(\theta, \phi)}{R_{id}(\theta)} - 1) \cdot 100\% \tag{17}$$

and provides, in percentage, how big the measured cosine response R is relative to the ideal $R_{id}=\cos(\theta)$.

Total error of cosine response will be calculated in two ways. Both ways will assume isotropic light incoming from all angles. The first method calculates the relative error in percent of the device compared with the ideal:

$$\epsilon_{tot} = \frac{\int_0^{2\pi} \int_{-\frac{\pi}{2}}^{\frac{\pi}{2}} R(\theta) \sin(\theta) d\theta d\phi}{\int_0^{2\pi} \int_{-\frac{\pi}{2}}^{\frac{\pi}{2}} R_{id}(\theta) \sin(\theta) d\theta d\phi} 100\% \tag{18}$$

with $R_{id} = \cos(\theta)$. This way of calculating the error tells us something about how much the device over/under-estimates measurements under isotropic light conditions. This quantity will be most useful in characterizing the devices for dosage measurements for EPP patients, as light from all angles is important when calculating the dose.

The second method calculates the difference between the ideal and measured cosine response in percentage. It is inspired by the error f2 defined by CIE 069-1987, but is modified by: the angular range of integration is the entire semicircle, not just between ±85°. Because the devices are likely to have some azimuth angle dependency, presented value will be the average of f2* calculated for both vertical and horizontal rotation.

$$f2^* = \int_{-\frac{\pi}{2}}^{\frac{\pi}{2}} [R(\theta) \sin(\theta) - R_{id}(\theta) \sin(\theta)] d\theta \tag{19}$$

2.6.2 Responsivity

Responsivity is how a sensor/photodiode reacts when intensity of incoming light is changed. The photodiode works by absorbing incoming energy, light, and turning it into electrical energy; output. It is this output devices use to measure irradiance, radiance, and everything else measured by electrical devices. The responsivity, R can be defined in terms of incoming power P of light and current I converted from the light:

$$R = \frac{I}{P} \tag{20}$$

and depends on wavelength.

For currents smaller than the threshold current, R is close to a constant. When the current reaches the threshold current point, the photodiode reach saturation and can not convert any more power, so an increase in irradiance will not be detected by a photodiode. So, for currents smaller than threshold current, we expect to get:

$$I \propto P \quad , I < I_{treshold} \tag{21}$$

Professional radiometers measure raw data in number of counts. This is then converted to a calibrated output in some units. Output of the devices are usually power per time per area, or lux. These output are all proportional to the output of the photodiode. Classification of responsivity is done by varying the irradiance incident on the devices, and noting the resulting outputs.

2.7 Correlation of variables

It would be beneficial to gain information regarding the correlations of the different values and indices calculated from measured irradiance by the instruments.

The Spearman correlation test gives a correlation factor, $-1 < \rho_s < 1$, and is for unique data defined by Equation 22. It has an advantage over the Pearson correlation test, in that the Spearman correlation test is not as sensitive to large deviations (extrema) in measurements.

$$\rho_s = 1 - \frac{6 \sum_{i=1}^{n} (\text{rank}(x_i) - \text{rank}(y_i))^2}{n^2(n-1)} \tag{22}$$

The rank is found by the following algorithm:

1. Sort data set (x_i, y_i) by ascending x-value.

2. The first x-value has rank 1, the second rank 2, and so on: $\text{rank}(x_k) = k$

3. Sort the data set by ascending y-values.

4. The first y-value has rank 1, the second rank 2, and so on: $\text{rank}(y_k) = k$

If there is a strong, positive correlation between x and y, ρ_s is close to 1, and if the correlation is strong but negative, ρ_s is close to -1. If there is a weak or no correlation, ρ_s is close to 0.

2.8 Method of least square: Finding models

When investigating relations between indices, a suitable model is made if possible. The model is based upon the method of *least square*[4].

To explain the idea, consider measurements that give n data points $(x_i, y_i), i \epsilon [1, n]$ with x_i being the independent variable, and y_i the dependent (on x) variable. By assuming there exist a function, f(x), that we are measuring with some inaccuracy, we want fit f(x) as best we can to the measured data. This is done by minimizing the distance between a measured data point, (x_i, y_i), and the data point from the model x_i, $f(x_i)$. The distance can be expressed as

$$(y_i - f(x_i))^2$$

and the residual (distance) squared, S, for all data point, is the distance from the measured to predicted data point:

$$S = \sum_{i=1}^{n} (y_i - f(x_i))^2 \qquad (23)$$

The goal of the method of least square is to minimize the sum in Equation 23. The function, f(x), can be assumed to be a polynomial of degree m, with coefficients α_i;

$$f(x) = \alpha_0 + \alpha_1 \cdot x + \alpha_2 \cdot x^2 + ... + \alpha_m \cdot x^m = \sum_{i=0}^{m} \alpha_i \cdot x^i \qquad (24)$$

Equation 24 in matrix notation is:

$$\boldsymbol{X}\vec{\alpha} = \vec{Y} \qquad (25)$$

with $\boldsymbol{X}$ is the matrix of data points x_i, $\vec{Y}$ is the vector of corresponding measurements y_i, and the vector $\vec{\alpha}$ is the m-dimensional vector corresponding to:

$$\vec{\alpha} = \begin{bmatrix} \alpha_0 \\ \alpha_1 \\ \vdots \\ \alpha_m \end{bmatrix}$$

Solving Equation 25 for the unknown constants:

$$\vec{\alpha} = (\boldsymbol{X}\boldsymbol{X}^T)^{-1}\boldsymbol{X}^T\vec{Y} \qquad (26)$$

---

[4]For a complete explanation of the method of least square, see any linear algebra textbooks. For instance, see *Linear Algebra and its applications* by Lay, D.C, published by Pearson.

For linear model through origin, Equation 25 is modified with $\alpha_0 = \alpha_2 = \alpha_3 = ... = \alpha_m = 0$. $\boldsymbol{X}$ is the a matrix with measurements in the second column, and zeroes elsewhere. The matrix-multiplication $\boldsymbol{X}\boldsymbol{X}^T$ is then the inner product of the second row of the matrix, $\vec{x}$. Equation 26 is reduced to:

$$\begin{aligned}
\alpha_1 &= (\vec{x}\vec{x}^T)^{-1}\vec{x}^T\vec{Y} \\
&= (\vec{x} \cdot \vec{x})^{-1}\vec{x} \cdot \vec{Y} \\
&= \frac{\sum_i x_i y_i}{\sum_i x_i^2}
\end{aligned} \tag{27}$$

2.8.1 Evaluating the regression functions

To evaluate the functions found, three sizes will be given with each model: The R^2-value, RMSD-value and RMSRD-value.

The R^2 value is a unit-less number between 0 and 1. It is defined by the square of residual between predicted and measured data, divided by the square of residual between measured data and the mean of these data:

$$R^2 = \frac{\sum(f(x_i) - y_i)^2}{\sum(y_i - \bar{y})^2} \tag{28}$$

R^2 can be interpreted as how good the model explains the measurements; if $R^2 = 1$, the model 100% accurately predicts all measurements, but if $R^2 = 0$, the model does not give any insight into predicting the measurements.

Root-mean-square, RMS, is an analysis multi-tool; take to root of the mean of some data. By finding the RMS of different data, different information regarding spread can be found. RMSD, or root-mean-square deviation, is a way of analysing the difference in estimated values, from the model, and measurements. It is defined by:

$$RMSD = \sqrt{\frac{\sum_i(f(x_i) - y_i)^2}{n}} \tag{29}$$

Note that RMSD has the same dimension as y. A low RMSD would mean a low average spread of data point, y_i, around the predicted model.

Another value of interest is the RMS of relative deviance:

$$RMSRD = \sqrt{\frac{\sum_i(\frac{f(x_i) - y_i}{y_i})^2}{n}} \tag{30}$$

The RMSRD i usually multiplied by 100% to get a percentage. RMSRD is an estimate for the error of the value produced by the regressed function, in percentage of the value itself.

2.9   Total uncertainty

Uncertainty in results are usually estimated by RMSRD (Equation 30), but for combined uncertainties the total uncertainty Δx is the root of sum of squares of individual uncertainties Δx_i:

$$\Delta x = \sqrt{\sum_{i=1}^{n}(\Delta x_i)^2} \tag{31}$$

This is only valid if the individual uncertainties are uncorrelated.

3 Instruments

In the thesis, two types of instruments were used: Dosimeters meant to measure a dose in the visual part of the spectrum, and radiometers, used to classify the dosimeters and to obtain solar spectrum data. The instruments chosen to be tested is the SunSprite RGB, by SunSprite, Phillips Actiwatch Spectrum Plus and SunSense RGB, by SunSense. To control them, and to gather extra data, the cosine irradiance radiometers Ramses 82E6 and 80E2 radiometers will be used, as well as the scalar irradiance radiometer Ramses 84EE. The Ramses radiometers are produced by Trios.

3.1 Radiometer

The E6 device measures in the UV region, while the E2 measures visible light. Both of them have 256 channel devices, with silica photocells, and are cosine irradiance devices [Trios, 2017]. The 84EE is a scalar irradiance device. More data are shown in Table 1, retrieved from manufacturer manual for instruments Trios [2017]. The validity of the cosine irradiance instruments have been examined by Tveiteråsen [2013].

Table 1: Table of radiometer specifications. From product sheet [Trios, 2017].

Device ID	80E2	82E6	84EE
Type	Irradiance	Irradiance	Scalar irradiance
Spectral region [nm]	319.5 - 951.8	279.5 - 501.9	319.5 - 951.8
Usable channels	194	104	194
Accuracy [%]	6-10	6-10	5

When measurements were made, the radiometers were mounted with the sensor tip/diffuser straight up, at the same position. The devices was from time to time be moved, due to involvement in other projects. Because of that, a designated rig was placed on top of the university building *Biologen*, so the instruments could easily be put back at the same spot when returned.

3.1.1 Instrument inner workings

The Ramses radiometers uses the same inner construction; an MMS-1 spectrometer made by Zeiss [Zeiss, 2017]. The light is lead to the spectrometer from the diffuser (tip of instrument) via optical fibre to the spectrometer. A flat field grating reflects and splits the light into a spectrum of colours, and

directs it at the photodiode array. The light that reach an individual photodiode is a narrow interval of wavelengths, so each channel has its associated wavelength.

The accuracy related to the spectrometer depends upon the quality of the grating and number of channels. Few channels gives the choice of few, narrow measurements (selected, few parts of the spectrum measured), or the channels must have a broader interval of wavelengths hitting it (collecting more of the total light energy, thus not making a spectrum in the output). Figure 9 shows a sketch of the inner workings of the Zeiss MMS-1 spectrometer, with a colour spectrum at the photodiode array to indicate that different wavelengths hit different parts of the array; therefore different diodes.
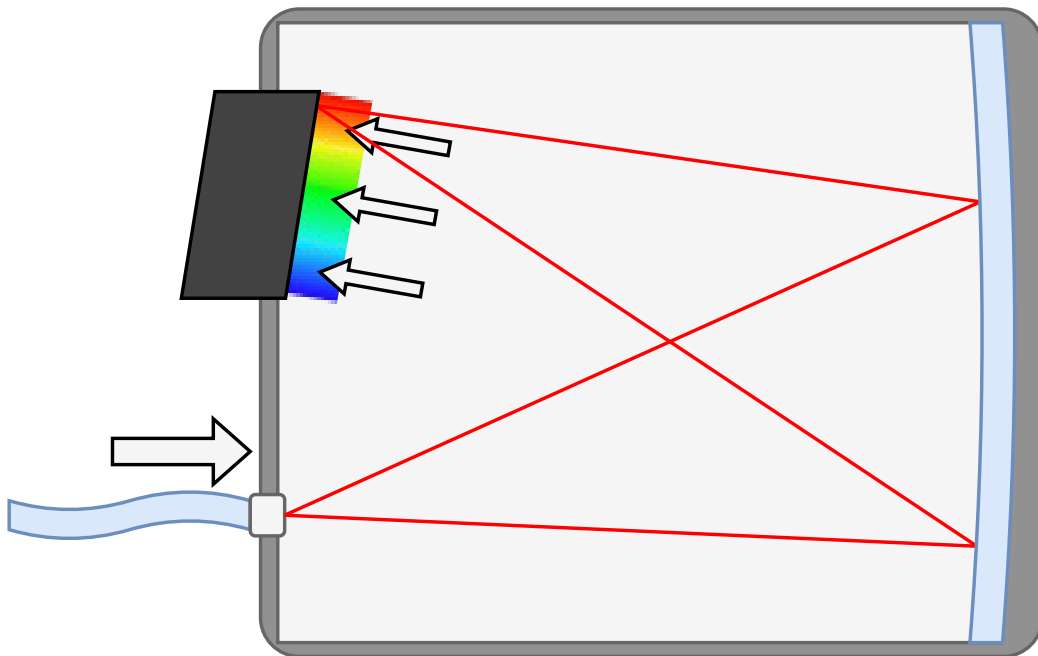
Figure 9: Sketch of inner workings of the spectrometer MMS-1. Light enters chamber through optical fibre (lower left), gets scattered onto flat field grating (blue area, right). From there, it is reflected back to the photodiode array (black parallelogram), where the light is turned into electrical signals. Different coloured light is scattered differently, and therefore hits different photodiodes (channels), as indicated by the colour spectrum next to array. Based on info and illustrations from Zeiss [2017]

The grating in MMS-1 is designed to let light with a narrow wavelength intervals hit more than one photodiode. This is meant to improve accuracy, as no light gets caught in between photodiodes. This must be kept in mind

when evaluating data. Even though a channel has a designated wavelength associated, in also gathers light from the surrounding wavelengths.

3.1.2 Calibration

As the data used is measured over a large timespan ($\sim$ 6 months), some calibration is required. This is done using a standard, relative calibration method. By making every variable constant, measurements can be made from time to time, to use as calibration:

- Light bulb: The same calibration light source is used every time. It shines close to a black body, and has spectrum that is constant over time. It is heated the same way each time (from 0 V to 12 V should take 5 min., then another 5 min. to let it stabilize). To preserve the light bulb when switched off (after calibration), the voltage is lowered from 12 V to 0 V over 5 min.

- Placement: The light bulb is mounted in a housing and the radiometer is placed in two cradles. They are then placed at the same distance, by measuring the distance from the foot of the light bulb housing, to the nose of the detector.

- Measurements: A few test spectra are made, to check for stability. If it is stable, three spectra are taken and used as a measurement in the relative calibration.

From the measured spectra, drift factors can be made by dividing the spectrum values for the initial reference spectrum by the spectrum values for the current spectrum. Using interpolation, factors can be obtained for all times between the measured spectra. Multiplying these with he measured spectrum from the field, the relative calibrated spectrum is obtained.

All relative calibrations are made with respect to the first spectrum measured with this set-up. The first spectrum was made just when the devices arrived newly absolute calibrated from manufacturer. By comparing the calibration spectrum at later times to the first, any drift in the devices should be seen. Relative calibration is also a easier than absolute calibration, as the absolute one requires that you know at a given distance the exact spectral irradiance emitted by the calibration lamp.

The stability of the calibration lamp is monitored by comparing the drift-factors with different radiometers.

3.2 SunSprite

The SunSprite, made by the company SunSprite, is a small, clip-on device that measures UV and visible light. It is battery powered, but is solar charged, and requires no external charger. The device comes with a detailed instruction manual, a quick start guide, and a downloadable app (originally only available for Apple products, now also for Android).

The device is simple in construction: a plastic housing with ten diodes, one button and a magnetic attachment. It also houses the photocells and battery. The device measures illuminance in lux, [lx], but provides data in their own unit of GLux, not to be confused with giga-lux. GLux is an abbreviation of GoodLux, and is a SunSprite defined unit to make the device easier to use for the common-man. SunSprite has a pre-set, not adjustable "goal" of 10 000 lx for 30 minutes a day. When the button on the device is pressed, it will light some of the diodes, depending on how far you have come on your goal. Each diode represents 10% towards the goal. For example, if three diodes are lit, and the fourth is flashing, it means you have had 30% of the exposure required, and the flashing light tells you that you are in sufficient beneficial sunlight. If the goal is achieved, it will flash, and you can restart it by holding the button for a few seconds.

The device can be linked to a smartphone using bluetooth. On the provided app, you can see graphs of your light exposure, and get a live reading on the illuminance value and UV index measured by the device.

3.3 Philips ActiWatch Spectrum Plus

The Phillips ActiWatch Spectrum Plus is a watch-like device intended for clinical studies of patients activity behaviour [Phillips, 2016]. It comes with a complete software (Windows only) for extracting and analysing data, but also to configure the ActiWatch in different ways. The device can go up to 50 days without recharge, depending on data sampling rate.

ActiWatch has a single button, used to either activate the device or start recording, or can be held to make a mark on the recording. This mark is nothing more than a mark that shows up at that exact time when analysing data, and if it is to be useful one must remember/write down the message. The display only shows what time it is, and gives an indication if the device is in operation or not.

ActiWatch monitors both activity (accelerometer) and full visible light spectrum. It has four different diodes, to cover the entire visible spectrum. According to the website Phillips [2016] operates between 400 nm to 700 nm, but through correspondence via e-mail with Phillips Support more precise

data was obtained, presented in Table 2. ActiWatch is also equipped with a capacitive sensor to detect when the device is off-wrist. This pauses data recording.

Table 2: ActiWatch diode specifications. Interval information is from e-mail correspondences with Phillips Support.

Colour	Top [nm]	Span [nm]
Red	615	570 - 750
Green	525	495 - 570
Blue	465	380 - 495
White	605	380 - 750

No additional data was obtainable for action functions for the diodes. The diodes are however placed in a well-like hole under the display, with no diffuser.

The software provided with the ActiWatch, Actiware, lets you connect the device, to program/start the device, and to extract data. It also lets you have many users, so if several patients are using the device, they each get one profile. The data it extracts is presented in tables and graphs, and the software has a versatile tool for producing reports.

Before the device can be used, it must be configured using the Actiware software. When configuring the device, several options are available.

- User: Several users can be configured in the Actiware. This option lets you select which one is using the device for this session.

- Active sensors: Select which sensors you want to use during this data collection session.

- Data sampling rate: Options on data collection frequency. Maximum frequency is one sample per 15 seconds. Note that increased sampling rate affects power consumption.

- Starting time: Select the time you want data collection to start.

- Optional; stop time: Select time when data collection should stop.

Other options include manual entering calibration coefficients for data calculation.

Another version of the Phillips ActiWatch Spectrum has been investigated by Price et al. [2012]. That version had a rectangular windows for the diodes.

Prize et al. reported a cosine response good, as long as the window is in the way of incoming light. It was also reported that the white light data was a linear combination of the red, green and blue diode data.

A version of ActiWatch has also been investigated by Figueiro et al. [2012]. Even though not stated clearly, only through a reference to Prize et al., the device tested here is probably the same as that tested by Price et al. [2012]. They both show similar results.

3.4   SunSense RGB

SunSense currently makes two devices; SunSense One and SunSense Pro. SunSense One has a small display, and measures UV index. SunSense Pro measures UV light as well as RGB, and communicates to a smartphone with SunSense app using bluetooth. Both of the devices are small, and easily attachable, and both of them are made for UV measurement and UV dosage estimation.

The one we received for testing, was a prototype of a SunSense RGB. The SunSense RGB shares much similarities with SunSense Pro; it has RGBW sensor, UV sensor, and communicates with a smartphone using bluetooth. The maximum response for each of the five sensors in SunSense RGB are at 330 nm (UVA), 360 nm (UVB), 465 nm (blue), 520 nm (green) and 630 nm (red) [SunSense, 2017]. The response functions for the RGBW sensor of SunSense RGB are shown in Figure 10.

The SunSense RGB is connected to Android or Apple smart phone using bluetooth, and calculates UV index and dosage from the sensors in the SunSense app. When fully developed, it is planned to have capabilities of calculate APLD. This is the reason it has been investigated in this thesis.

The SunSense RGB is equipped with a slightly transparent diffuser on top of the detector.

The SunSense RGB tested did not have calibrated diodes, and all measurements are presented relative to the max. The app was not fully functioning, and only available relevant feature was display of current data. Because of some communication problems, not all data sent from SunSense RGB was received and displayed on the phone.
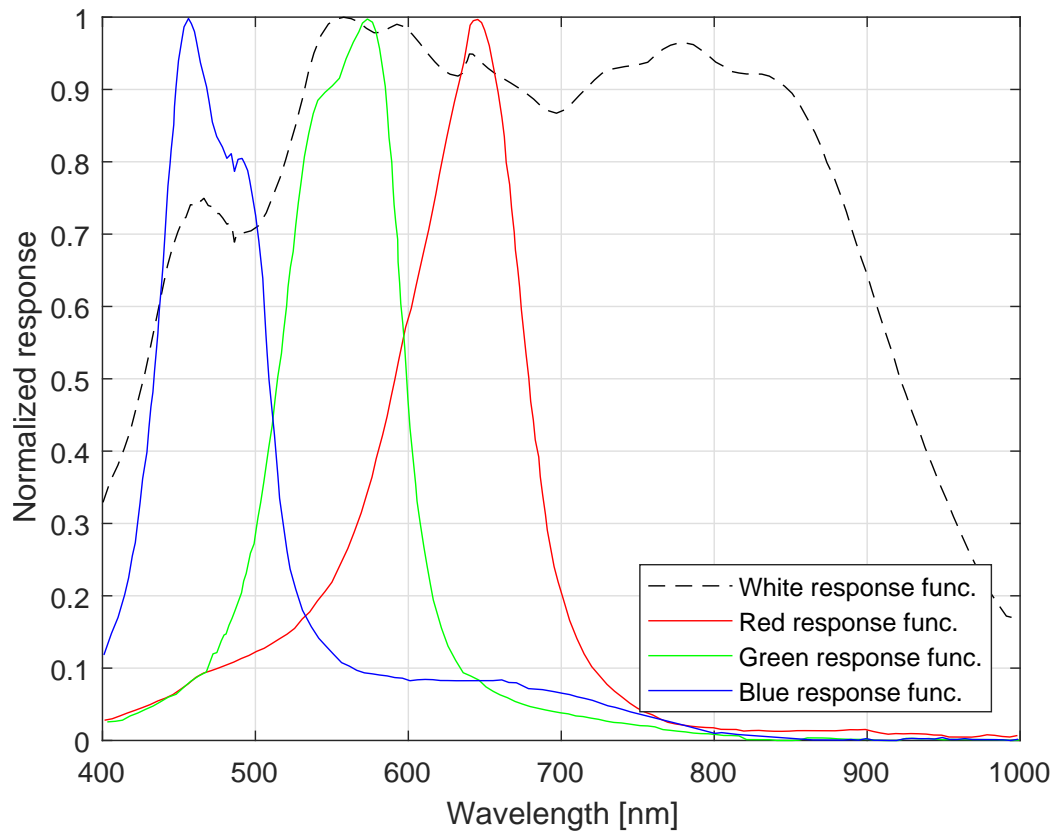
Figure 10: Response functions of the red, green, blue and white diode in the RGBW sensor in SunSense RGB. Provided from personal communication with SunSense.

4 Method

4.1 Evaluating the devices

The overall goal is to find devices suitable for EPP patients to use for dosage calculations, or similar. The devices will be evaluated in the following ways:

- Ease of use

- Possibilities and limitations

- Accuracy

- How construction of devices influence measurements

If the devices prove to be somewhat practical, examination on what they measure with respect to the solar spectrum will be done. By consulting with manufacturers, available documentation and making own measurements, the photocells of the devices should be classified as thoroughly as possible. Preferably with a function describing the response of the diodes, as a function of wavelength of the incoming light. From here on one must compare the measurements the devices provide with what could be useful for an EPP patient. See Section 2.1 for what could be considered useful for an EPP patient. Using the information obtained, conclusions as to the usefulness can be made.

4.2 Classifying the devices

4.2.1 Measuring cosine response

Irradiance radiometers does not register light from different directions equally well; light incoming perpendicular to the photodiode surface normal would not register at all. This is called cosine response, and have been thoroughly examined for the Ramses devices by Tveiteråsen [2013]. A diffuser is a device/object fitted on top of radiometer sensors to scatter light in a specific manner. The diffuser will scatter light in such a way that ideally only the cosine component of the incoming light will be proportional to the light that hits the detector, i.e. the plane diffuser must have the same transmittance for different directions of the incoming light (the amount of light that hits it, is already proportional to the cosine component). For scalar irradiance detectors, the diffuser should be a sphere with no cosine dependence, i.e. receives the same amount of light independent of the angle of the incoming beam.
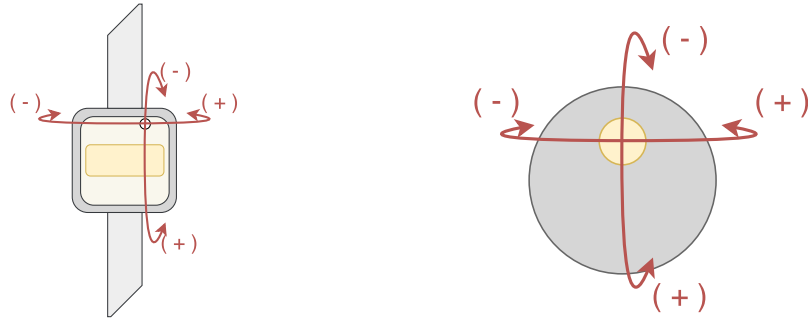
Figure 11: Sketch of ActiWatch (left) and SunSense (right), seen head on, with two axis (horizontal and vertical) of rotation, and indications of positive and negative angles.

When measuring the cosine response of the devices, the following set-up was used. A sketch of the set-up can be seen in Figure 12.

- For stability during measurements, everything is mounted on a optical table.

- A standard optical fibre lamp was used for light source.

- A lens was used to make the light spread out from the optical fiber as parallel as possible. This is to help any inaccuracies in placement of the sensor.

- The sensors were mounted in the centre of the turntable. To validate the centring, a laser was mounted on the table and pointed on the tip of the sensor. When turning the table, the laser does not change position if the device is correctly placed.

- Measurements on each device were done in a single run.

    For the ActiWatch Spectrum Pro: Four measurements were made on each angle measured. The first measurement was discarded due to large deviance, likely caused by reflection of an arm that had to go under the light beam when adjusting the angle.

    For the SunSense RGB one measurement was made on each angle of measure. The SunSense and light source proved so stable that no more measurements were needed.

- All other light sources in the room were turned off. Any close objects that might reflect stray light onto the sensor were removed.

- When measurements were made, the only variable was the angle of the rotary table.

Figure 11 indicates what is meant by horizontal and vertical rotation of the ActiWatch (left part of figure), and SunSense (right). Positive and negative end of axis is also indicated, and origin is assumed to be just on the tip of the sensors.
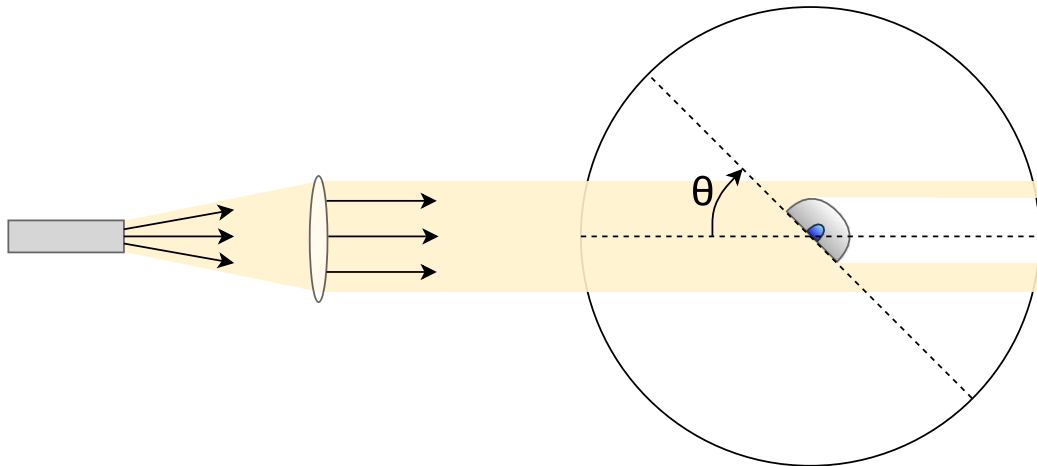
Figure 12: Sketch of set-up for cosine response measurement. Device (grey semicircle) is placed in the middle of turn table (black circle). A light source (gray rectangle) shines light on a lens that focuses it to parallel beam.

4.2.2 Measuring responsivity of sensors

To measure the output of the devices when the incoming intensity changes, a set up as shown in Figure 13 was used. The following set-up was used:

- For stability during measurements, everything is mounted on a optical table.

- A standard optical fibre lamp was used for light source.

- An IR (infrared) filter was mounted just in front of the lamp, and is used to remove any near-infrared radiation. The photodiodes of SunSense (see Figure 10, white diode) measure into the near-IR region, and the grey filters used had only approximately constant transitivity in visual range, so the transmittance in IR region varied with filters.

- A lens was used to focus the light source just behind the tip of the sensor. This is to make the light as strong as possible. It is placed after the IR filter.

- Grey filters were mounted in a lens holder between the focusing lens and the devices.

- Measurements were made in a single run.

  When measurements were made on the ActiWatch, four measurements were made on each filter. The first measurement in each set was however rejected, as filter change heavily influenced results, as the ActiWatch recorded during filter change (every 15 seconds).

  When measurement were made on SunSense, it was stable enough to make a single measurement with each filter.

- All other light sources in the room were turned off. Any close objects that might reflect stray light onto the sensor were removed.

- When measurements were made, the only variable was the filters. Everything else was kept constant.

Change of intensity is made by changing the filter (transparent grey). Filters used have a small change in transmittance in the visual part of the spectrum, and are not treated as constant in this thesis.
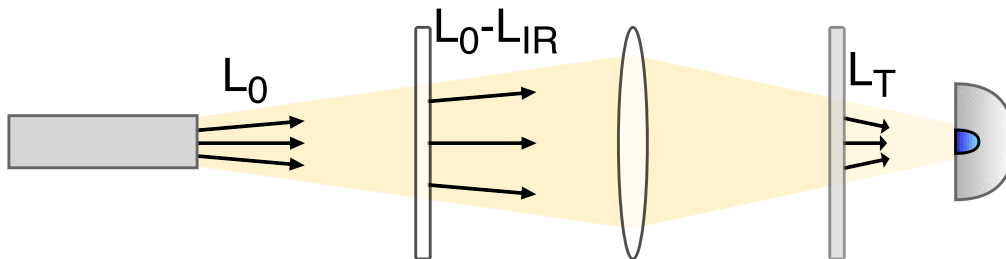
Figure 13: Sketch of measurement set-up when checking responsivity. The light source (grey box, left side) shines constant light with radiance L_0 through a filter (white rectangle) removing infrared radiance. The beam is then focused by a lens (white ellipse). The filter (transparent grey) has a near constant transmittance for visual light, reducing the radiance to L_T. The device (grey, semicircle) is placed so the light covers the sensor (blue area).

The grey filters used are labelled with optical density; OD. The transmitted radiance, L_T, is the radiance incident on the filter, $L=L_0-L_{IR}$, and OD

in Equation 32.

$$L_T = L \cdot 10^{-OD} \tag{32}$$

The transmittance T is defined by the ratio of transmitted and incoming light, which can be expressed with OD as a variable. See Equation 33.

$$T = \frac{L_T}{L} \cdot 100\% = 10^{-OD} \cdot 100\% \tag{33}$$

Corrections were made with regards to OD. The OD was not found sufficiently constant over the sensors spectral range, and OD was interpreted from manufacturer data sheet. OD was found for the top wavelengths of each diode in the devices tested. Figures 49, 50 and 51 in Appendix Section A.2 for manufacturer provided graphs, showing how OD vary with wavelength.

4.3 Solar spectrum data

Three radiometers, mentioned in Section 3.1, were mounted on top of the University of Bergen building; *Biologen*. They have been there periodical from spring to autumn 2016. Measurements by these radiometers will provide the irradiance data for calculating illuminance, UV index, porphyria light indices (see Sections 2.2.4, 2.1.1, 2.1.3), and the values the devices would have measured.

An added bonus of the measurements being done on top of the *Biologen*, is that our measurement station and that of NRPA is only about 300 m away. To check the validity of the data gathered from these radiometers, comparisons of calculated UV index and measured UV index (NRPA) will be done. To do this, a software for reading data from plotted graphs must be used to extract data from NRPA's graphs of UV index on the course of the day. The software *WebPlotDigitizer v3.8* was chosen. Any attempts of correcting mistakes will be discussed later.

4.4 Simulating solar spectrum data

To strengthen any correlation the instruments might find, simulated spectra were generated using the AccuRT software. The AccuRT software uses a satellite measured solar spectrum data outside the atmosphere to generate solar spectrum at distances in atmosphere and in water. AccuRT does this by solving the RTE discussed in Section 2.3, Equation 12, for horizontal slabs.

AccuRT lets the user specify variables for both a simulated detector and weather. Variables for detectors include choice of irradiance and radiance detector, and placement of detector (in height for irradiance, and height and

angle for radiance). Weather/atmosphere conditions can also be specified, such as clear or cloudy, with or without aerosols. The individual modules can be modified as well, such as cloud thickness, particle concentration/size etc. Several other options can be used, such as ground material.

By investigating the simulated spectra for both clear weather, different layers of clouds and with/without aerosols at varying zenith angles, the theoretical correlation can be calculated and compared with the measured.

Four simulations were done, meant to represent:

- Clear weather

- Clear weather with aerosols

- Thick cloud layer

- Thin cloud layer, with aerosols

All simulations had most of the parameters set equally, to get comparable results. Simulations were done with solar zenith angle between 0° and 89°, with step 1°. To get a full spectrum of visual and UV light, the simulations would mimic a detector at 1 m above the ground, registering at wavelengths of 280 nm with step 3 up to 800 nm. The bandwidth for the detector channels was all set to 3 nm, to minimize oscillation of data due to individual absorption lines, and to better mimic an actual detector. The simulations were done over land by setting the lower slab vacuum (no ocean).

AccuRT uses horizontal slabs for approximating the atmosphere, and does not take into account the curvature of the earth. For most angles the error is small, but at larger zenith angles the approximation will loose its accuracy. Because earth's atmosphere curves around the earth, it will have a finite depth at 90° zenith angle. The horizontal slab will not possess the same property, and as the zenith angle approaches 90°, the depth will keep on increasing.

5 Results and discussion

5.1 Testing SunSprite

The SunSprite device was quickly rejected. It was easy to use, and very intuitive, but was not able to give any useful information that might be used for EPP patients to determine dose. The data the device gathered was only accessible through real time, or in graphs in an app, but without accurate units for time and lux. See Figure 14 for screen-shot of data provided after a small test period. Because of this, the SunSprite was not classified.

Figure 14: Data available from SunSprite app. The graph shows illuminance in "GoodLux", GLux, on the vertical axis, and time in hours and minutes on the horizontal axis. Notice the cut of on the graph at about 12 GLux.

For this device to be useful, it would need to have implemented a way to export the data in a more useful way (for EPP patients), either with more useful graphs, or by a table with appropriate columns.

As later is shown (Sections 5.8.2 and 5.8.3), there is a strong correlation between illuminance and (optimized) PL index. If the device is thoroughly classified, and found data can be extracted in a sensible way, it could be used as a dose-rate-meter.

5.2 Testing Phillips ActiWatch Spectrum Plus

The Phillips ActiWatch Spectrum Plus is easy to use by itself, but the software could be a bit overwhelming. It should not be very hard to learn the essential for an EPP patient, or a young EPP patient's parents. The ActiWatch lacks the real time insight to the data it measures, like the SunSprite and SunSense have. It must be connected to a computer with the correct software (Windows only, as of May 2017) to be read. The device will therefore serve more as a way of determining the accumulated dose after expose, more than a real time device for determining when an EPP patient must take cover. This is mostly relevant if exposure time comes as intervals; for instance recess in school/kindergarten.

Another note on the ActiWatch, is that it is a wrist wearable. This puts the device in danger of being covered by sweaters, jackets or similar. Clothes would block most of the irradiance, rendering the device un-precise. Figueiro et al. [2012, Figure 6] compares how a wrist-wearable devices compares to one mounted next to the eye. It is there found that wrist-wearable devices measure less than one mounted next to the eye.

The orientation of the watch will also influence the measurements. Depending on the orientation of the wrist, reading on the device could be different. Orientation should be done to best mimic the exposure of the face, as the face is the most exposed area for an EPP patient. One might try mounting the device outside the clothing, but the device will auto shut-down when of wrist, because to the capacitive sensor. The sensor can be tricked by placing a conductor on the back, where the wrist should be. This solution could be unstable, and has not been tested in this thesis.

5.2.1 ActiWatch illuminance measurements

A comparison measurement between the E2 radiometer and ActiWatchs' measured illuminance was done on the second of June, 2016. The results are plotted against time in Figure 15, and against one another in Figure 16. One would expect some linear correlation between these measurements, as both devices measures irradiance. The Spearman rank was calculated for the correlation between the two illuminance measurement sets, by ActiWatch and E2:

$$\rho_s = 0.71$$

indicating there might be some positive correlation. It appears that the ActiWatch device might not be useful for illuminance measurements. As can be seen in Figure 17, the same trend can be seen by individual measurements for all four photodiodes in the ActiWatch device.

41
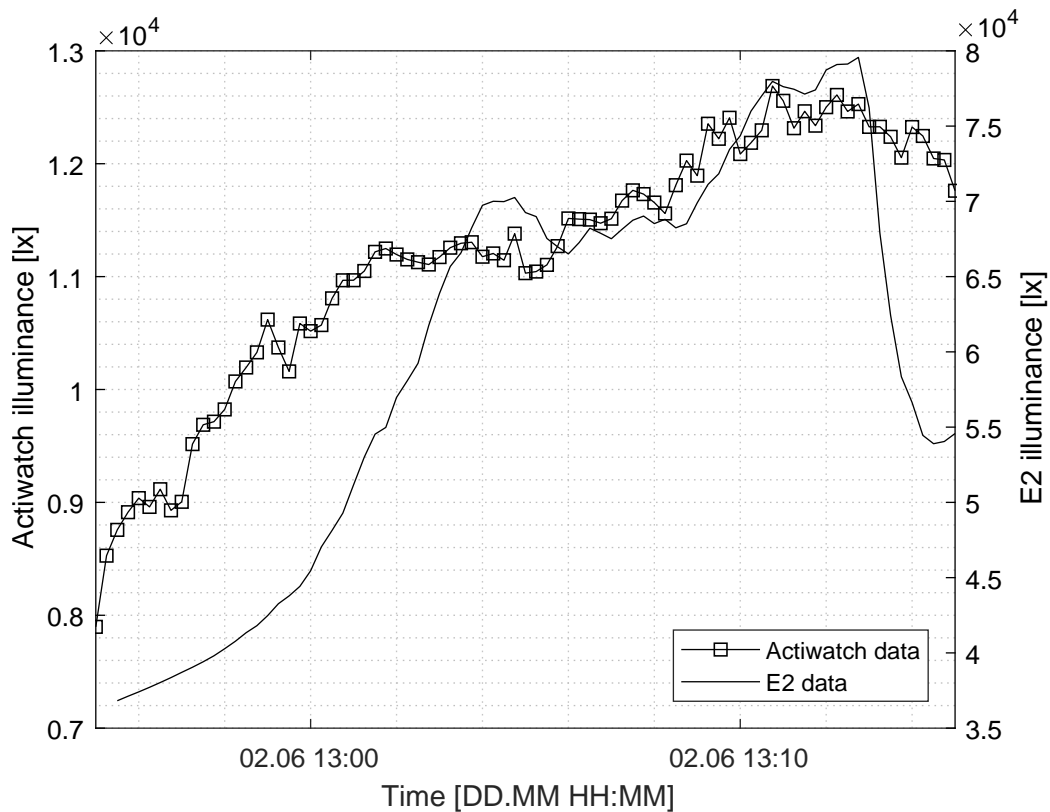
Figure 15: Figure shows measurements made by ActiWatch (square points on hard line, left y-axis) and E2 (hard line, right y-axis) on 02.06.2016. For ActiWatch the illuminance is an output from ActiWare. The illuminance-values from E2 are calculated on measured the irradiance from E2.

As can be seen by Figures 16 and 17, the slope is the same for all sensors on the ActiWatch. This indicate that the sensor on the ActiWatch does not measure the same as the E2 radiometer. The poor correlation between measurements by the radiometer E2 and the ActiWatch could have one or more origin(s):

- Cosine response: ActiWatch's photodiodes sits in a cylindrical hole in the display face, covered by the same glass as the rest of the display. Incoming light must then have sufficiently low zenith angle to make it down the hole and onto the photodiode. This affects what light the photodiode detects, and could also explain why E2 measures higher values than the Actiware (see Figure 16). This is investigated in Section 5.3.1.

- Curvature of the display: The glass and display has a slight curvature,

42
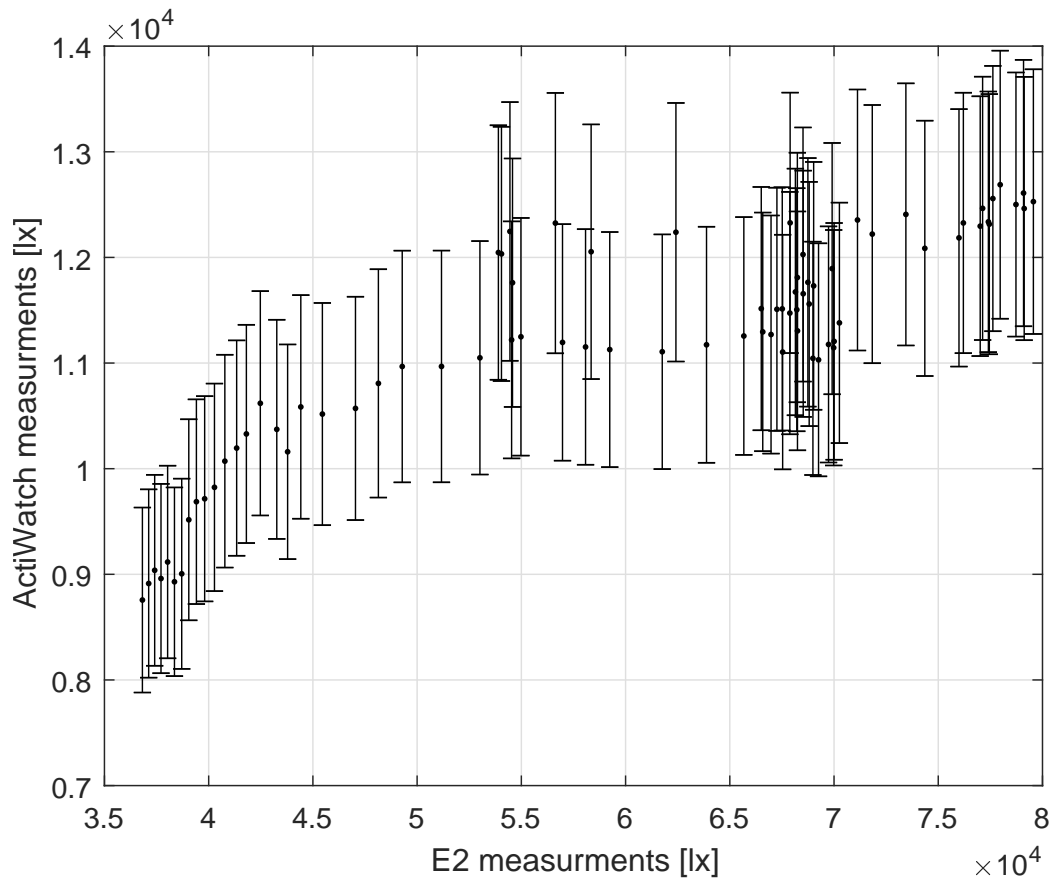
Figure 16: Plot of measured illuminance by E2 and ActiWatch. Error bars are 10% of ActiWatchs' measurements.

affecting the transmittance angle of the light.

- Heat: The second of June, 2016 (our day of measurements), was a warm one. The heat could influence the internal circuits in the device, or affect the protective glass.

- Over stimulation: The photodiodes in ActiWatch are not meant to be used as radiometer, and therefore might not handle the strong light as much as we would like.

- Contaminations: A small, but possible source for errors are contaminations. Especially grease from fingers on the glass, above the sensors.

To see if our faulty measurements were correlated with the cosine response of the ActiWatch, the average incoming light angle was calculated for our
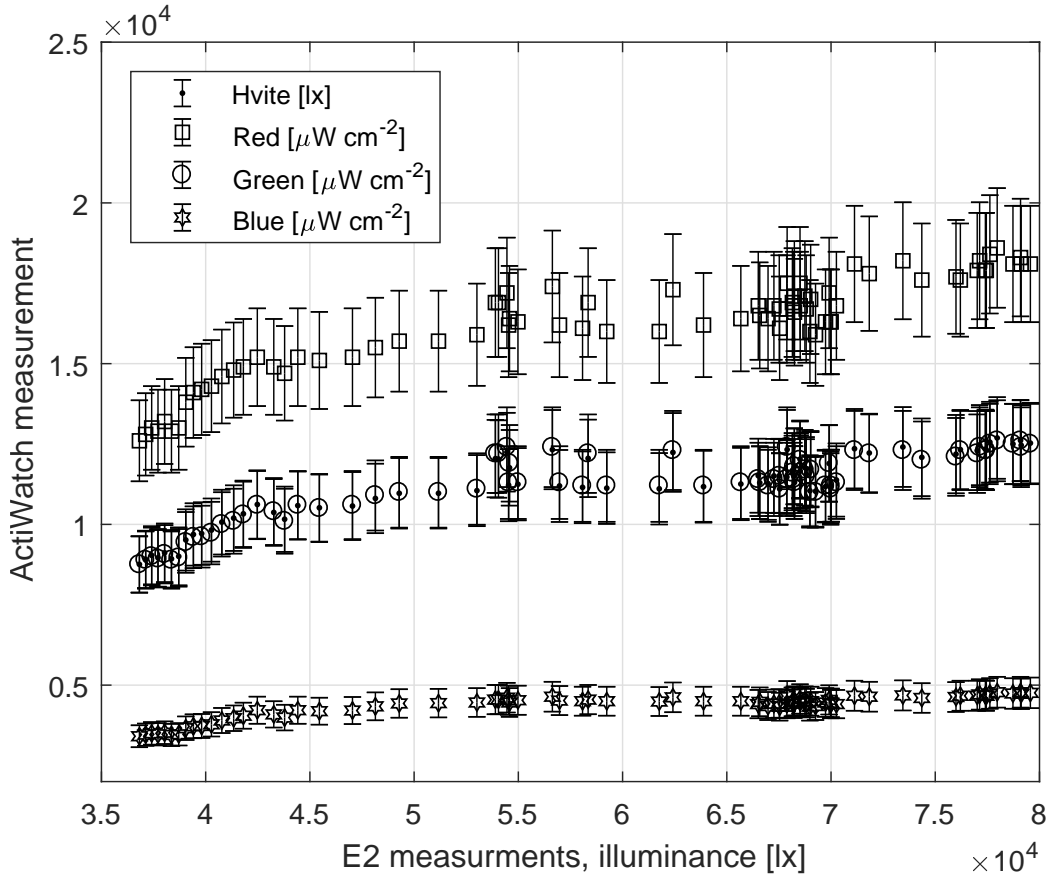
Figure 17: Plot of measured illuminance by E2 vs all measurements from ActiWatch, on 02.06.2016. Error bars are 10 % of ActiWatchs' measurements. Units in legend are for ActiWatch.

day of measurements (Figure 18). The calculations for that plot are made by dividing measurements from the cosine radiance radiometer (E2) with measured spectrum from the scalar irradiance radiometer (EE), as explained in Section 2.5. This number, between 0 and 1, is then converted to an angle by finding the inverse cosine.

From Figure 18, it is clear that light at shorter wavelengths (in the visible spectrum) originates slightly closer to the horizon than light at longer wavelengths. Under a clear sky, red light is not scattered as much by the atmosphere as blue light, and so we would expect less red light at angles further from zenith, as can be seen in Figure 19. It is also notable that overall, average angle does not change much in short wavelengths. The change in average angle is largest for wavelengths >500 nm from 13:00 till 13:05. Comparing this with the measurements by ActiWatch and E2 in Figure 15, this is
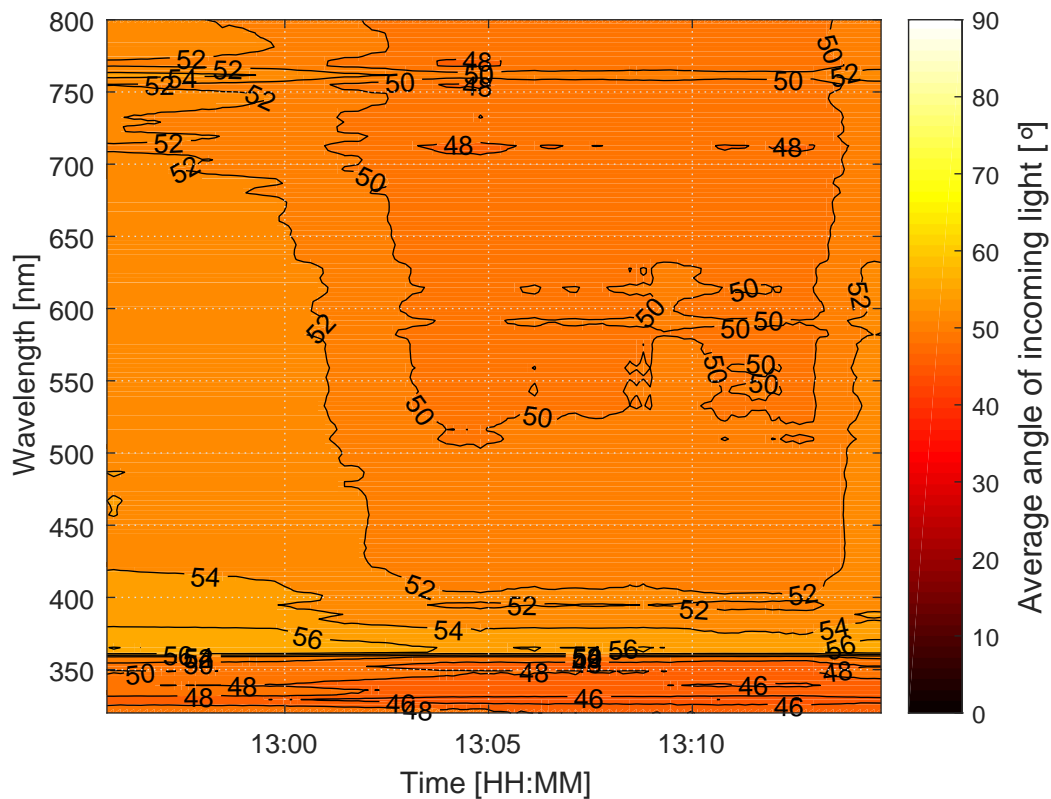
Figure 18: Contour plot of how the average angle of the incoming light changed with time of the day we compared ActiWatch and E2 (x-axis) for different wavelengths (y-axis). The average angle is calculated by dividing the irradiance (light incoming on a surface) with the scalar irradiance (all light incoming to a sphere/semi-sphere). Colour-bar displays average incoming angle. Zenith angle in Bergen on 02.06.2016 was 38.2° [NRPA, 2016]

where illuminance calculated from E2 measurements changes the most, while those from ActiWatch does not show the same behaviour.

Average angles in Figure 18 corresponds well with simulated average angles at solar zenith angle of 40° in Figure 19, except for the shortest wavelength, where we measured average angle being smaller, therefore closer to zenith. It was hypothesised that this could be because of two reasons:

1. Our radiometers are too inaccurate to correspond well with simulated data.

2. Our radiometers have parts of the horizon covered by buildings and mountains; therefore lowering average angle for diffuse light.

The spectra have been calibrated as they should, and because E2 and EE are

45
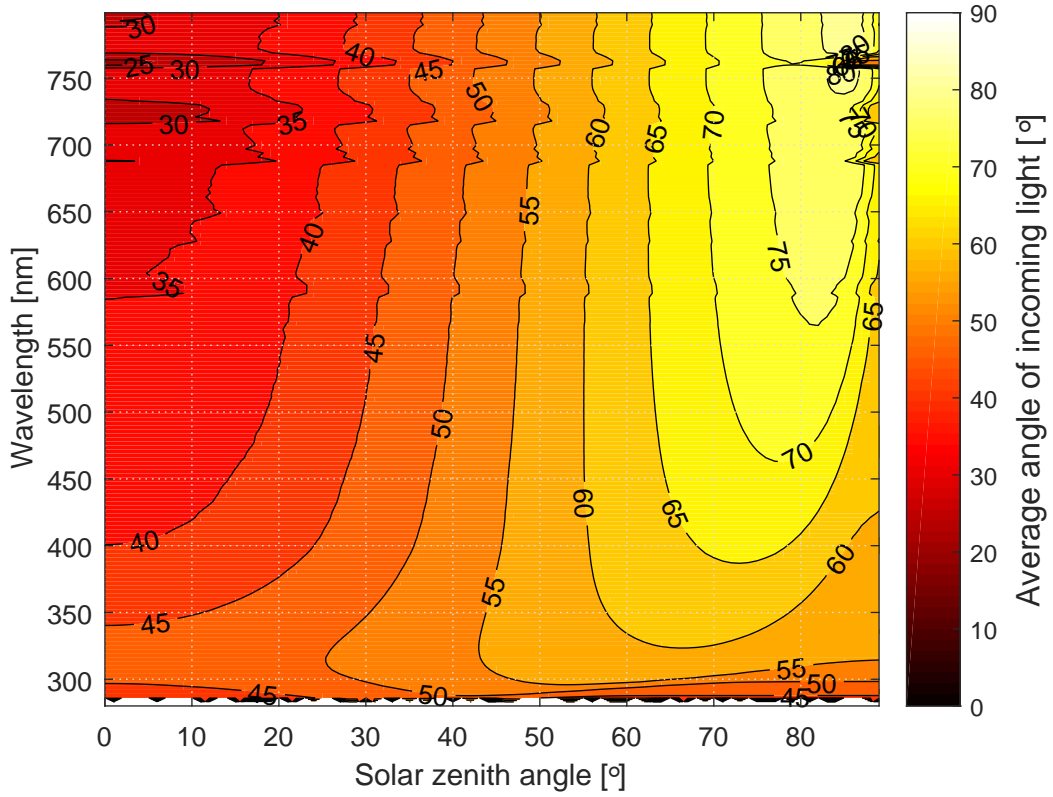
Figure 19: Average angle calculated from irradiance, angle has same reference axis as the zenith angle.

basically the same device with different diffuser (remember: E2 is a cosine irradiance radiometer, and EE is a scalar radiometer). Any error should therefore be more or less be evened out when the fraction is calculated (see Equation 14). To investigate the second reason, a new simulation was done.

Simulation was done under the same conditions as before, but with a radiance radiometer measuring at polar angles lower than 84°. When integrating the irradiance;

$$
\begin{aligned}
F_{partial} &= \int_{\Omega} L(\theta, \phi) d\Omega \\
&= \int_{0}^{2\pi} \int_{0°}^{84°} L(\theta, \phi) \sin(\theta) d\theta d\phi
\end{aligned}
\tag{34}
$$

An equivalent equation is used to calculate cosine irradiance, except with an extra cosine factor. See Equations 2 and 3. These calculations gives scalar and cosine irradiance with 6° above the horizon blocked. Calculated average angle is presented in Figure 20. This gives better correspondence in UV

46

region, but makes correspondence in longer visual spectrum worse. It should not be ruled out that the blocking of the horizon influence the data, but it is probably not much.
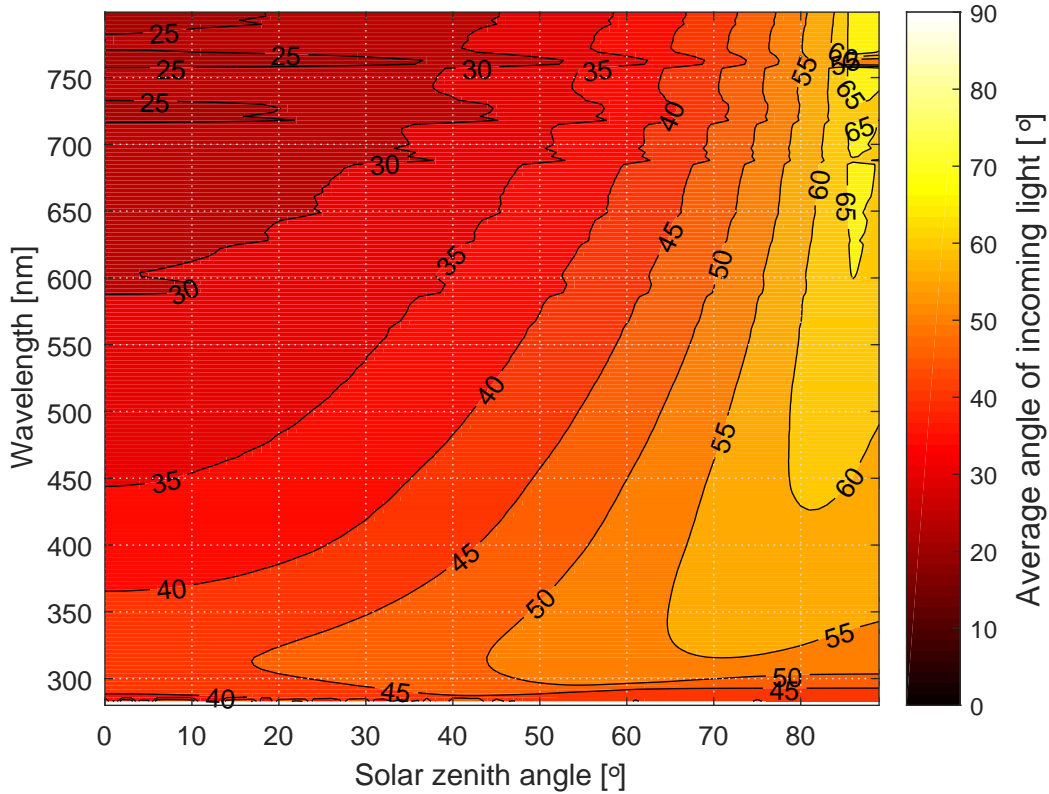
Figure 20: Average angle of incoming light calculated from irradiance, which in term is calculated from simulated radiance values. The radiance values are for polar angles < 84°, to simulate obstacles (buildings, mountains) blocking 6° from horizon.

It is concluded that the invariance between simulated average angle and measured is likely due to error in UV measurement, as is a known source of error for the visual radiometers (as tested by Tveiteråsen [2013]).

5.2.2 ActiWatch for (optimized) PL index measurements

After calculating (optimized) PL indices from the measurements on 2.6.2016, these were compared with the measurements of the ActiWatch. See Figures 21 and 22. The same trends as in Section 5.2.1 have been found.

In Figures 21 and 22, the ActiWatch measures almost no difference in PLi or optPLi. Due to the large error bars and the flatness of the curves,

47
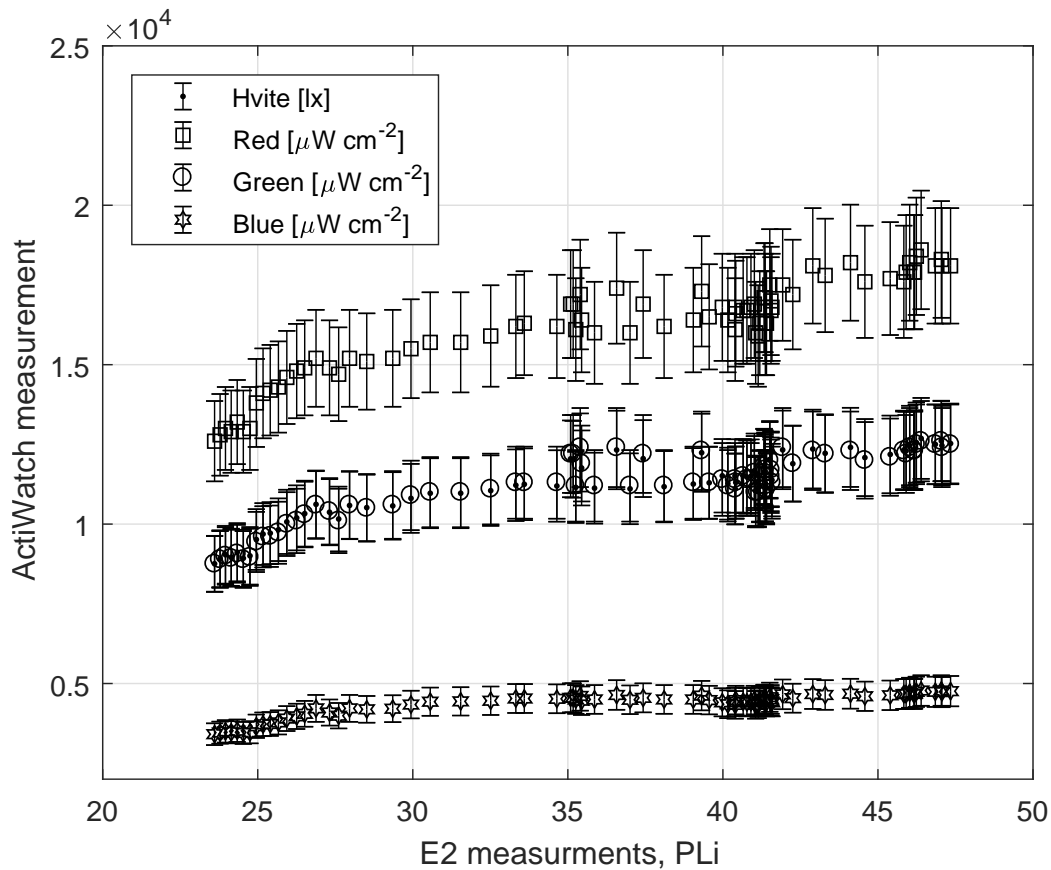
Figure 21: Plot of measured PL index by E2 (x-axis) vs all measured quantities of ActiWatch (y-axis), on 02.06.2016. Units in legend are for ActiWatch diode.

it can be seen from the figures that the ActiWatch can not tell indices 30 or 55 apart. This has a huge impact on DPLD, and could potentially cause overexposure for EPP patients.

5.3 Classifying Phillips ActiWatch Spectrum Plus

5.3.1 ActiWatch cosine response

As the ActiWatch had poor correlation with measurements by E2, see Section 5.2.1, it was hypothesised that this could be caused by poor cosine response on the device. Measurements were made using set-up described in see Section 4.2.1. All measurements are plotted in Appendix A.1.

The measurements presented in Appendix A.1, Figures 46, 47 and 48 all show four data points for each angle. The first point in each set usually devi-
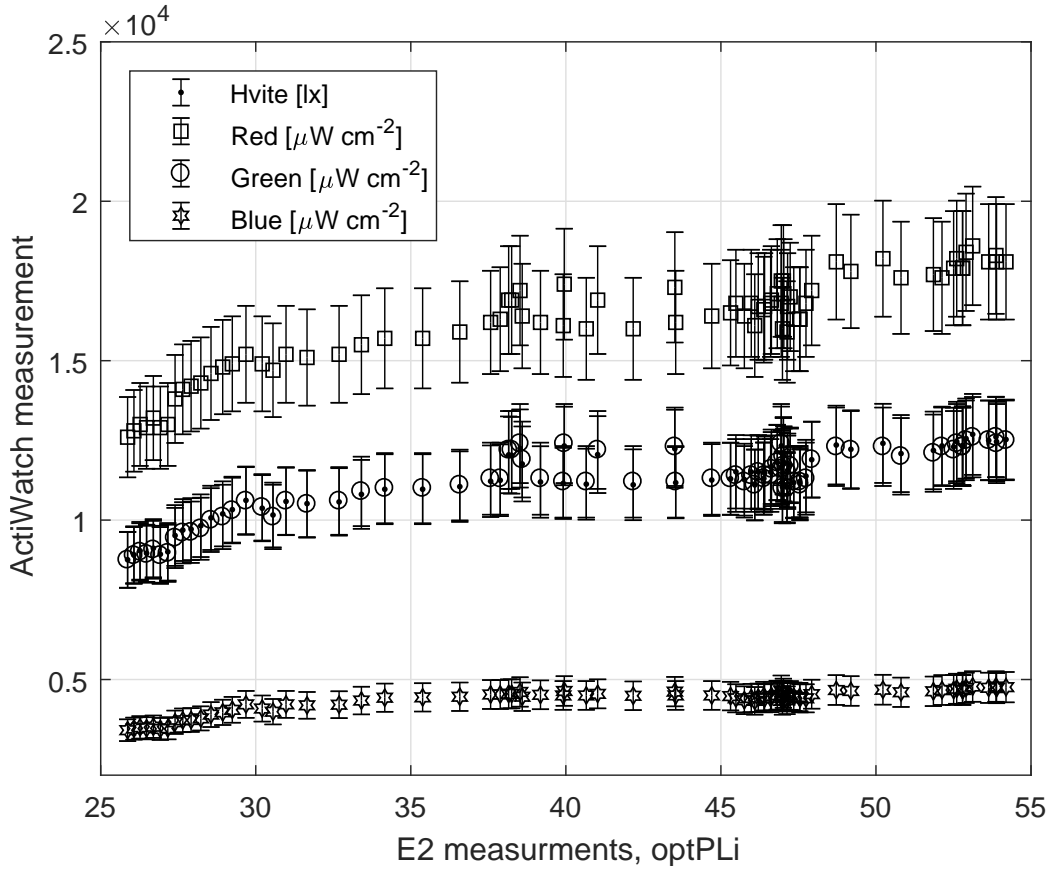
Figure 22: Plot of measured optimized PL index by E2 (x-axis) vs all measured quantities of ActiWatch (y-axis), on 02.06.2016. Units in legend are for ActiWatch diode.

ates noticeably, and are excluded in further calculation. Probable reason for the deviation is that adjustments to the angle happens a few seconds before time stamp of first measurement at that angle. The angle adjustments causes varying reflection in display glass, changes relative diode position (to incoming light), and also introduces some extra light from hands and clothing, that might reflect light to the photodiodes.

The excluded data is interesting nonetheless, as they unveil a big problem with the ActiWatch: sudden large deviations in both directions at the edge of its field of view (discussed later in this section). These mistakes make measurements at some point even higher than what the light source provide, based on what the ActiWatch measures head-on. Some data at the edge of the field of view also gives no values (out of range), NaN. These inaccuracies are ignored when discussing field of view, but must be kept in mind when

evaluating the overall usefulness and accuracy of the device.
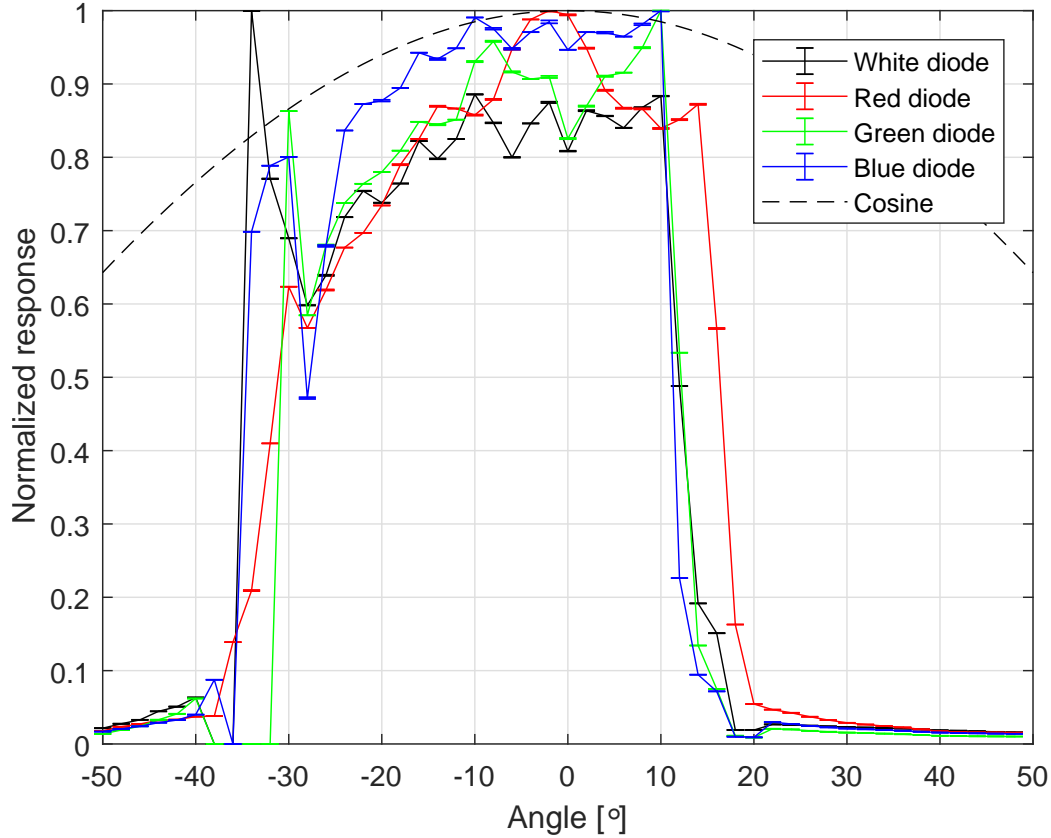
Figure 23: Measurements of cosine response of the ActiWatch, with varying vertical angle. Each diode response normalized to 1 at its maximum. Points are mean of three measurements at the same angle, and errorbars are the standard deviations of these. Negative angles correspond to looking up on the device from below, and positive angles correspond to looking down on the device from above. Angles are explained in Figure 11

Figure 23 shows the measurements made for vertical angles, with measurements for each diode normalized to its own maximum measurements. Note the steep drops for all photodiodes between angles $\sim -30°$ to $-38°$ and $\sim 10°$ to $18°$, and the drop of response at $-28°$. To closer investigate the behaviour from $\sim -30°$ to $-38°$, a second measurement was made, with $1°$ angle step. These data are presented in Figure 24. There are some discontinuities in measurements. The discontinuities can be seen as breaks in the line between points, and are caused by ActiWatch reporting values that are not numbers (NaN).

The two data sets (full angular spectrum and problem part of the angular
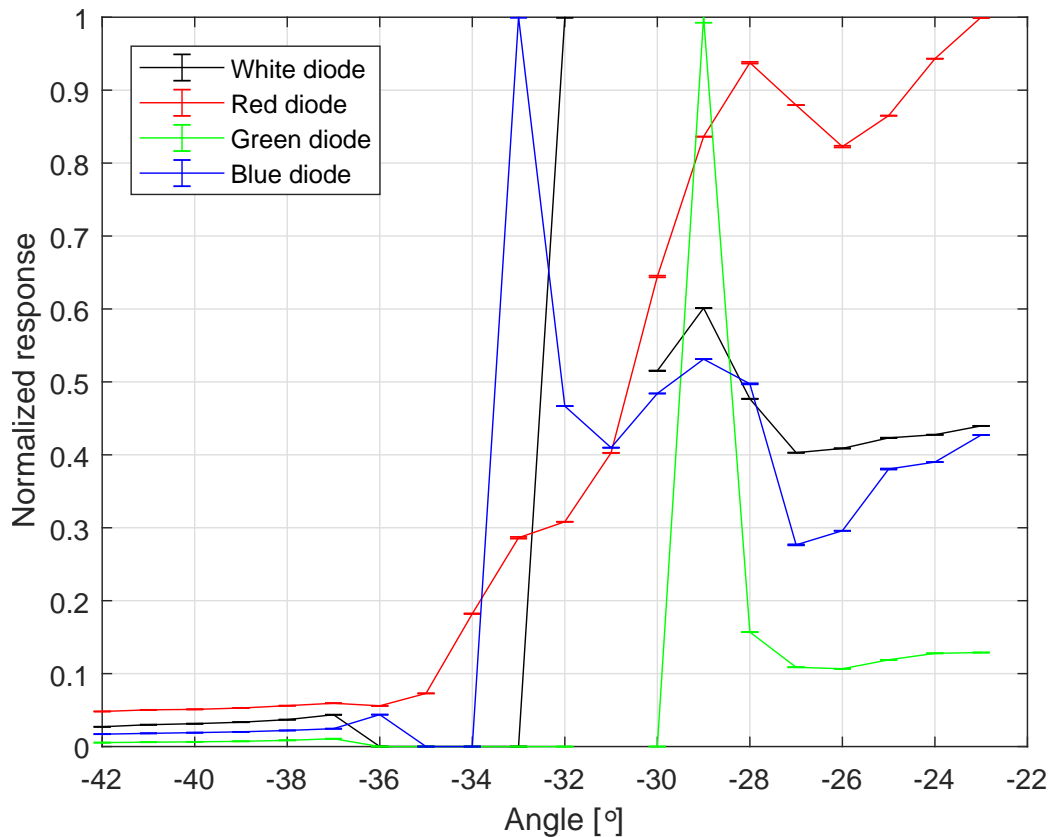
Figure 24: Normalized cosine response for selected problem area for the ActiWatch. Measurements are made with 1° step. Points are mean of three measurements, errorbar are belonging standard deviation.

spectrum) are shown together in Figure 25. The measurements with step 1° is plotted in dashed line, and is normalized with the maximum of original data (hard line), for comparison.

The vertical cosine response has a narrow field of view, and shows large deviations in measurements at the edge of the field of view. This irregularity of the measurements are probably due to the photodiodes sitting in a hole, and is therefore very sensitive to small change in angle. Internal reflection in the display glass could also be a source for this.

The ActiWatch's photodiodes are placed in a hole in the display face, with the same glass covering the entire display. Because of this, the diode will not register much of the light incident at an angle larger than what it can "see" out of its hole. From Figure 23, it can be seen that the ActiWatch registers light incoming from ∼ 14° from below, and ∼ 24° from the top; for a total field of view of 38°.
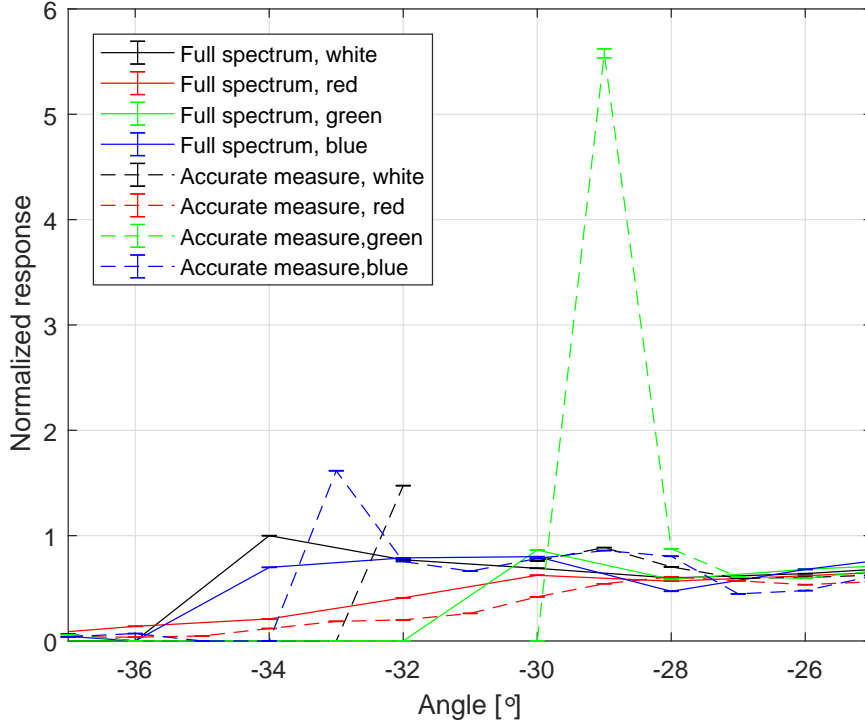
Figure 25: Data from Figures 23 (hard lines) and 24 (dashed line) compared. Points are mean of three measurements, error are the belonging standard deviation. Data for each diode is normalized to measured maximum from the full test. The discontinuity in lines represents data not detected by ActiWatch.

Errors under isotropic light was calculated for the cosine response of ActiWatch. Results are presented in Table 3. The errors presented are so big that the device should not be classified as an irradiance measurement device. The errors are, for all diodes, -80% (rounded of to nearest 10th). Comparing with findings of another ActiWatch device - Phillips ActiWatch Spectrum - as examined by Figueiro et al. [2012], the f2* error of that device was -30.9%, -39.4% and -57.2% for the three diodes [Figueiro et al., 2012, Figure 4]. The ActiWatch Spectrum Plus, tested by us, is therefore worse than its predecessor.

Since the ActiWatch only sees a small portion of all the angles of incoming light, its representation of irradiance is poor. This also explains the poor correspondence of illuminance measurements with E2 in Section 5.2.1. Comparing the average angle of incoming light (Figure 18) to the cosine re-
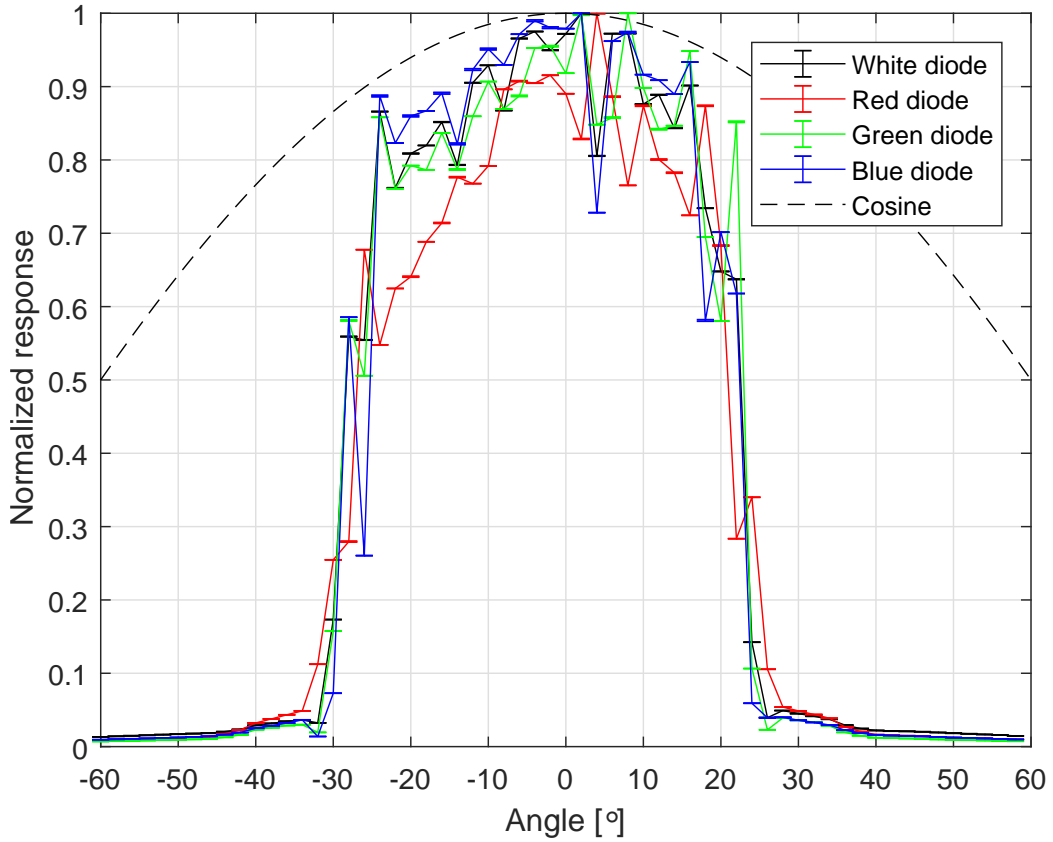
Figure 26: Figure shows measurements of cosine response of the ActiWatch, with vertically horizontal angle. Each diode response normalized to 1 at its maximum. Points are mean of three measurements at the same angle, and errorbars are the standard deviations of these. Negative angles corresponds to looking on the device from the right, and positive angles correspond to looking down on the device from the left.

Table 3: Errors in cosine response of ActiWatch. Row two shows ratios of deviance from ideal curve, Equation 18, row three shows difference in percentage, Equation 19.

	Red diode	Green diode	Blue diode	White diode
ϵ_{tot} [%]	-82.39	-81.81	-82.43	-79.97
f2* [%]	-82.35	-81.77	-82.39	-79.93

sponse of the ActiWatch, it's clear why ActiWatch's measurements are so much lower than E2's (Figure 16), as the average angle of incoming light is low compared with what the ActiWatch detects. Also, as noted before in

Section 5.2.1, the slope of E2's measurements and Actiwatch's are different. E2's rise with a convex curvature; ActiWatch's data with a concave. The origin of the slope in the figure is that the sky cleared up in that period of time; from slightly cloudy to clear. Clouds contributes negatively to the irradiance. ActiWatch's field of view makes it unable to detect changes in clouds outside its own field of view. E2, on the other hand, would detect this, as E2 has a much better cosine response (for a comparison of E2 cosine response and a cosine function, see Tveiteråsen [2013, Figure 4.13]). E2's measurements gradually go up as the clouds disappear, while ActiWatch only notices what is more or less above it.

The results of our tests show that ActiWatch Spectrum Plus is worse than the ActiWatch Spectrum investigated by Price et al. [2012] and Figueiro et al. [2012]. Based on Price et al. [2012, Figure 1], ActiWatch has the projection problem of photodiodes being placed in a well. The problem is larger for the small, circular opened well of ActiWatch Spectrum Plus when compared with the larger, rectangular opening of ActiWatch Spectrum.

5.3.2 Responsivity of sensor in ActiWatch

The ActiWatch was set-up as described in Figure 13 (Section 4.2.2). Because of troubles with the ActiWatch, data was only gathered for the last six filters in Table 8. Two runs were made, with the second having lower starting intensity than the first run. In both the first and second run it registered "NaN" for the first few filters. Because the ActiWatch already has been proven not useful for EPP patients (Section 5.3.1), no further investigations were made.

Corrections to OD was done as described in Section 4.2.2, using the wavelength corresponding to the top of the response function for the ActiWatch diode (see Table 2). The results are presented in Figure 27 and Table 4.

Table 4: Results from responsivity test on ActiWatch. Column two provides the inclination for the function $y = ax$

Diode	Inclination	R^2	RMSRD [%]
Red	$154 \cdot 10^3$	0.998	10.3
Green	$111 \cdot 10^3$	0.981	8.0
Blue	$79 \cdot 10^3$	0.957	5.6
White	$120 \cdot 10^3$	0.961	10.6

The results show that the sensors follow a straight line with an expected percentage error of 10.25%, 8.04%, 5.61% and 10.63% for the red, green, blue and white diode (values from Table 4).
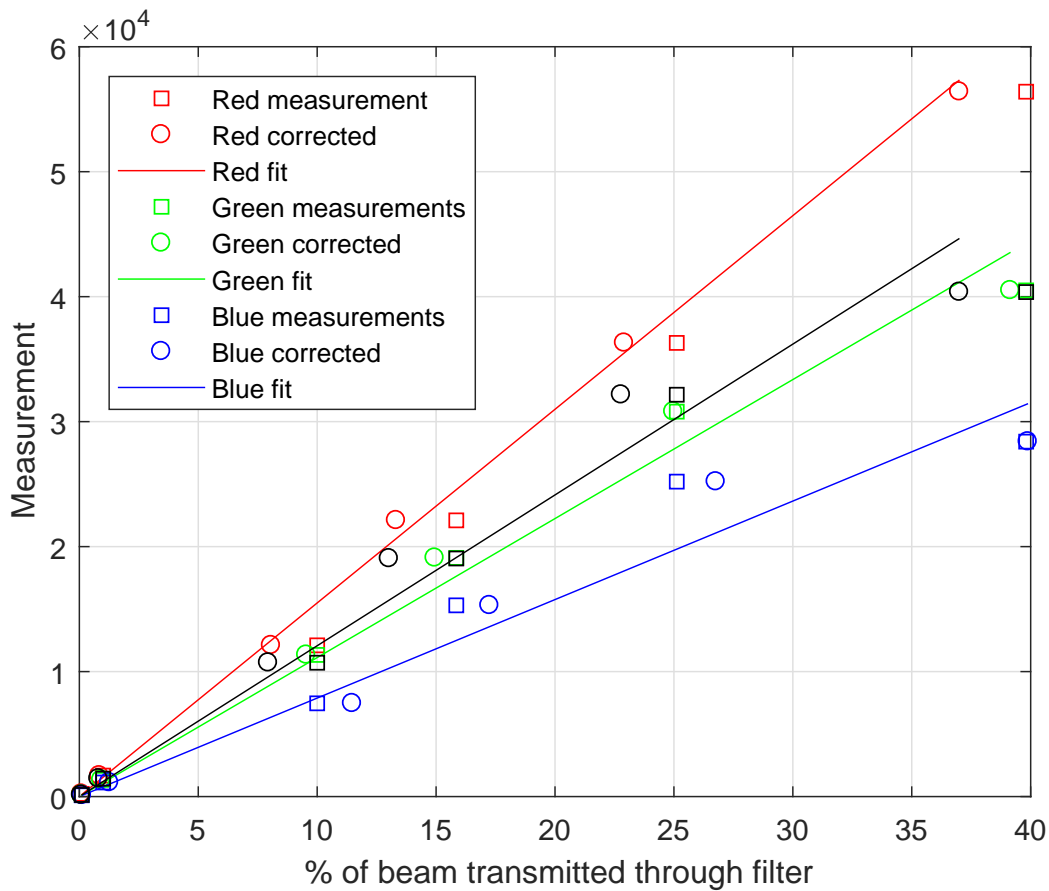
Figure 27: Measurements done on ActiWatch, with varying filters. Square points are plotted using states OD of filters, round points using OD at each diode for each filter. Fitted line is for corrected data.

5.3.3 Error in measurements

According to data sheet, the ActiWatch has an accuracy of "typical" 10% at 1500 lx [Phillips, 2016].

When doing cosine response measurement, three data points were obtained for each angle. Mean and standard deviance were calculated from these. Even though three data points for each set is a small sample, the stability of the light source and in the device was assumed to be good. Any large deviation in measurements within a set would likely be caused by faulty electronics, but was not observed within a data set. The largest deviations was seen when adjusting the angle close to where the ActiWatch has its limits of field of view. Large deviations, as can be seen as the first data point of each set in Figures 48 and 46, was likely caused by reflections of an arm

that had to go in under the front of the device to adjust measuring angle.

When measuring responsivitiy of the ActiWatch, the first measurement for each filter was very off, due to the process of changing filter. After that, the measurements were stable, and error is assumed to be in the decimals.

5.3.4 Evaluation of accuracy in ActiWatch Spectrum Plus

Total error was calculated by Equation 31 using relative cosine error (Table 3) and RMSRD error (Table 4). Total error is presented in Table 5. The errors represented are for isotropic light, and shows that the ActiWatch Spectrum Plus is not for measuring irradiance.

Table 5: Table of total relative uncertainty for RGB diodes of SunSense. Calculated using data from Tables 3 and 4.

Red [%]	Green [%]	Blue [%]	White [%]
83	82	83	81

Our findings are in correspondence with the one for ActiWatch Spectrum, as examined by Price et al. [2012] and Figueiro et al. [2012]. The placement of the photodiodes is not suitable for irradiance measurements, and is the largest contribution to errors in ActiWatch Spectrum Plus and the earlier model, ActiWatch Spectrum. The cosine response would probably improve if a diffuser was added to the device, as the construction would be more like that of SunSense.

5.4 Testing SunSense RGB

SunSense RGB was not for sale at the moment of test (first half of May, 2017), and the device tested was provided as a prototype/unfinished device from SunSense. Please note that changes might be made to the device that comes for sale.

The SunSense has the size of a coin (measures about 23x5 mm), and comes with a wristband and a clip. The wristband lets users wear the device on the wrist, while the clip lets users put it anywhere. The clip will be most useful for EPP patients, letting them clip the device on their jacket collar, facing forward. Light incoming at the face will then be registered by the device sitting close.

SunSense has an app, that still was under development. It's planned to include dose calculating for EPP patients. It also lets the user read live values measured by the SunSense. The app is necessary for measurements and readings, as the SunSense RGB has no display.

Measurements done with the SunSense are not absolute at the moment, as the photodiodes on the prototype have not been calibrated.

5.5 Theoretical test of SunSense (output)

As stated in Section 3.4, response functions for the RGBW sensor in SunSense were obtained through personal communication with SunSense. Calculations are done, assuming that the response functions provided are valid.

5.5.1 Comparison of theoretical SunSense output and (optimized) PL index

PL index and optimized PL index is what EPP patients have use for, and so theoretical output of SunSense was only compared with these indices. The correlation between what the SunSense (theoretically) would output and these indices was calculated. Calculations can be seen in Figure 28 for PL index and Figure 29 for optimized PL index.

The same regression and analysis method is done on these theoretical data as on measurements by the actual indices in Sections 5.8.2 and 5.8.3. The aim of the calculations is to see if the sensor *could* be used in a device in such a way it is useful for EPP patients. Calculations are presented in Table 6. From this table, it is clear that there are good correspondences between the output of the diodes and both PLi and optimized PLi. The blue diode seems especially useful, with an RMSRD of about 6.1% for PLi measurement, and 1.5% for optimized PLi. The usefulness will, as clearly shown in the ActiWatch device, depend on how the sensor is placed in the device, and how the orientation is (Section 5.3.1). If carefully designed, it would be promising.

This investigation of SunSense output should be validated when the device is finalized. Either by finding the correct action functions of the photodiodes, and compare with the ones provided by manufacturer, simply compare the output of the SunSense with output of a radiometer like Ramses.

5.6 Classifying SunSense RGB

5.6.1 SunSense RGB cosine response

Measurement for the cosine response of SunSense RGB was done in the same way as described in Section 4.2.1. Measurement were made for both vertical and horizontal rotation, and results are plotted in Figures 30 and 32. Data in plots are for red, green, blue and white diode, all normalized to its respective maximum.
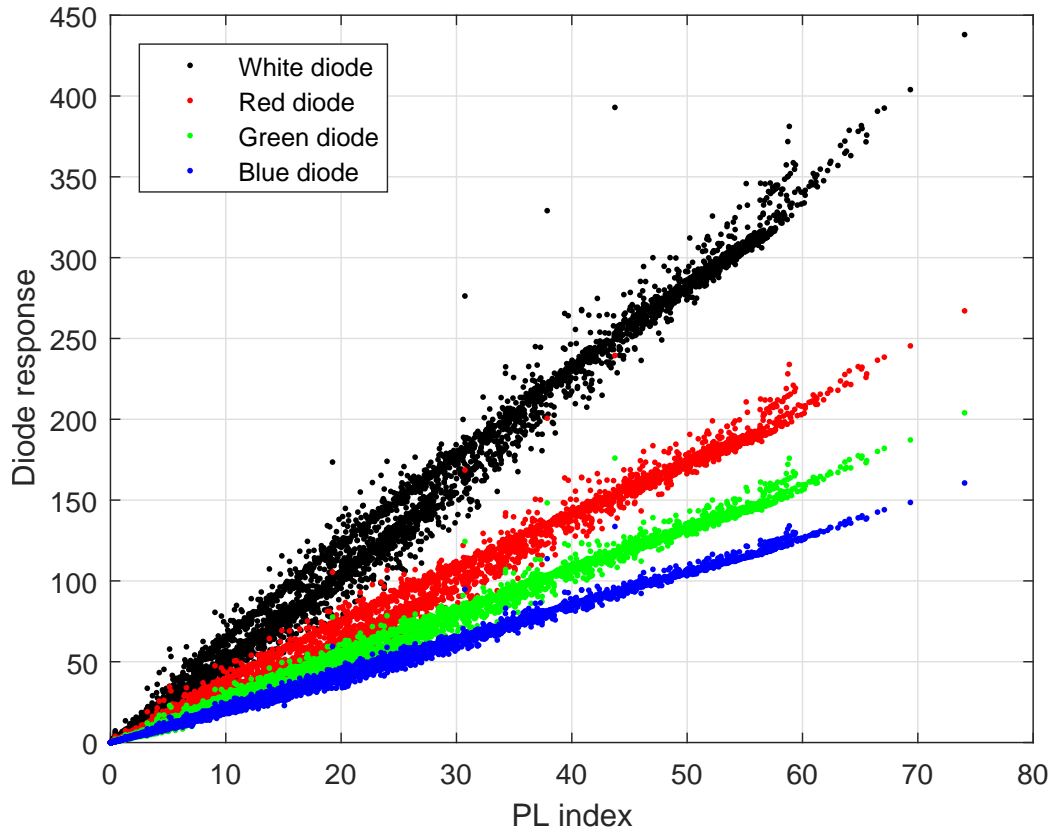
Figure 28: Plot of calculated PL index vs theoretical diode measurements. Note: The response (y-value) is multiplied by a constant for aesthetics; for the actual device they will need calibration.

Table 6: Models for (optimized) PLi and the RGBW diode in SunSense. R, G, B and W are used as variable names for the individual diodes.

Equation	R^2	RMSD	RMSRD [%]
$PLi = 0.12 \cdot W + 0.42$	0.9937	1.3	12
$PLi = 0.43 \cdot R + 0.48$	0.9933	1.4	12
$PLi = 0.45 \cdot G + 0.41$	0.9954	1.1	9.6
$PLi = 0.47 \cdot B + 0.20$	0.9978	0.78	6.1
$optPLi = 0.14 \cdot W + 0.22$	0.9984	0.75	7.1
$optPLi = 0.49 \cdot R + 0.28$	0.9983	0.78	7.0
$optPLi = 0.51 \cdot G + 0.22$	0.9992	0.52	4.4
$optPLi = 0.54 \cdot B - 0.02$	0.9999	0.16	1.6
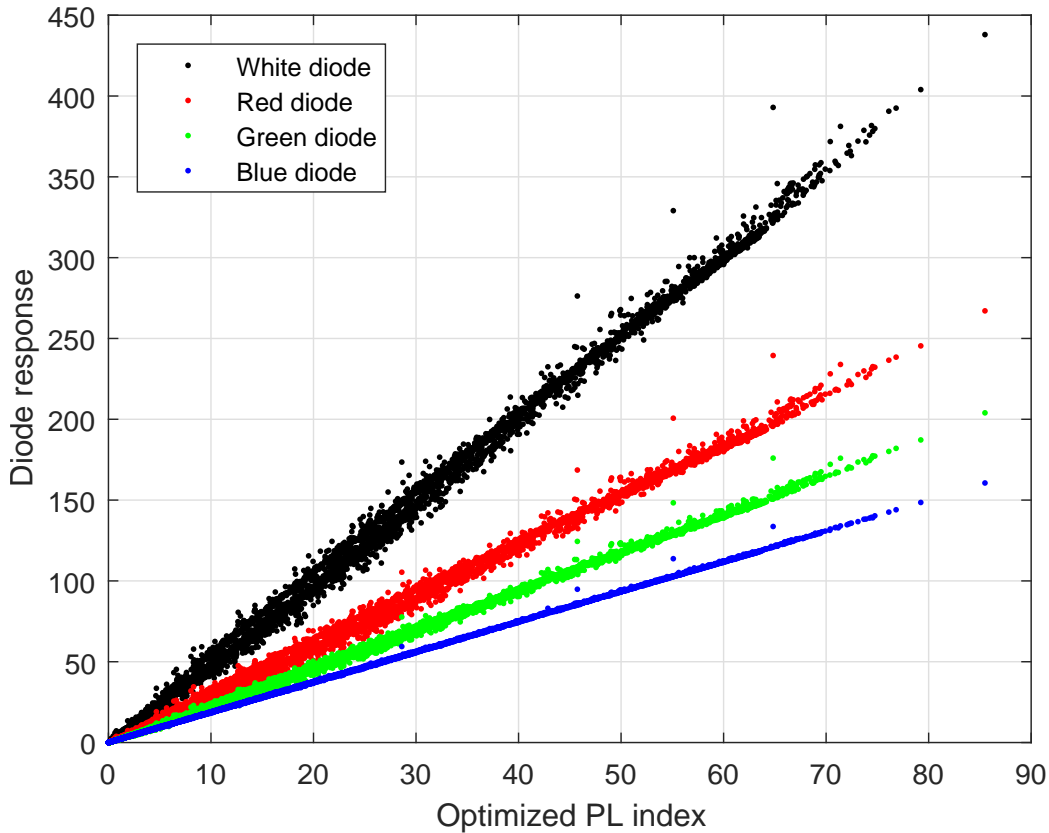
Figure 29: Plot of calculated optimized PL index vs theoretical diode measurements. Note: The response (y-value) is multiplied by a constant for aesthetics; for the actual device they will need calibration.

The relative error ϵ, see Equation 17, is presented in Figures 31 and 33. The results show that SunSense measurements are mostly lower than the ideal, except for some angles in vertical direction. This is likely due to the curvature of the surface of SunSense, and the slight offset of the diffuser. When measuring, SunSense was mounted so the cross section of the coin-like device was vertical, and no considerations were made as to the offset of the sensor from the centre. Another source of error is the distance from the diffuser and the photodiodes. The photodiodes are not elevated up to the diffuser, and so some space are left between them.

Relative error less than 10% occur differently for horizontal and vertical rotation. For horizontal rotation, the absolute error is less than 10% for angles −30° to 30°, and for vertical rotation −45° to 20°. The absolute error also gradually goes up from there.

To better understand how much the error in SunSense's cosine response
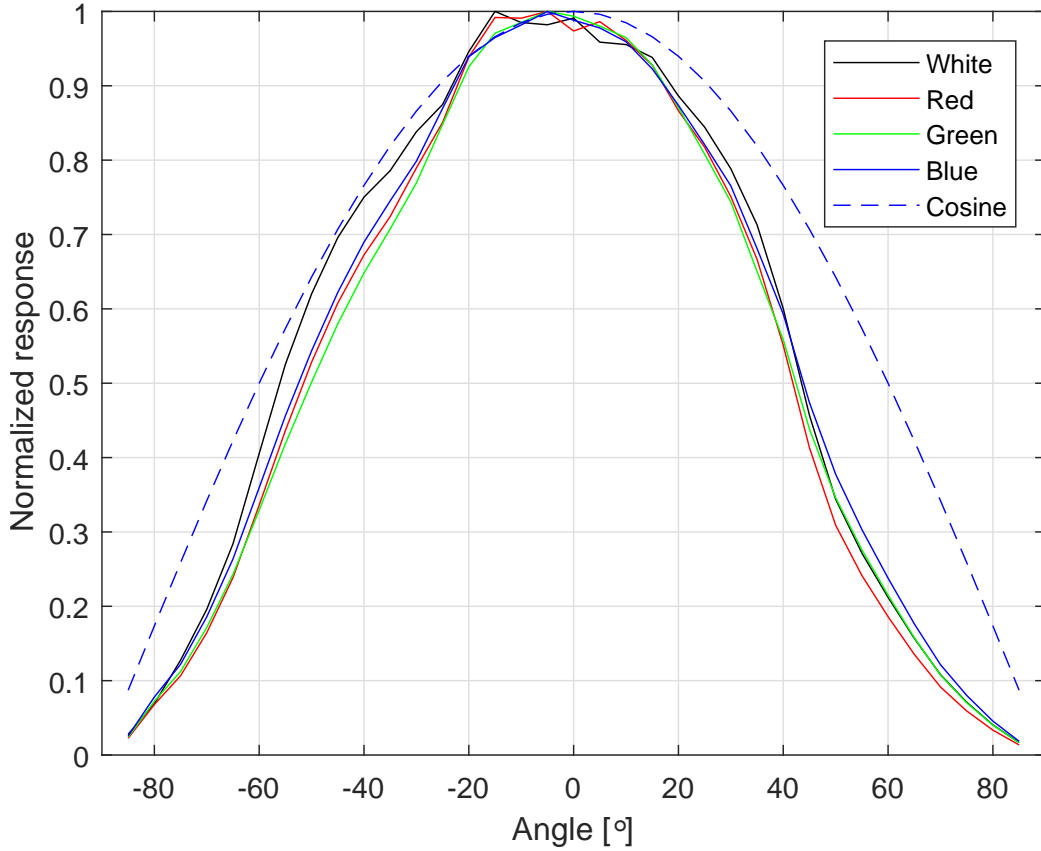
Figure 30: Cosine response for SunSense RGB, rotated along horizontal axis. Normalised to maximum. Cosine curve has its maximum at the same place as white diode (0°). Measurements are done with 5° step.

matters, the total relative error was calculated, as shown in Equation 18, and difference-error, as in Equation 19, were calculated. Results are presented in Table 7, as a percentage of what SunSense would measure compared with the ideal measurement.

Table 7: Errors in cosine response of SunSense. Row two shows ratios of deviance from ideal curve, Equation 18, row three shows difference in percentage, Equation 19.

	Red diode	Green diode	Blue diode	White diode
ϵ_{tot} [%]	-27.5	-28.1	-23.8	-21.7
f2* [%]	-26.6	-27.3	-23.2	-19.7

As Table 7 shows, SunSense underestimates the light under conditions
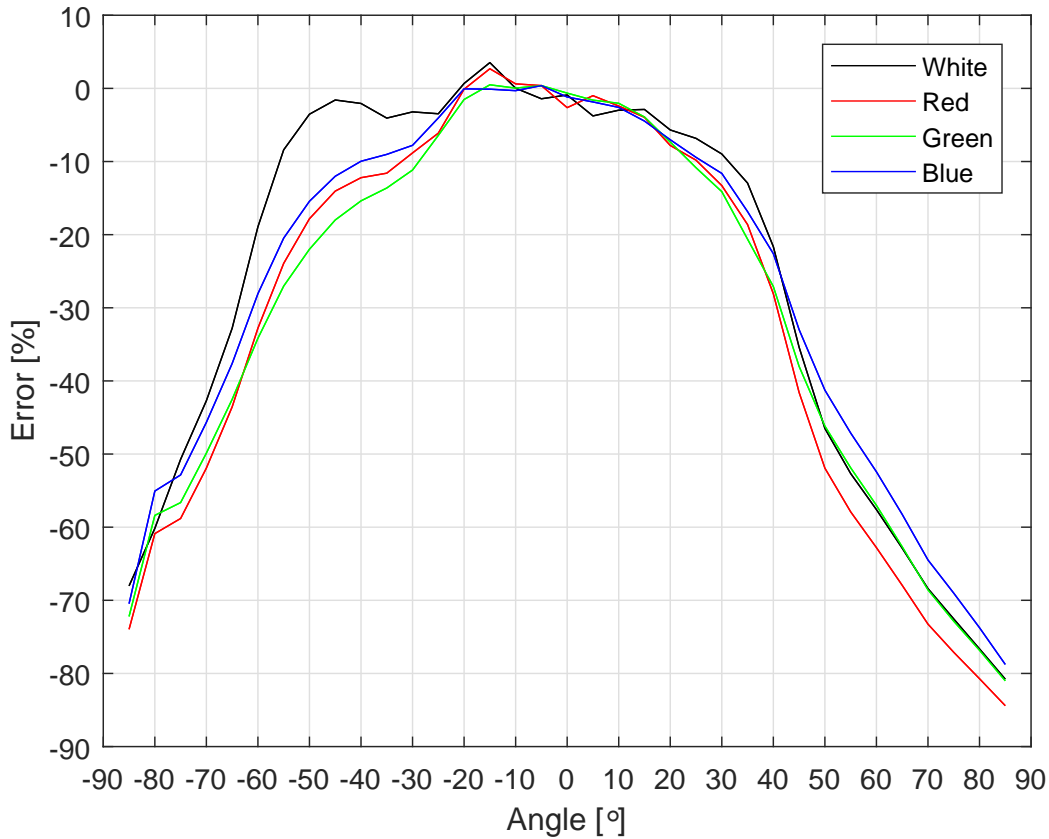
Figure 31: Measurements for cosine response relative to ideal measurement in percentage for horizontal rotation. Extrema at low angles are ignored.

of isotropic light. In practice, this suggests that the sensor must be placed strategically for increased accuracy. As the face is the part of the body most exposed for an EPP patient, it is natural to mount the SunSense facing somewhat forward. As can be seen in Figure 19, the average angle of blue light (400 nm) ranges from about 40° at a zenith angle of 0°, to 65° when the sun is closer to the horizon on clear weather days. The zenith angle, in Bergen, varies from 36.9° to 83.8°, and therefore limits the variation of average light to 52° and 66°, for light at 400 nm. The error of cosine response of SunSense is less than 10% for a larger interval of angle than what the average angle varies. This adds to the argument of placement of SunSense, and how it will be important in dosage measurement accuracy for EPP patients.

Comparing SunSense with the dosimeters by Lighting Research & Technology Centre - Daysimeters - as investigated by Figueiro et al. [2012], SunSense does not perform as well. Figueiro et al. finds an f2-value of 11.6%, 9.9% and 10.1% for the three channels of the Daysimeters, much lower when
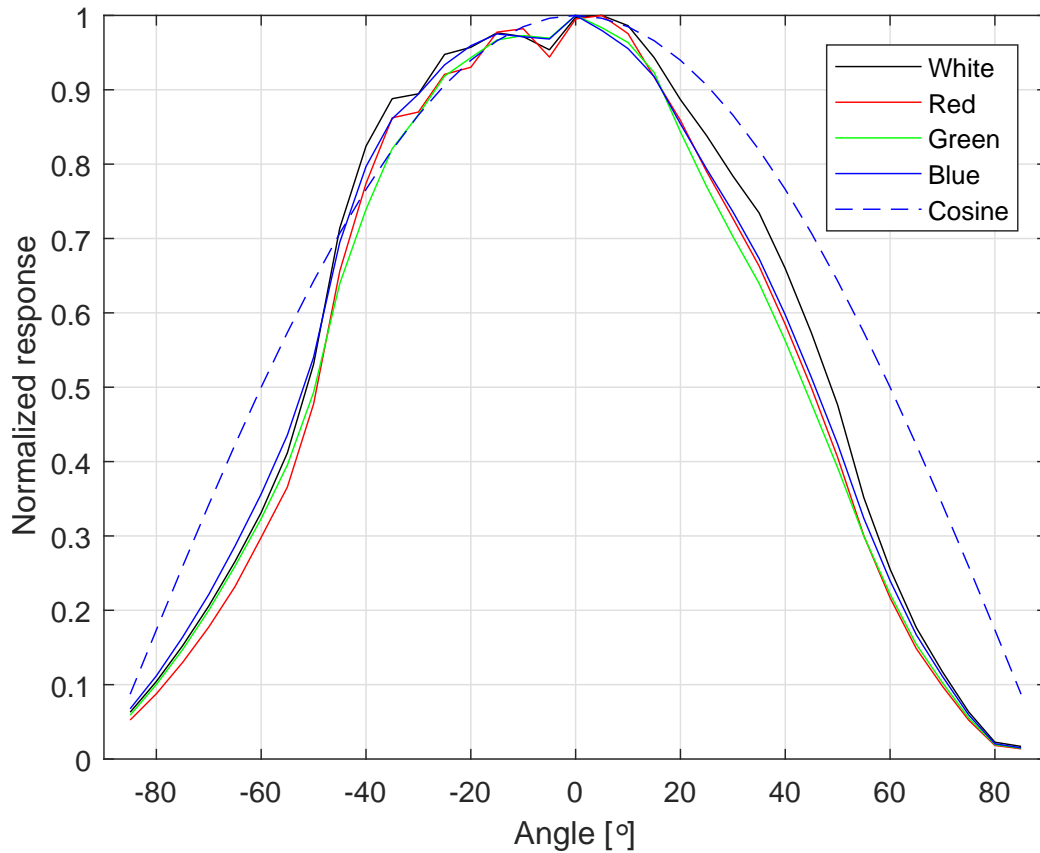
Figure 32: Cosine response for SunSense RGB, rotated along vertical axis. Normalised to maximum. Cosine curve has its maximum at the same place as white diode (0°). Measurements are done with 5° step.

compared to that of SunSense. The Daysimeters has an opal glass diffuser, which likely is the reason for the good results it shows.

5.6.2 Responsivity of sensor in SunSense RGB

Measurements were performed as described in Section 4.2.2 for the SunSense RGB. Intensity of the light source was regulated so that it was below saturation when set-up with the most transparent filter. Measurements were made on the red, green, blue and white diodes with each filter. The filters used are shown in Table 8.

The OD of the filters, shown in Table 8, is actually the OD at a specific wavelength; 546.1 nm. The photodiodes in SunSense does not measure at this specific wavelength, so new OD was interpreted from Figures 49, 50 and 51. OD was interpreted for manufacturer provided maximum wavelengths for
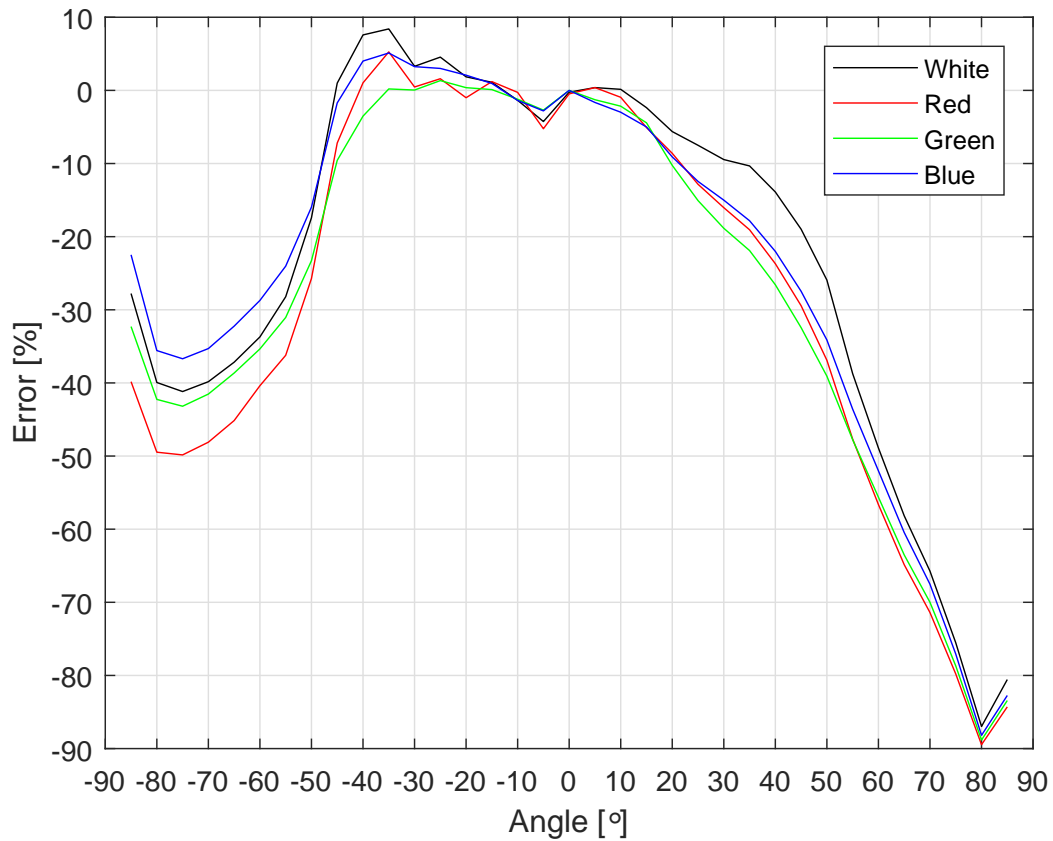
Figure 33: Measurements for cosine response relative to ideal measurement in percentage for vertical rotation. Extrema at low angles are ignored.

Table 8: Table of filters used for responsivity measurements, with optical depth OD, and transmittance in %. OD provided by manufacturer, and is the OD at 541.6 nm. Transmittance calculated by Equation 33.

Filter name	Optical depth	Transmittance [%]
FSQ-OD05	0.05	89.1
FSQ-OD20	0.2	63.1
FSQ-OD40	0.4	39.8
FSQ-OD60	0.6	25.1
FSQ-OD80	0.8	15.9
FSQ-OD100	1.0	10.0
FSQ-OD200	2.0	1.0
FSQ-OD300	3.0	0.1

each diode (450 nm, 550 nm and 650 nm). Note that these wavelengths are

Table 9: Table of interpreted OD for each diode and filter. Figures used can be seen in appendix, Figures 49, 50 and 51.

Filter name	OD red diode	OD green diode	OD blue diode
FSQ-OD05	0.040	0.041	0.043
FSQ-OD20	0.25	0.20	0.22
FSQ-OD40	0.45	0.40	0.43
FSQ-OD60	0.67	0.60	0.59
FSQ-OD80	0.89	0.81	0.78
FSQ-OD100	1.1	1.0	0.98
FSQ-OD200	2.1	2.0	2.0
FSQ-OD300	2.9	3.0	3.0

actually the centre of FWHM (Full Width at Half Maximum) of the curves. See Figure 10. Figure 34 shows the data measured plotted vs both filter OD, and interpreted OD for each diode.

Note that the white diode is not included in the linearity measurements. The grey filters used had only (approximately) constant OD in the visible spectrum, and the white diode extends into both UV and IR region (see Figure 10). An IR filter was used, but did not show the expected results, and measurements were therefore rejected. The varying results for the white diode was therefore expected to be caused by a) large variation in OD in the grey filters over response function range, and b) failure to sufficiently block IR light. Because sufficient filtering proved difficult in IR- and UV-region, the white diode was excluded. UV diode was also not tested, because the light source did not radiate enough light in UV-region to get measurements over the complete range for the diodes.

Linearity should be tested over the entire region of the photodiodes: from close to no output to close to saturation. To test the responsivity of the UV diode, a plank-like light source, with sufficiently hight temperature, or a UV lamp could be used.

Even though the OD changes in the wavelength interval of the photodiodes, the choice of maximum wavelength should help reducing the error. This is still a source of error, and actual responsivity might be better than the one that was found. Better measurements could be made with a laser for each diode, shining at Because sufficient filtering proved difficult in IR- and UV-region, the white diode, as well as UV diodes, were excluded: close to the peak of the response curve. When adjustments to filters are made, the interpreted OD would not vary as much, due to the narrow wavelength light emitted from the laser.

When finding linear fit, two assumptions were made with regards to regression: a) The fit is linear, and b) the line passes through origin. a is assumed because the photo-diodes usually behave linearly, until it gets close to saturation (see Section 2.6.2). All measurements were made with intensity values lower than $< 90\%$ of saturation. b is assumed because a transmittance of 0 should cause no read on the device. The only light source in the room was that of the beam, and the device was confirmed to read zero when sensor is covered (i.e. dark current is too small to give any readings). Results are presented in Table 10.

Table 10: Results from responsivity test on SunSense RGB. Column two provides the inclination for the function $y = ax$

Diode	Inclination	R^2	RMSRD [%]
Red	$59 \cdot 10^3$	0.97	12
Green	$61 \cdot 10^3$	0.98	10
Blue	$33 \cdot 10^3$	0.99	6.1

5.6.3 Error in measurements

Measurements on the SunSense were made by manually reading of values from the app. All readings are done when device and light source are stable. The device provided stable readings, and so errors in measurements are assumed to be in decimal point, and therefore much less than the values registered.

5.6.4 Evaluation of accuracy in SunSense RGB

In characterizing the SunSense, relative uncertainty related to cosine response and uncertainty related to responsivity have been calculated. The uncertainties are for each of the colour photodiodes. Uncertainty in cosine response was calculated for isotropic light conditions, see Table 7. Uncertainty in responsivity was calculated for the deviance of measurements to a linear function, see Table 10.

The total relative uncertainty of measurement output of SunSense is calculated by Equation 31.

Although Table 11 shows that the blue diode is the best for measuring a PL dose, the uncertainty is high (24.6%, Table 11). Underestimation of 25% could potentially cause overexposure for EPP patients. The main cause of the high uncertainty is due to the high uncertainty in the cosine response of
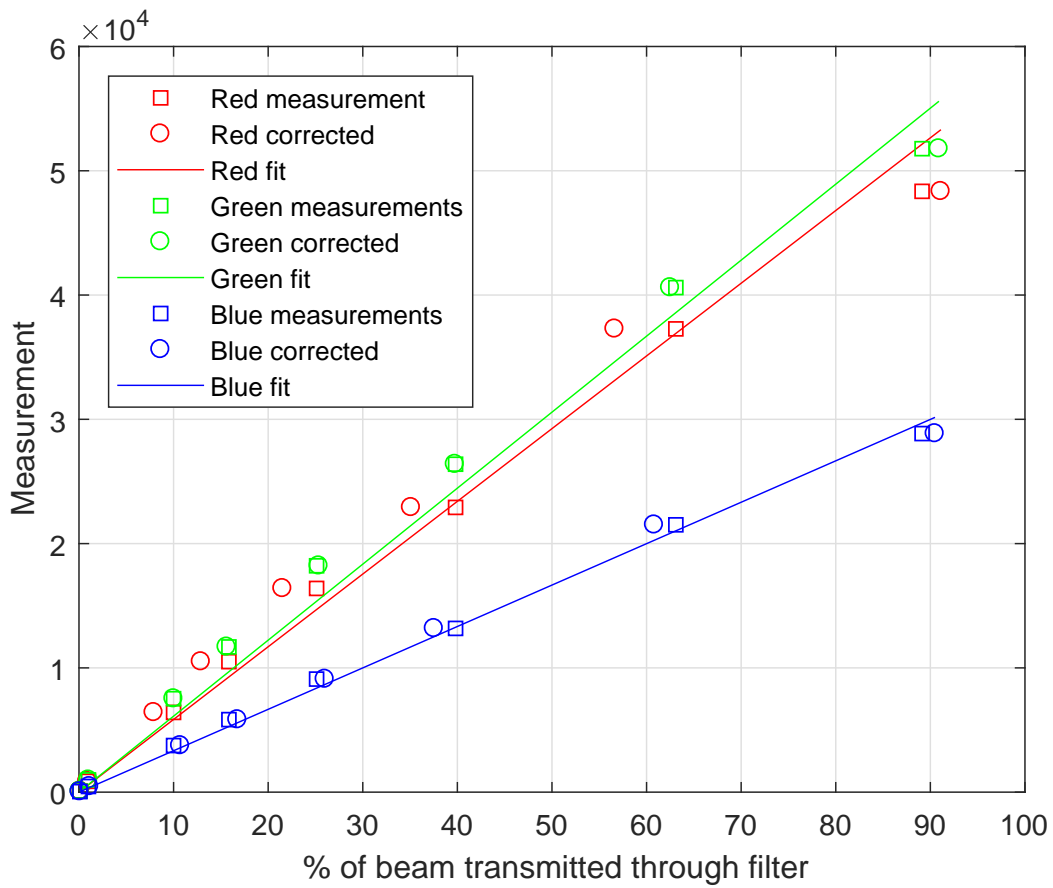
Figure 34: Measurements done on RGB diode of SunSense, with varying filters. Square points are plotted using states OD of filters, round points using OD at each diode for each filter. Fitted line is for corrected data.

Table 11: Table of total relative uncertainty for RGB diodes of SunSense. Calculated using data from Table 7 and 10.

Red [%]	Green [%]	Blue [%]
30.1	29.9	24.6

SunSense. It must therefore be stressed that placement of the SunSense will be important in measuring PL dose.

5.7 Using the Ramses instrument for UV index measurement

All calculations of UV indices are done with measurements from the Ramses E6 instrument, which was placed in Bergen. The instruments used by us and by the NRPA were placed only 300 m apart. There was, however, a large deviation in calculated UV index compared with the UV index measured by NRPA.
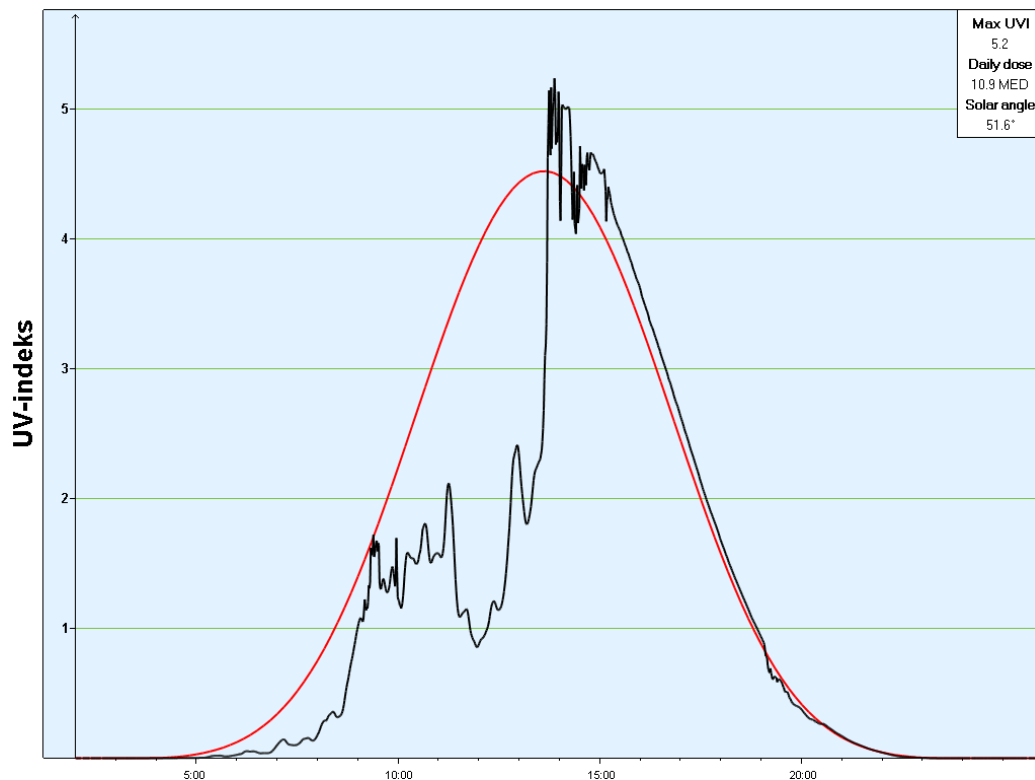
Figure 35: Figure shows NRPA's predicted UV index for clear sky (red curve), and NRPA's measured (black curve) UV index in Bergen, on 31.05.2016. Graph from NRPA [2016].

Figure 35 shows UV index (black) on the 31st of May, 2016, as measured by NRPA. The maximum UV index for that day was 5.2. Calculations on the same day, with data from Ramses E6, gave UV index of 10. This lead to the question of the validity of our calculated UV indices, and attempts were made to improve our measurements.

5.7.1 First attempt of correcting Ramses E6 data

The action spectra for the UV index gave highest sensitivity between 250 nm and 298 nm, and from there decreasing rapidly (see Equation 5). The solar spectrum is rapidly increasing from about 300 nm and out. The problem of our over estimated UV indices is partially caused by these steep curves. The Ramses E6 device measures irradiance at many wavelengths. However, it does have a certain bandwidth (6 nm.), so even though irradiance spectrum is measured for a wavelength λ_n, it actually measures irradiance for $\lambda_n \pm 3$ nm. The response spectrum for each channel is approximated to a normal distribution, a Gaussian function, centred at λ_n, and with a FWHM of 6 nm. This, combined with the steep inclination of the spectrum, makes the results larger than the actual value.

To accommodate for this, an approximation was made. This was done using the method of finding the mean of the wavelength, $\overline{\lambda}$, using some weighing function, $w(\lambda)$. According to the hypothesis that the error is larger when the inclination close to the response function of the channel is large, the registered spectrum values should be higher than the actual values. By using the solar irradiance spectrum itself, $F(\lambda)$, and assuming the channels of the instrument has a Gaussian response function, $G(\lambda_n)$, centred at λ_n and a FWHM of 6 nm:

$$G(\lambda_n) = A e^{-4ln(2)\frac{(\lambda-\lambda_n)^2}{FWHM^2}} \tag{35}$$

with A some normalizing coefficient. The expectation value was calculated using the product of the Gaussian function and solar spectrum as weighing function:

$$\overline{\lambda}(\lambda_n) = \frac{\int_0^\infty \lambda G(\lambda_n)F(\lambda)}{\int_0^\infty G(\lambda_n)F(\lambda)}d\lambda \tag{36}$$

with λ_n being the instrument channel wavelength, $\overline{\lambda}_n$ being the new wavelength for the measurement. This calculation makes the wavelengths in the steep region (> 300 nm) slightly larger, and thus reducing the UV index slightly.

Calculations after this corrections gave a UV index of 8. The deviance, from 5, was not acceptable.

5.7.2 Second attempt at correcting Ramses E6 data: Black body-calibration

When calibrating the Ramses devices, see Section 3.1.2, the lamp used has a spectrum close to that of a black body at equilibrium; absorbing all incoming

light, and emitting light through Planck radiation, described by Planck's law. The following assumptions were made:

1. The lamp shines as a perfect black body with constant temperature T.

2. The device measures accurately at sufficiently large wavelength; at relatively low irradiance gradient.

The first assumption is reasonable, because the calibration lamp was chosen because it shines close to a black body.

The second assumption is a result of a previous assumption made in Section 5.7.1: The inaccuracy of the Ramses E6 device is higher when the gradient of the spectrum is high. This means that for parts of the spectrum where the gradient is low, the instrument should measure somewhat accurate. Using this assumption, we use the measured spectrum of the lamp (in lab environment), and found the Planck curve that best fitted the measured spectrum at high wavelengths ($\lambda > 350$ nm). Then it was a matter of finding some constants of calibration that put the measured data on the Planck curve.

After the black body calibration, the correction from Section 5.7.1 was applied. The solar spectrum is much steeper than any Planck curve, and the Planck correction could not solve this problem, and UV indices were still higher compared with NRPA.

5.7.3 Third attempt at correcting Ramses E6 data: Comparing with NRPA

NRPAs radiometer for UV measurements was placed some 300 meters from our measurement site. By trusting the official measurements from NRPA, we could compare our measured UV index with theirs. A few UV index graphs were chosen from NRPA's website [NRPA, 2016], see Figure 37. When selecting what UV index graphs to compare, days of clear weather were chosen. From these days we could expect two things:

- Smooth graphs due to little or no clouds

- Relatively high maximum UV index

Data for clear days was chosen because NRPA's radiometer and ours were placed a short distance apart, clouds would interfere with the validity of the comparison; If a cloud cast a shadow on our instrument for a while, it would give a "false result" when compared.

The mean ratio between NRPAs maximum UV indices and the ones calculated from the E6 radiometer, was 0.85 (see Table 12). From examining

how the ratio varied over all our chosen days, a suitable time-dependent function was applied, that would modify our UV measurements closer to NRPAs. The function that suited our need best turned out to be a sinusoidal squared curve, with one period per two days, and matched with maximum ratio to top of curve. The maximum difference in ratio gave a phase shift in the cosines function of -1.775, corresponding to the minimum of cosine function coming at about 02.00 in the morning. The function best suited was $0.85 \cdot \cos^2(\pi x - 1.775)$, x being time measured in Matlab's convenient DateNum format ($\Delta x = 1$ corresponds to a change in time of 24 hours). The proposed cosine function is plotted as a dashed line, with all UV index ratios in Figure 36.

Table 12: Overview of days chosen for UV comparison, with some information on the days. *Zenith angle is from NRPA [NRPA, 2016]

Date	UVi$_{max}$ NRPA	UVi$_{max}$ E6	Ratio	Zenith angle* [°]
25.05.2016	4.5	5.3	0.85	39.4
26.05.2016	4.7	5.4	0.88	39.2
27.05.2016	4.7	5.4	0.87	39.0
16.08.2016	4.3	4.8	0.89	36.8
04.09.2016	2.9	3.8	0.76	53.3

As can be seen in Figure 36, the ratio is closest to 1 at ∼13.00, when the Sun is at it's highest position. This suggests that the deviance in measurement is closely related to the zenith angle. Irradiance measured by E6 is the component perpendicular to a horizontal surface. That means that the measurements are the cosine component of the irradiance. The deviance in measurement difference could be related to this. Reflection in the diffusing crystal in E6 radiometer could very well give origin to some deviance.

Note that at low UV values, at night, there are a lot of extrema in the ratio of NRPA's UV indices and ours. This is simply due to both of the measurements being close to zero, and small differences turn huge when divided. They have been ignored when analysing.

5.7.4 Validity of the corrections

When all corrections are done, our measured UV index was much closer to NRPA's than in the beginning. In the third assumption, corrections were made only with respect to clear days. On clear days, the intensity of light is higher than on cloudy/very cloudy days. By using the same time-dependent
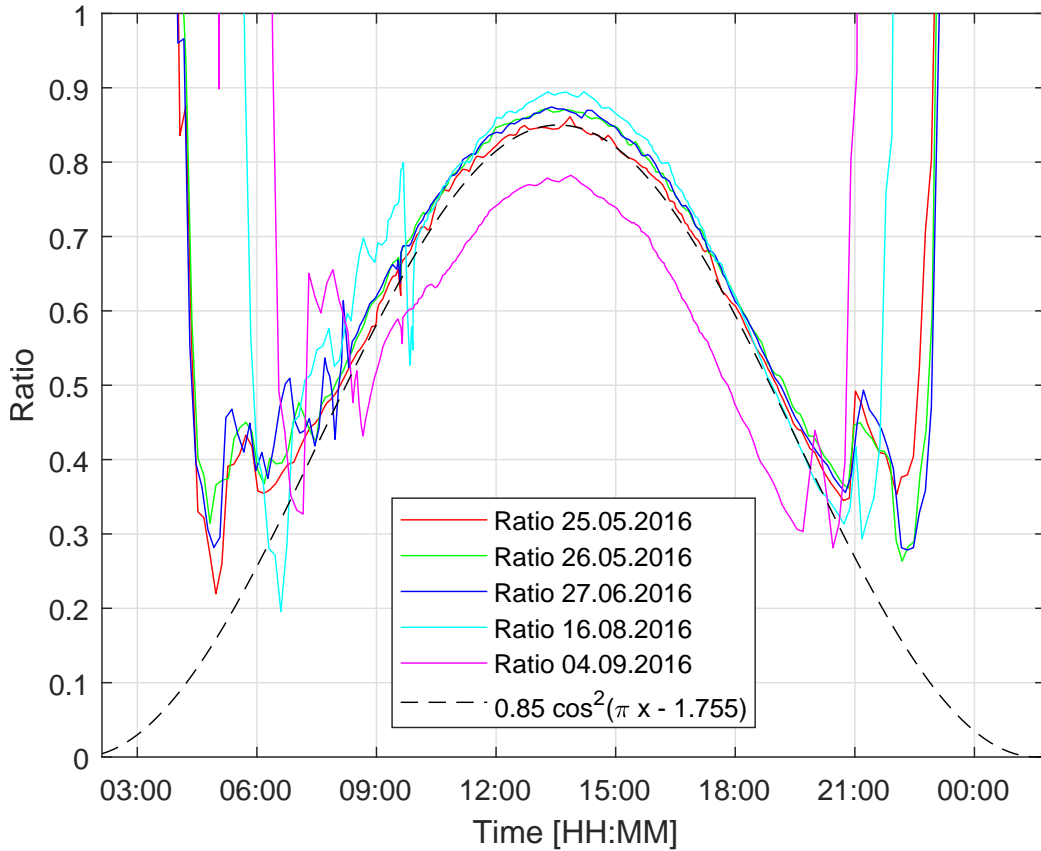
Figure 36: Ratio of NRPA's UV index and Ramses E6 measurements for all chosen days. Dashed line is the guessed correlation cosine function.

correction function on all days, the UV index from Ramses E6 ended up lower than that of NRPA. Some of the error could also originate from irregularities in clouds over Ramses E6 and NRPA's instrument.

The most important thing with regard to minimizing error in PL dose, is to minimize error at large PL indices. Large PL indices are probably found when the UV index is high. Because of this, the gain from our third correction, in high-UV index region, is probably higher than the issues it spawns at low UV indices.

5.8 Index comparison: Simulated and measured

To better determine if the devices this thesis tests are suitable for EPP patient, comparisons between the different values the devices measures/estimates were made. The indices are compared with each other. They are compared with simulated indices from the radiative transfer tool, AccuRT, to
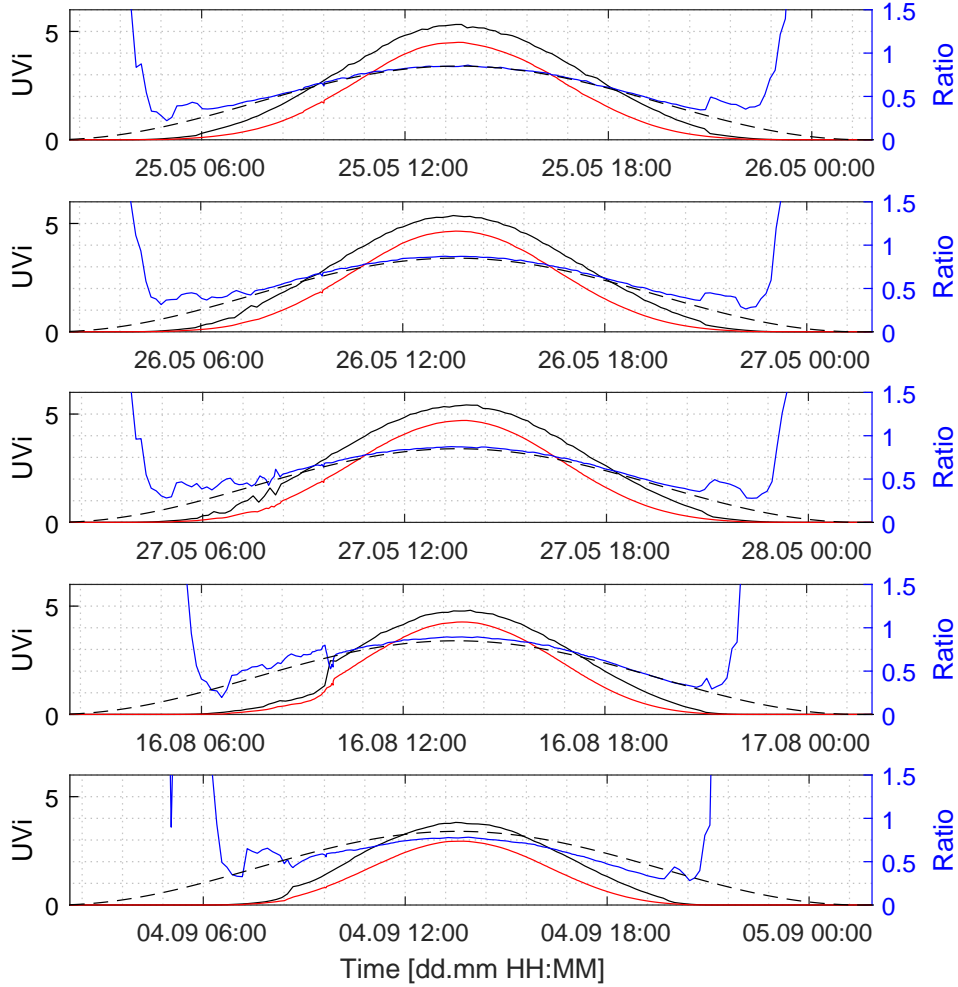
Figure 37: All chosen dates for comparison. Hard black line (Ramses E6's UVi) and red line (NRPA's UVi) on left y-axis, blue line (ratio of the two UVi's) and dashed black line (fitted $\cos^2$ function) on right y-axis. x-axis shows time in format [dd.mm HH:MM]. NRPA data from NRPA [2016].

strengthen any correlations or conclusions.

Data from AccuRT has a larger uncertainty at large zenith angle. AccuRT uses horizontal slabs to approximate the atmosphere, and does not take the curvature of the earth into account. For small zenith angles, this does not have any significance, but at large zenith angles the actual distance through the atmosphere will be shorter than the simulated.

72

5.8.1 Comparing (optimized) PL index and UV index

Note: The action functions for calculating PL index (Figure 5) and UVi (Figure 4) was plotted in Matlab.

After corrections were made, as described in Section 5.7.1, 5.7.2 and 5.7.3, measured data of UV indices and PL indices was plotted in Figures 38 and 39 to investigate any correlations.
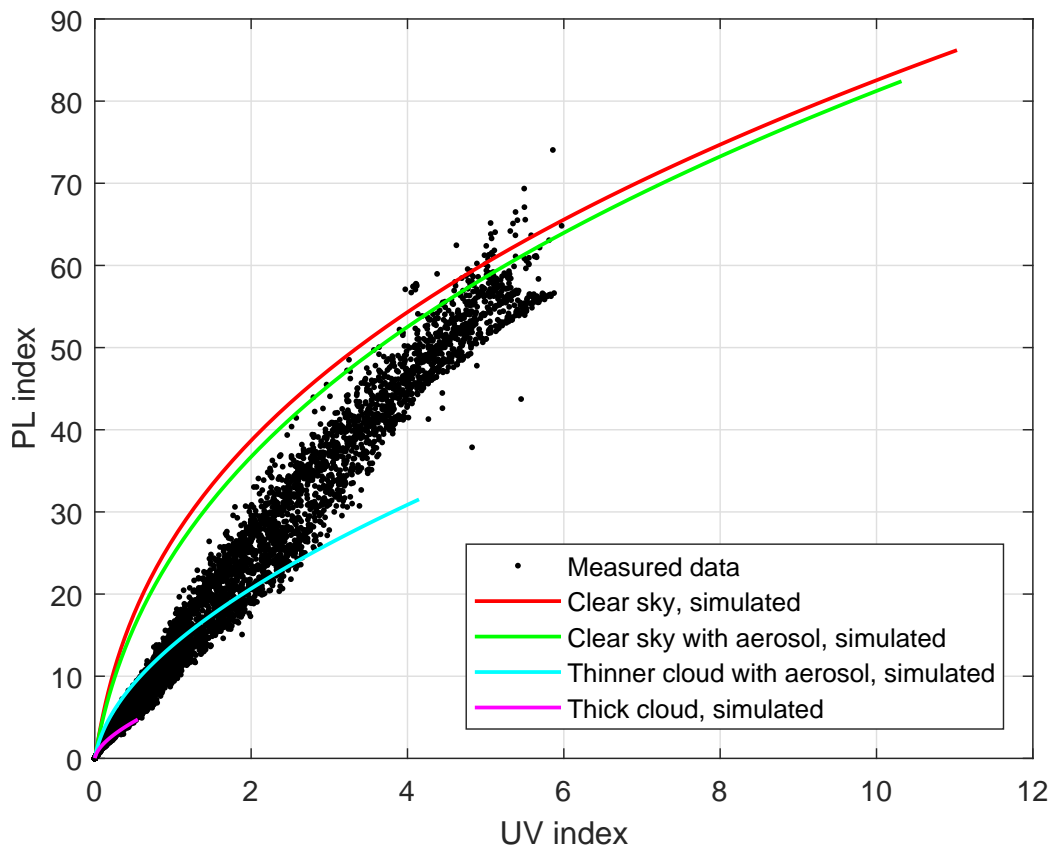
Figure 38: Plot of measured and simulated UV indices and PL indices.

The indices from E2 and E6 measurements are for low values somewhere between the indices calculated from simulated irradiance spectrum. From Figure 18 we can see that the average angle of incoming UV radiation is higher than for longer wavelengths. It is possible that the measured indices have higher (optimized) PL index compared to indices from simulations at the same UV value, due to our instrument not seeing the sky as a full hemisphere above itself. Our detector is placed in Bergen, "the city of seven Mountains", and mountains and building cover part of the horizon. This influences light with large average incoming angle, mostly diffuse; shorter wavelengths (in

73
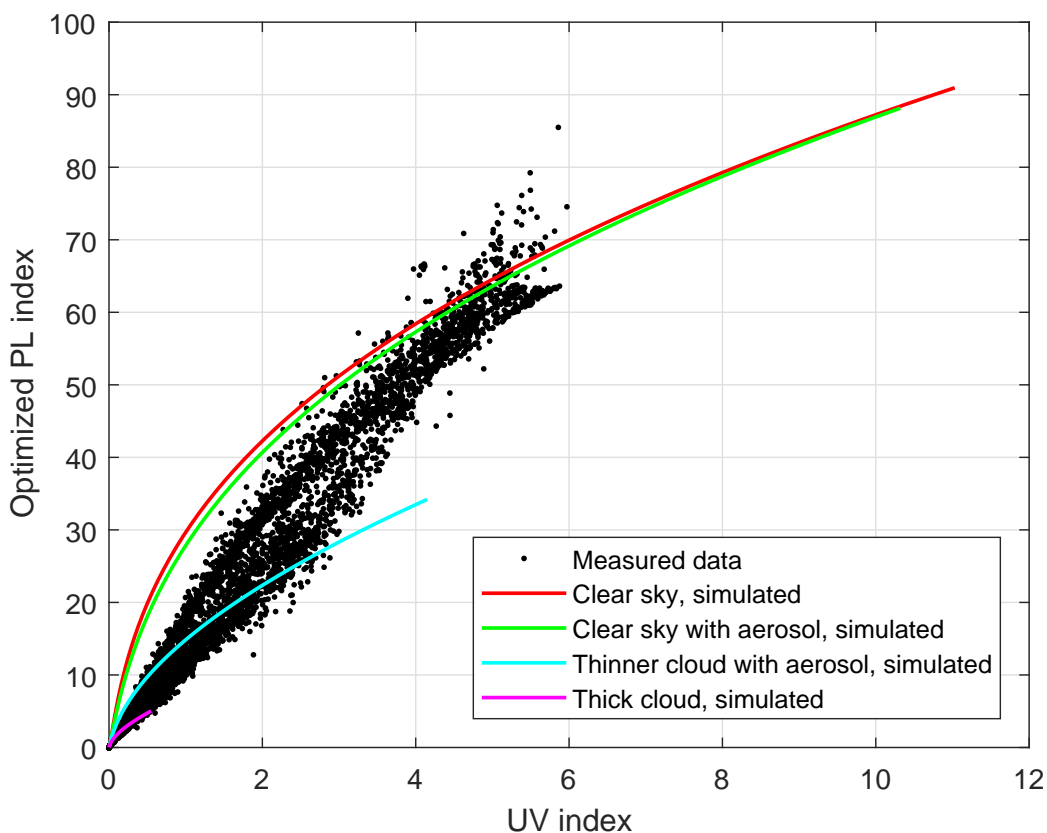
Figure 39: Plot of measured and simulated UV indices and omptimized PL indices.

the visible spectrum). So even though the measurements does not match the simulations perfectly, the difference has been explained, and data can be trusted.

Simulations shows that the correlation between (optimized) PL index and UV index also depends on weather conditions. The same trend can be seen as a spread in measured data in the same figure (Figures 38 and 39). A single model would then be wrong for some weather conditions. A model for each weather condition would be plausible, but since the correlation depends too much on how much of the sky close to the horizon is visible, it would be impractical; bearing to wrong. A finale method could be a "worst case scenario" model; make a model for highest possible (optimized) PL index for the lowest UV index. The usefulness of the model would be strictly limited to either predicting the worst that could happen, or overestimating DPLD. Either way, it would probably not benefit EPP patients significantly.

There is a lesson to be learned here, with regards to trying to make a

model for the correlation between UV index and (optimized) PL index. The correlation will depend on the field of view of the detector, not to mention the exposed areas of the EPP patient. The correlation will not be the same in Bergen as in an open field; and not the same on top of a building in Bergen as in the streets below.

5.8.2 Comparing PL index and illuminance

Calculated PL indices and illuminance from Ramses data was plotted together with simulated indices in Figure 40. As can be seen, there appear to be a positive, linear correlation between illuminance and PL index. The Spearman test, Equation 22, gave

$$\rho_s = 0.9969,$$

indicating a strong positive correlation between the measured illuminance and PL index. To investigate the correlation, the method of least squares was used to find the line best fit with data points. The correlation is shown in Table 13.

Table 13: Model for PLi and illuminance

Equation	R^2	RMSD	RMSRD [%]
$PLi = 0.0006 \cdot Lux + 0.4$	0.9953	1.14	9.7

Figure 40 shows PL index and illuminance calculated using both measured irradiance data (black dots) and simulated (hard lines) irradiance from AccuRT. The simulations are made with different weather conditions. For low indices the measured data fits better with simulated than for higher indices. At high illuminance values, the measured PL index is somewhat lower than the simulated. The simulated data giving highest illuminance values are for low zenith angles, close to 0°. These zenith angles are not found in Norway. The zenith angle goes to about $\sim 53°$ for Bergen, on 21.06.2016 [NRPA, 2016]. That means that the irradiance values will not occur in Bergen. The highest illuminance values probably comes from a sky covered with a thin cloud layer, but with exposed Sun. The thin layer of clouds acts as a redirector for sunlight, scattering it at all angles. That way, there is more incoming light at the detector; so irradiance is higher. Such light would be shifted toward red, from blue. The illuminance is more sensitive in the red/green part of the visible spectrum than the PL index, and would thus be relatively higher than the PL index.
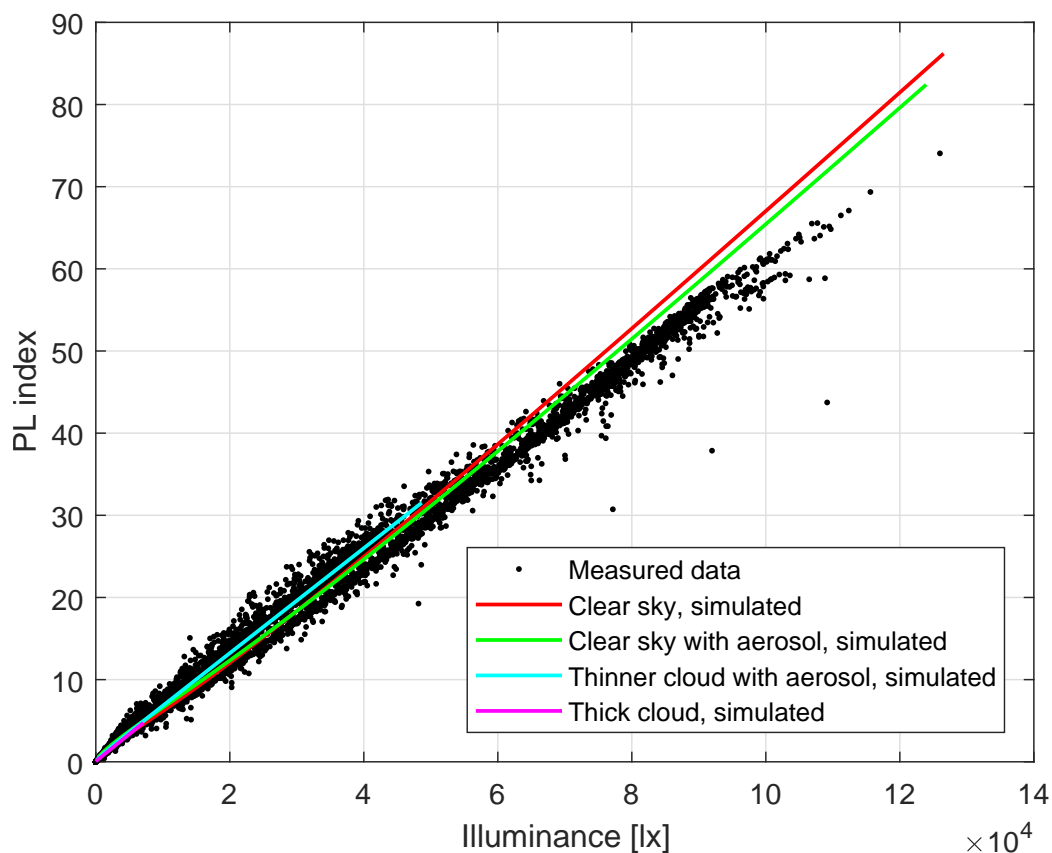
Figure 40: Porphyria light index v.s. illuminance. Plotted are both simulated (with different weather conditions), and measured data. Note: Thick cloud, simulated data is barely visible close to origin.

5.8.3 Comparing optimized PL index and illuminance

Calculated optimized PL indices and illuminace from Ramses data was plotted together with simulated indices in Figure 41. The data points seem to be linear, much closer to the theoretical lines than the PL indices plotted in Figure 40. The Spearman correlation test, Equation 22, gave

$$\rho_s = 0.9929,$$

suggesting a strong, positive correlation between the measured illuminance and the optimized PL index. The method of least square was used, assuming linear correlation, and the line in Table 14 was found. The line for optimized PL index v.s. illuminance is a better fit than that for PL index v.s. illuminance. This is probably caused by the action spectrum of optimized PL is shifted more to higher wavelengths; thus having more in common with the

76

luminosity function.

Table 14: Model for optimized PLi and illuminance

Equation	R^2	RMSD	RMSRD [%]
$optPLi = 0.0007 \cdot Lux + 0.2$	0.9992	0.53	4.6
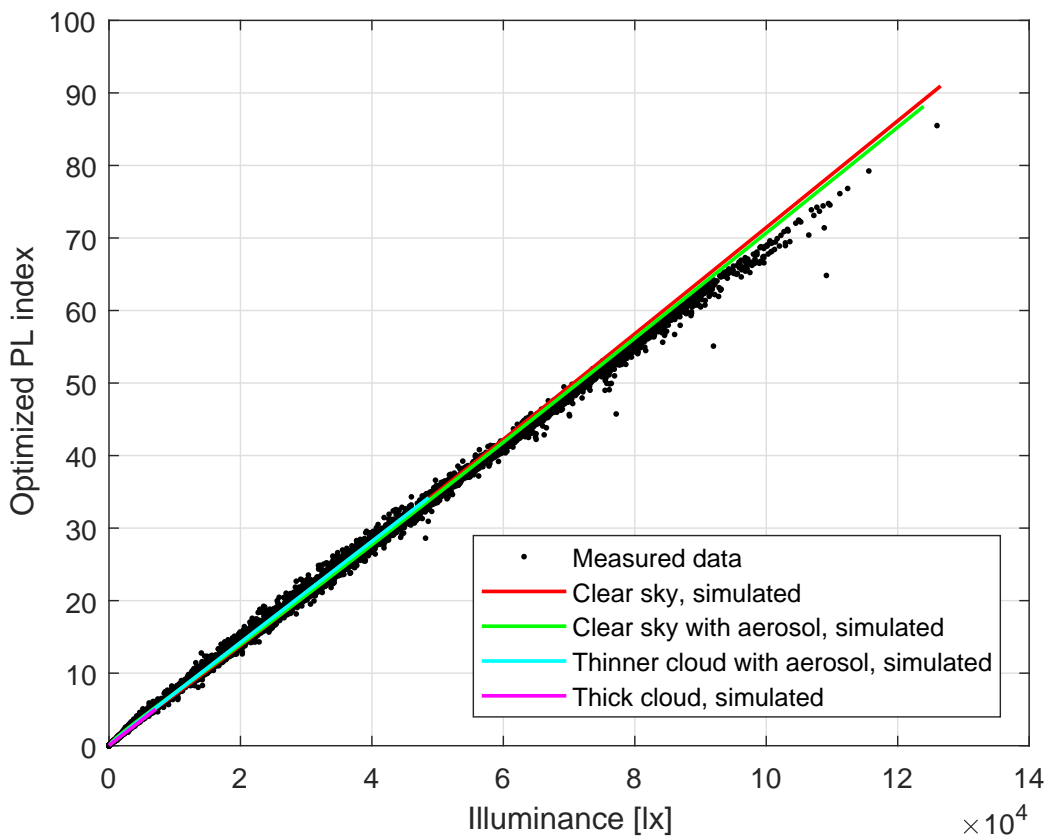
Figure 41: Optimized porphyria light index v.s. illuminance. Plotted are both simulated (with different weather conditions), and measured data. Note: Thick cloud, simulated data is barely visible close to origin.

Another cause for optimized PL index fitting better with simulated than the regular PL index, has its source in the same argument made for why measured data for PL index and illuminance are shifted compared with simulated data (see Section 5.8.2): A thin layer of clouds, not covering the Sun, could redirect more sunlight towards the sensor than just a blue sky, especially for

longer wavelengths (red/green). As can be seen in Figure 5, the optimized PL index action spectrum is relatively much more sensitive to light at longer wavelengths, when compared with the PL index action spectrum. The optimized PL spectrum therefore resembles the luminosity efficiency function more than the PL spectrum. Therefore, the optimized PL index would also get the benefit of the thin layer of clouds, just like the illuminance, making it hug the simulated data better.

5.9   Porphyria light dosage calculation

Inspired by the DUVD (Equation 6), the daily porphyria light dosage, DPLD, is calculated in similar terms. Daily dose was calculated for all available in the data set from the Ramses devices, and compared with maximum UV index for that day. The data is presented in Figures 42 and 43. The Spearman rank was calculated for the data sets, presented in Table 15. It indicates a somewhat weak, positive correlation.

Table 15: Calculated Spearman rank for the correlation of maximum UV index and (optimized) DPLD.

DPLD and max UVi	optDPLD and max UVi
0.885	0.889

To further investigate any correlation, a linear fit using the method of least squares (Equation 26) was found for both cases. The model found had a large deviation (see TAble 16), and are therefore not suited to make accurate estimations for daily doses for EPP patients. All data related to the fit is presented in Table 16. The cause for the large RMSRD for the fit between optimized DPLD and maximum UV index are caused by the large deviations at low maximum UV indices.

A "worst case" scenario forecast could be to use the fitted line plus RMSD. As Figures 42 and 43, these lines are better for estimating the maximum DPLD. However, since the goal is to accurately estimate DPLD, it is still not advisable.

Because of this, NRPA's UV forecast should not be used for estimating dose based on the maximum UV index of the day.

Another comparison was made; comparing (optimized) DPLD with the average UV index between 13:00 and 15:00. The time interval was chosen because UV index forecasts are available as an average of UV indices around 14:00. See for instance `https://www.yr.no/uv-varsel/?spr=eng`.
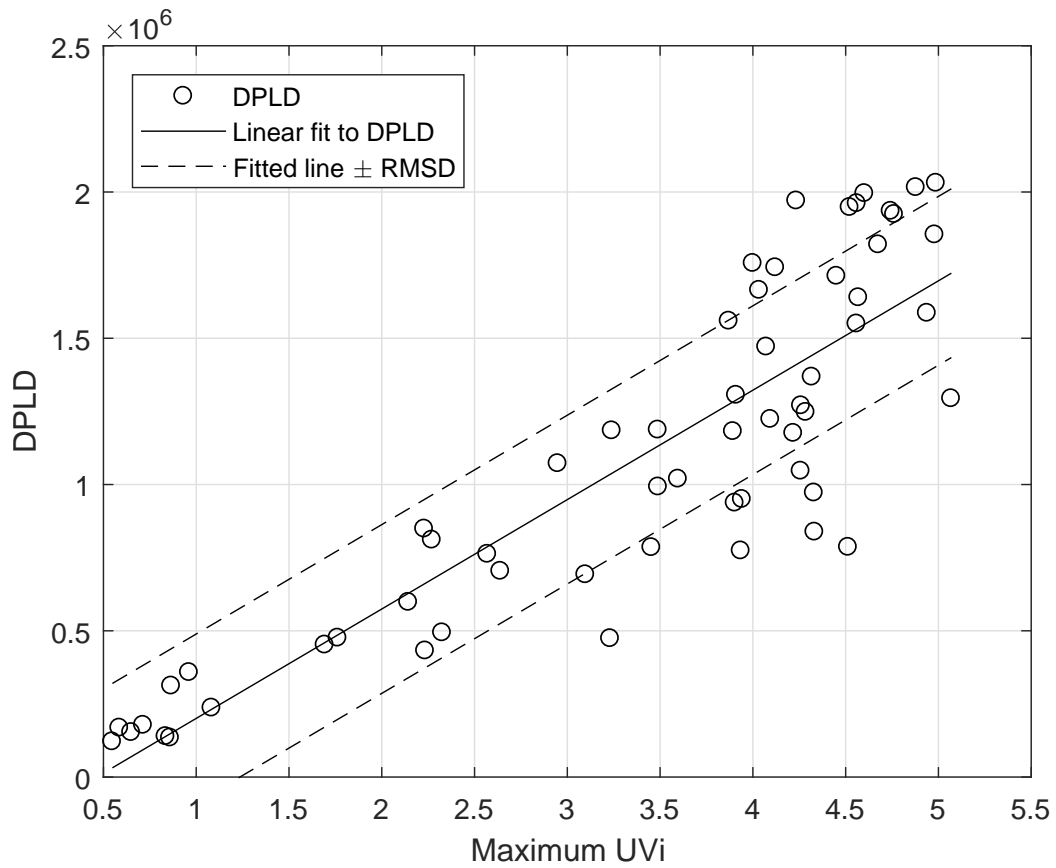
Figure 42: Plot of maximum UV index (x-axis) and daily PL dose (y-axes). Also shown is a linear fitted line (hard), with $\pm$ RMSD (dashed). Number of days: 60.

Table 16: Data for fitted lines for (optimized) DPLD and maximum UV index. Row 2 and 3 are inclination and constant term in $y = ax + b$.

	DPLD and max UV	**optDPLD and max UV**
a	$3.74 \cdot 10^5$	$4.25 \cdot 10^5$
b	$-1.73 \cdot 10^5$	$-2.23 \cdot 10^5$
r^2	0.76	0.75
RMSD	$2.88 \cdot 10^5$	$3.35 \cdot 10^5$
RMSRD [%]	60.7	165

Calculations were made, showing a better correlation between (optimized) DPLD and average UV index than with maximum UV index. The Spearman rank for these correlations are presented in Table 17.

Figures 44 and 45 show the data plotted, along with fitted lines and
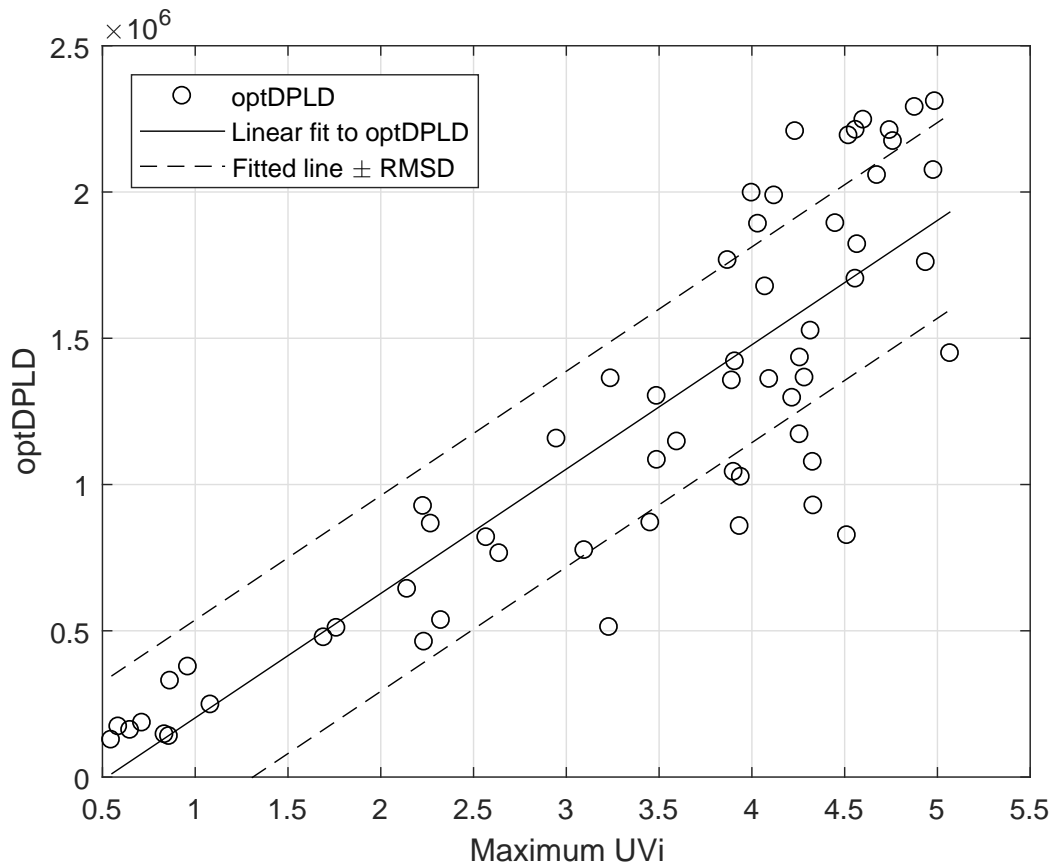
Figure 43: Plot of maximum UV index (x-axis) and daily optimized PL dose (y-axis). Also shown is a linear fitted line (hard), with ± RMSD (dashed). Number of days: 60.

Table 17: Calculated Spearman rank for the correlation of mean UV index and (optimized) DPLD.

DPLD and mean UVi	optDPLD and mean UVi
0.956	0.959

different error lines. Data for fitted lines are presented in Table 18. Error bars in the figures are the calculated standard deviations from the data sets used to calculate average UV index. The hard lines are the best fitted linear function, using the method of least squares. The dashed straight lines are the fitted lines ± RMSD. The dotted lines are the fitted lines multiplied by either (1+RMSRD) or (1-RMSRD). When calculating, RMSRD is converted from percentage to decimal. All data is shown in Table 18. As can be seen from the figures (Figure 44 and 45)

Table 18: Data for fitted lines for (optimized) DPLD and mean UV index between 13:00 and 15:00. Row 2 and 3 are inclination and constant term in $y = ax + b$.

	DPLD and mean UV	optDPLD and mean UV
a	$3.35 \cdot 10^5$	$4.47 \cdot 10^5$
b	$0.751 \cdot 10^5$	$0.716 \cdot 10^5$
r^2	0.91	0.91
RMSD	$1.81 \cdot 10^5$	$2.03 \cdot 10^5$
RMSRD [%]	27.4	27.9
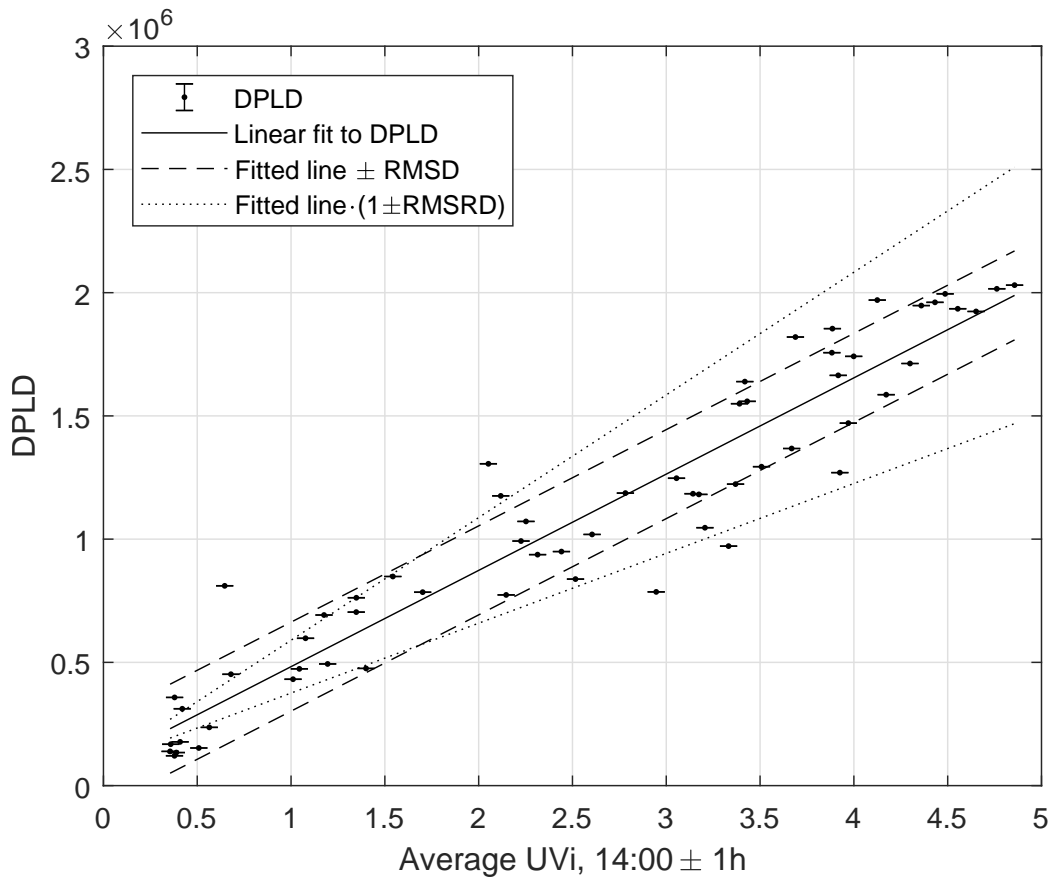
Figure 44: Plot of average UV index between 13:00 and 15:00 (x-axis) and daily PL dose (y-axis). Horizontal error bars are standard deviation in the average UV index. Also shown is a linear fitted line (hard), fitted lines with $\pm$ RMSD (dashed), and fitted lines adjusted with RMSRD (dotted). Number of days: 60.
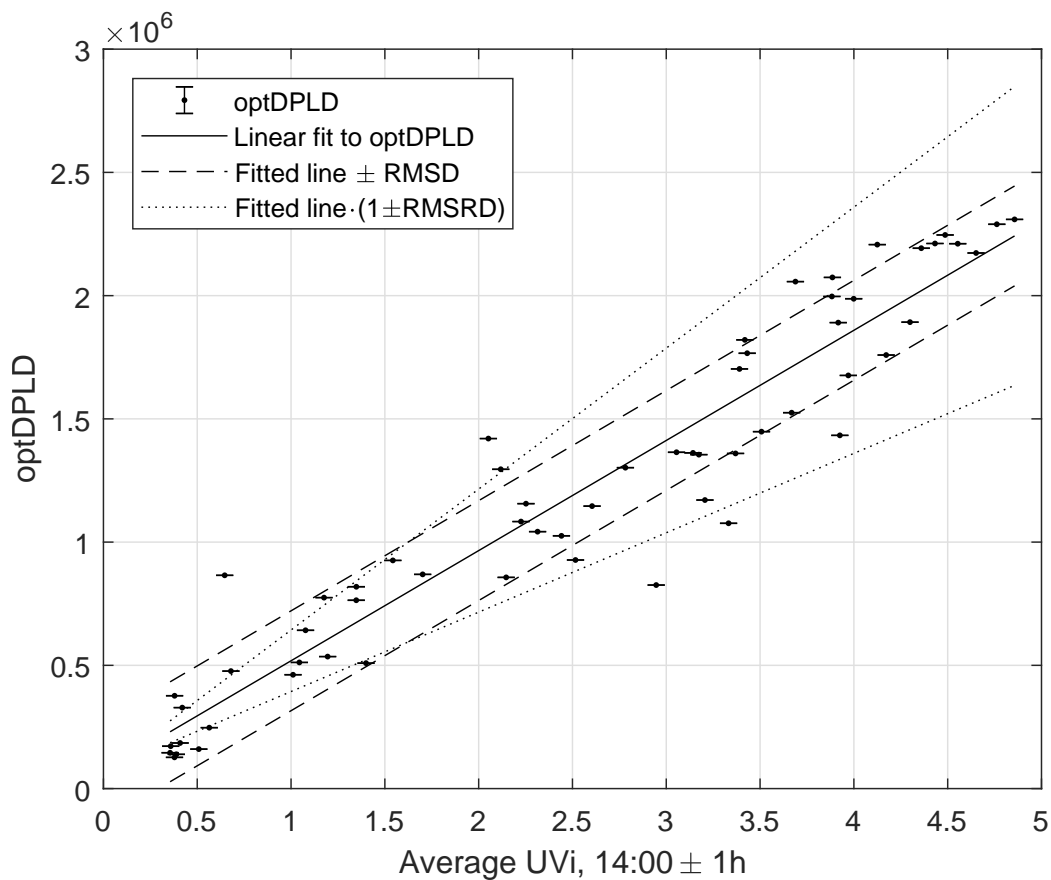
Figure 45: Plot of average UV index between 13:00 and 15:00 (x-axis) and daily optimized PL dose (y-axis). Horizontal error bars are standard deviation in the average UV index. Also shown is a linear fitted line (hard), fitted lines with ± RMSD (dashed), and fitted lines adjusted with RMSRD (dotted). Number of days: 60.

Because the correlation is better between the (optimized) DPLD and mean UV index than with maximum UV index, it is a better choice for forecasts for EPP patients. Because there is a certain correlation, days can be planned from UV index forecast, as long as it is understood that the errors are big. Worst case scenarios can be used, by choosing either the fited function + RMSD, or the fited lines multiplied by the factor (1+RMSRD), with RMSRD in percentage. The latter have the benefit of estimating above all data point except two, as can be seen in Figures 44 and 45.

6 Conclusion

6.1 Regarding SunSprite

The SunSprite does not provide a useful way of estimating dose, as measurements are only presented in an inaccurate graph (Figure 14).

SunSprite is therefore **not advisable** for dose measurement for EPP patients.

6.2 Regarding Phillips ActiWatch Spectrum Plus

The ActiWatch Spectrum Plus provides full insight into measurements, but is proven inaccurate compared with Ramses E2 (Figure 16). The cosine response of ActiWatch was close to zero for a wide part of the spectrum (Figures 23 and 26). It also shows spiky measurements around angles where cosine response drops (Figure 24), and was unstable when measuring responsivity under laboratory conditions (see Section 5.3.2).

ActiWatch perform well on responsivity (Table 4).

Phillips ActiWatch Spectrum Plus is not an improvement of the earlier model, Spectrum, when compared with the findings of Price et al. [2012] and Figueiro et al. [2012].

Phillips ActiWatch Spectrum Plus is **not advisable** for dose measurement for EPP patients, as the device is "blind" on angles that should receive light to accurately estimate PLi and DPLD.

6.3 Regarding SunSense RGB

SunSense RGB has a better cosine response (Figure 30 and 32) compared with the ActiWatch. The relative error is small for angles around the maximum, and increases with increasing angle (Figure 31 and 33). Under isotropic light from all angles, the SunSense measures 22% to 28% less than an ideal reference device. This depends upon the diode used (Table 7). The blue diode is the most useful diode for (optimized) PL index measurement (Table 6), and also shows the smallest error under isotropic light conditions. Because the error in cosine response largely depends on angle of incoming light - the orientation of the SunSense - it will be most useful if well placed and oriented.

When compared with the Daysimeter [Figueiro et al., 2012], produced by Light & Research Technology Center, SunSense shows it has room for improvements. The large difference in f2* cosine response error is likely due to choice of diffuser.

The app used with SunSense RGB will be able to provide accumulated DPLD based on its measurement, making it practical and easy for EPP patients.

SunSense RGB will be most **useful** for EPP patients when correctly oriented and well placed.

6.4 DPLD forecast

A significant correlation between maximum UV index and (optimized) DPLD was **not found** (Table 16), and the maximum UV index therefore serves little use for EPP patients.

A correlation was found between average UV index between 13:00 and 15:00 and (optimized) DPLD was found, suggesting that some UV index forecasts **could be used**, but should be used very careful, as the deviations are high (see Table 18). UV index forecasts could be used to plan ahead, but a good dosimeter is advised to avoid overexposures.

6.5 UVi measurement with Ramses E6

It was noticed that calculation of UV index from Ramses E6 data gave large deviation from measured UV index a few hundred meters from our station. Corrections were made, to get close to NRPA's measurements, using three methods (Section 5.7); Compensation for wide bandwidth, correcting for drifting measurements at low wavelengths (UV region) and lastly finding a simple time-dependent model to adjust the indices closer to NRPA's.

UV indices calculated with Ramses E6 should be **compared and** (if necessary) **corrected**, and should not be blindly trusted.

6.6 Estimating PL index

Even though there is some correlation between UV index and the PL indices, this does not agree with results from simulations (Figure 38 and 39). It is **not advisable** to estimate PL index from UV index, especially not for DPLD.

According to the models found, and presented in Table 13 and 14, there appear to be a **strong correlation** between the light perceived by the eye (luminosity) and the PL indices. EPP patients can use accurate lux-meters, like SunSense, to get an instant reading of the illuminance, and take precautions immediately. This can be done either by just evaluation the lux value, or doing a simple calculation to find the suitable PL index. From the PL index it should be easier to take suitable precaution.

7 Further work

7.1 Further classification of SunSense RGB

Because the tests in this thesis were carried out on a prototype of the SenSense RGB, and it may be changed on release, a new study of cosine response and responsivity should be carried out. The response functions of the diodes should also validated. A final comparison test between a professional radiometer and SunSense RGB could also be carried out, to confirm the correlations found.

Linearity for UV photodiodes were not carried out in this thesis, because the light source used did not radiate much light in the UV-region. To find the linearity if the UV photodiodes, use a Planck-like light source (with sufficiently high temperature), or a UV lamp. To check the linearity over the full range of the diode, the maximum radiance should be just below saturation of the photodiodes.

Linearity measurements for the white diode were excluded in the results of this thesis, because sufficient filtering in IR and UV region was not achieved. Better/more filters, covering a larger range could be used to find the linearity of the white diode.

7.2 Measurement of UV index using Ramses E6

The instrument should probably be thoroughly investigated, as the UV indices calculated from normaly calibrated spectrum are much higher, at some cases almost twice, than the actual UV index. The methods explained in this thesis (Section 5.7) helped for clear weather days, but

7.3 Impact of ActiWatch cosine response on previous studies

Phillips ActiWatch Spectrum Plus is used in many studies today. However, ActiWatch does not measure the irradiance it is supposed to, results of studies may be on false foundation. The impact of ActiWatch's cosine response should be investigated.

Abbreviations

APLD: Accumulated Porphyria Light Dose. Measurement of how much porphyria light the patient have been exposed to.

CIE: International Commission on Illumination.

DPLD: Daily Porphyria Light Dose. Relative measurement of energy accumulated by protoporhyrin IX.

DUVD: Daily UV Dose. Measurment of accumulated UV light, weighted by a erythremal function, in a day.

EPP: Erythropoietic Protoporhyria.

FECH: Ferrochelatase. Enzyme responsible for PPIX-haem reaction.

FWHM: Full width at half maximum. Used in statistics, and is the full width (Δx) of the Gaussian function at half its maximum($\frac{1}{2}y_{max}$).

Lux: Here: used as abbreviation for illuminance. From the unit of illuminance, lux [lx]

MED: Minimal erythema dose. Unit of UV dose.

NaN: Not a number. A value (usually measurement) that is not valid, i.e. not 0 or any other value.

NRPA: Norwegian Radiation Protection Agency (Statens Strålingsvern). Responsible for measurement public advice regarding radiation in Norway.

OD: Optical Density. In this thesis: labels on filters used for responsity measurements.

OptPLi: Optimized Porphyria light index. See Section 2.1.3

PLi: Porphyria light index. See Section 2.1.3.

PPIX: Protoporhyrin IX, last intermediate molecule before haem in haem synthesis. See Section 1.3.

RGB: Red, green and blue.

RGBW: Red, green, blue and white.

RMS: Root-mean-square. A method for statistic purposes; its the root of the mean of the squares of data.

RMSD: Root-mean-square deviation. Used for statistic purposes, it is explained in Section 2.8.1, and defined by Equation 29

RMSRD: Root-mean-square of relative deviation. See Equation 30.

RTE: Radiative transfer equation. Describes the loss and gain of intensity of light travelling through a medium.

UVi: UV index, Ultra Violet index.

References

Aijoka, R. S., J. D. Phillips, and J. P. Kusjner. Biosynthesis of heme in mammals. *BIochimica et Biophysica Acta*, pages 723–736, 2016.

Akacem, L. D., K. P. W. Jr., and M. K. LeBourgeois. Bedtime and evening light exposure influence circadian timing in preschool-age children: A field study. *Neurobiology of Sleep and Circadian Rhythms*, 1(2): 27 – 31, 2016. ISSN 2451-9944. doi: https://doi.org/10.1016/j.nbscr.2016. 11.002. URL `http://www.sciencedirect.com/science/article/pii/ S2451994416300128`.

Besur, S., W. Hou, P. Schmeltzer, and H. L. Bonkovsky. Clinically important features of porphyrin and heme metabolism and the porphyrias. *Metabolites*, 4:977–1006, 2014. doi: 10.3390/metabo4040977.

BIPD, Bureau International des Poids et Mesures, 2017. Resolution 3 of the 16th CGPM (1979), 2017. URL `http://www.bipm.org/en/CGPM/db/16/ 3/`. Accessed: 19.05.2017.

Bonkowsky, H., J. Bloomer, P. Ebert, and M. Mahoney. Heme synthetase deficiency in human protoporphyria. demonstration of the defect in liver and cultured skin fibroblasts. *Journal of Clinical Ivestigations*, 56(5), 1975. doi: 10.1172/JCI108189.

Brainard, G. C., J. P. Hanifin, J. M. Greeson, B. Byrne, G. Glickman, E. Gerner, and M. D. Rollag. Action spectrum for melatonin regulation in humans: Evidence for a novel circadian photoreceptor. *Journal of Neuroscience*, 21(16), 2001. ISSN 0270-6474.

Brun, A. and S. Sandberg. Mechanisms of photosensitivity in porphyric patients with special emphasis on erythropoietic protoporphyria. *Journal of Photobiology B: Biology*, (10):285–302, 1991.

CGPM. Defintion of candela. Technical report, Bureau International Des Poids Et Mesures, 1979. URL `http://www.bipm.org/utils/common/ pdf/CGPM/CGPM16.pdf#page=100`.

CIE 069-1987. Methods of characterizing illuminance meters and luminance meters: Performance, characteristics and specifications. Technical report, Commission Internationale de L'Eclairage, 1987.

CIE 1924. Commission Internationale de l'Eclairage Proceedings, 1924. Technical report, Commission Internationale de L'Eclairage, 1926.

CIE S013/E2003. International Standard Global Solar UV Index. Technical report, Commission Internationale de L'Eclairage, 2003.

Collins, P. and J. Ferguson. Narrow-band UVB (TL01) phototherapy: an effective preventative treatment for the photodermatoses. *British Journal of Dermatology*, 132(6):956–963, 1995. ISSN 1365-2133. doi: 10.1111/j.1365-2133.1995.tb16955.x. URL `http://dx.doi.org/10.1111/j.1365-2133.1995.tb16955.x`.

Colour & Vision Research Laboratory, 2017. Luminance efficiency function data, 2017. URL `cvrl.org`. Accessed 23.05.2017.

Crawford, B. The scotopic visibility function. *Preceedings of the physical society*, 62(5), 1949.

de Bataille, S., H. Dutartre, H. Puy, J.-C. Deybach, L. Gouya, E. Raffray, M. Pithon, J.-F. Stalder, J.-M. Nguyen, and S. Barbarot. Influence of meteorological data on sun tolerance in patients with erythropoietic protoporphyria in France. *British Journal of Dermatology*, 175, 2016. URL `http://dx.doi.org/10.1111/bjd.14600`.

Elder, G., P. Harper, M. Badminton, S. Sandberg, and J.-C. Deybach. The incidence of inherited porphyrias in Europe. *Journal of Inheritable Metabolic Diseases*, 36:849–857, 2013. doi: 10.1007/s10545-012-9544-4.

Figueiro, M., J. Brons, B. Plitnick, B. Donlan, R. Leslie, and M. Rea. Measuring circadian light and its impact on adolescents. *Lighting Research & Technology*, 43(2):201–215, 2011. doi: 10.1177/1477153510382853. URL `http://dx.doi.org/10.1177/1477153510382853`.

Figueiro, M., R. Hamner, A. Bierman, and M. Rea. Comparisons of three practical field devices used to measure personal light exposures and activity levels. *Lighting Research & Technology*, 45(4):421–434, 2012. doi: 10.1177/1477153512450453. URL `http://dx.doi.org/10.1177/1477153512450453`.

Henriksen, T. E., S. Skrede, O. B. Fasmer, B. Hamre, J. Grnli, and A. Lund. Blocking blue light during mania markedly increased regularity of sleep and rapid improvement of symptoms: a case report. *Bipolar Disorders*, 16 (8):894–898, 2014. ISSN 1399-5618. doi: 10.1111/bdi.12265. URL `http://dx.doi.org/10.1111/bdi.12265`.

Henriksen, T. E., S. Skrede, O. B. Fasmer, H. Schoeyen, I. Leskauskaite, J. Bjrke-Bertheussen, J. Assmus, B. Hamre, J. Grnli, and A. Lund. Blue-blocking glasses as additive treatment for mania: a randomized placebo-controlled trial. *Bipolar Disorders*, 18(3):221–232, 2016. ISSN 1399-5618. doi: 10.1111/bdi.12390. URL `http://dx.doi.org/10.1111/bdi.12390`.

Holme, S. A., A. V. Anstey, A. Y. Finlay, G. H. Elder, and M. N. Badminton. Erythropoietic protoporphyria in the UK: clinical features and effect on quality of life. *British Journall of Dermatology*, 155(3):574–581, SEP 2006. ISSN 0007-0963. doi: {10.1111/j.1365-2133.2006.07472.x}.

ISO/CIE 17166/1999. Erythema reference action spectrum and standard erythema dose. Technical report, Commission Internationale de L'Eclairage, 1999.

Kimberly, B. and P. J. R. Amber lenses to block blue light and improve sleep: A randomized trial. *Chronobiology International*, 26(8):1602–1612, 2009. doi: 10.3109/07420520903523719. URL `http://dx.doi.org/10.3109/07420520903523719`.

Kyba, C. C. M., A. Mohar, and T. Posch. How bright is moonlight? *Astronomy & Geophysics*, 58(1):1.31, 2017. doi: 10.1093/astrogeo/atx025. URL `http://dx.doi.org/10.1093/astrogeo/atx025`.

Langendonk, J. G., M. Balwani, K. E. Anderson, H. L. Bonkovsky, A. V. Anstey, M. Bissel, J. Bloomer, C. Edwards, N. J. Neymann, C. Parker, J. D. Phillips, H. W. Lim, I. Hamzavi, J.-C. Deybach, R. Kauppinen, L. E. Rhodes, J. Frank, G. M. Murphy, F. P. Karstens, E. J. Sijbrands, F. W. de Rooij, M. Lebwohl, H. Naik, C. R. Goding, J. P. Wilson, and R. J. Desnick. Afamelanotide for erythropoietic protoporphyria. *New England Journal of Medicine*, 373:48–59, 2015. doi: 10.1056/NEJMoa1411481.

Lecha, M., H. Puy, and J.-C. Deybach. Erythropoietic protoporphyria. *Orphanet Journal of Rare Diseases*, 4, 2009. ISSN 1750-1172. doi: {10.1186/1750-1172-4-19}.

Magnus, I., A. Jarrett, T. Prankerd, and C. Rimington. Erythropoietic protoporphyria a new porphyria syndrome with solar urticaria due to protoporphyrinemia. *The Lancet*, 278(7200):448 – 451, 1961. ISSN 0140-6736. doi: http://dx.doi.org/10.1016/S0140-6736(61)92427-8. URL `http://www.sciencedirect.com/science/article/pii/S0140673661924278`.

Mahmoud, B. H., C. L. Hexsel, I. H. Hamzavi, and H. W. Lim. Effects of visible light on the skin. *Photochemistry and Photobiology,*, 84:450–462, 2008. doi: 10.1111j.1751-1097.2007.00286.x.

Marko, P., J. Miljikovic, P. Povalej, and A. Kansky. Erythropoietic protoporphyria patients in Slovenia. *Acta Dermatovenerol Alp Pannonica Adriat*, 16:99–102, 2007.

Meerman, L. Erythropoietic protoporphyria. An overview with emphasis on the liver. *Scandinavian Journal of Gastroenterology. Supplement*, (232): 79–85, 2000. ISSN 0085-5928. URL `http://europepmc.org/abstract/MED/11232498`.

Michalsky, J., L. Harrison, and W. Berkheiser. Cosine response characteristics of some radiometric and photometric sensors. *Solar Energy*, 54(6):397 – 402, 1995. ISSN 0038-092X. doi: http://dx.doi.org/10.1016/0038-092X(95)00017-L. URL `http://www.sciencedirect.com/science/article/pii/0038092X9500017L`.

Minder, E. I. Afamelanotide, an agonistic analog of a-melanocytestimulating hormone, in dermal phototoxicity of erythropoietic protoporphyria. *Expert Opinion on Investigational Drugst* , 19(10), 2010. ISSN 1354-3784.

Minder, E. I., X. Schneider-Yin, J. Steurer, and L. Backmann. A systematic review of treatment options for dermal photosensitivity in erythropoietic protoporphyria. *Cellularand Molecular Biology*, 55(1):84–97, 2009. ISSN 1165-1580. doi: 10.1170/T841.

Nielsen, K. P., A. Juzenas, P. Juzenas, K. Stamnes, J. J. Stamnes, and J. Moan. Choice of Optimal Wavelength for PDT: The Significance of Oxygen Depletion. *Photochemistry and Photobiology*, 81, 2005. doi: 10.1562/2005-04-06-RA-478.

NOAO. Recommended light levels (illuminance) for outdoor and indoor venues. Technical report, National Optical Astronomy Observatory, 2017. URL `www.noao.edu/education/QLTkit/ACTIVITY_Documents/Safety/LightLevels_outdoor+indoor.pdf`. Accessed: 19.05.2017.

NRPA, Norwegian Radiation Protection Authority, 2016. Today's uv index, 2016. URL `http://www.nrpa.no/uvnett/default_en.aspx`. Accessed: 21.05.2017.

Park, D., D. F. Kripke, and R. J. Cole. More prominent reactivity in mood than activity and sleep induced by differential light exposure due to seasonal and local differences. *Chronobiology International*, 24(5):905–920, 2007. doi: 10.1080/07420520701669677. URL `http://dx.doi.org/10.1080/07420520701669677`.

Phillips, 2016. Actiwatch spectrum plus, 2016. URL `http://www.bmedical.com.au/shop/actiwatch-spectrum-plus-philips.html`.

Price, L., M. Khazova, and J. O'Hagan. Performance assessment of commercial circadian personal exposure devices. *Lighting Research & Technology*, 44(1):17–26, 2012. doi: 10.1177/1477153511433171. URL `http://dx.doi.org/10.1177/1477153511433171`.

Puy, H., L. Gouya, and J. a. Deybach. Porphyrias. *The Lancet*, 375(9718):924 – 937, 2010. ISSN 0140-6736. doi: https://doi.org/10.1016/S0140-6736(09)61925-5. URL `http://www.sciencedirect.com/science/article/pii/S0140673609619255`.

Spelt, J. M. C., F. W. M. de Rooij, J. H. P. Wilson, and A. A. M. Zandbergen. Vitamin D deficiency in patients with erythropoietic protoporphyria. *Journal of Inherited Metabolic Disease*, 33(3):1–4, 2010. ISSN 1573-2665. doi: 10.1007/s10545-008-1037-0. URL `http://dx.doi.org/10.1007/s10545-008-1037-0`.

Srikanthan, N., B. Hamre, and A. Brun. Light filter protection as a preventive measure for the photodermatosis in erythropoietic protoporphyria. To be submitted.

Stockman, A. and L. Sharpe. Spectral sensitivities of the middle- and long-wavelength sensitive cones derived from measurements in observers of known genotype. *Vision Research*, 40:1711–1737, 2000.

Stockman, L., W. Jagla, and H. Jagle. A luminous efficiency function, v, for daylight adaptation. *Journal of Cision*, 5:948–968, 2005.

SunSense, 2017. Sunsense products, 2017. URL `http://getsunsense.com/products/`. Accessed: 01.05.2017.

SunSprite. *SunSprite Quick Start Guide*, 2017. URL `https://www.sunsprite.com/doc/SunSprite_quick_start.pdf`. Acessed: 21.06.2017.

Thapar, M. and H. L. Bonkovsky. The diagnosis and management of erythropoietic protoporphyria. *Gastroenterology & Hepatology*, 4(8):561–566, 2008.

Thunell, S., P. Harper, and A. Brun. Porphyrins, porphyrin metabolism and porphyrias. IV. Pathophysiology of erythyropoietic protoporphyria diagnosis, care and monitoring of the patient. *Scandinavian Journal of Clinical Lab Investigations*, 60:581–604, 2000.

Todd, D. Erythropoietic protoporphyria. *British Journal of Dermataology*, 131:751–766, 1994.

Trios, 2017. Ramses - Hyperspectral radiometer manual, 2017. URL `http://www.trios.de/index.php?eID=tx_nawsecuredl&u=0&g=0&t=1495609899&hash=2945ea4eef22862de2b3c4d11c043a38c4c10cb4&file=uploads/tx_cccascatalog/files/d02-010en201605_broschuere_ramses_01.pdf`. Accessed 23.05.2017.

Tveiteråsen, J. Characterization of hyper spectral irradiance and radiance sensors. Master's thesis, University of Bergen, 2013.

Wahlin, S., Y. Floderus, P. Stal, and P. Harper. Erythropoietic protoporphyria in Sweden: demographic, clinical, biochemical and genetic characteristics. *Journal of Internal Medicine*, 263(3):278–288, 2011.

Wahlin, S., N. Srikanthan, B. Hamre, P. Harper, and A. Brun. Protection from phototoxic injury during surgery and endoscopy in erythropoietic protoporphyria. *Liver Transplantation*, 14(9):1340–1346, 2008. ISSN 1527-6473. doi: 10.1002/lt.21527. URL `http://dx.doi.org/10.1002/lt.21527`.

Webb, A. R., H. Slaper, P. Koepke, and A. W. Schmalwieser. Know Your Standard: Clarifying the CIE Erythema Action Spectrum. *Photochemistry and Photobiology*, 87(2):483–486, 4 2011. ISSN 1751-1097. doi: 10.1111/j.1751-1097.2010.00871.x. URL `https://dx.doi.org/10.1111/j.1751-1097.2010.00871.x`.

Zeiss, 2017. MMS - Monolithic Miniature-spectrometer, 2017. URL `ftp://ftp.nist.gov/pub/physics/lunarproject/References/Spectrometers/ZEISS%20MMSOverview_t5U.pdf`. Accessed: 23.05.2017.

Zibordi, G. and B. Bulgarelli. Effects of cosine error in irradiance measurements from field ocean color radiometers. *Applide Optics*, 46(22):5529–5538, Aug 2007. doi: 10.1364/AO.46.005529. URL `http://ao.osa.org/abstract.cfm?URI=ao-46-22-5529`.

A Appendix: Data sets

A.1 Data sets for cosine response measurements of Ac-tiWatch Spectrum Plus
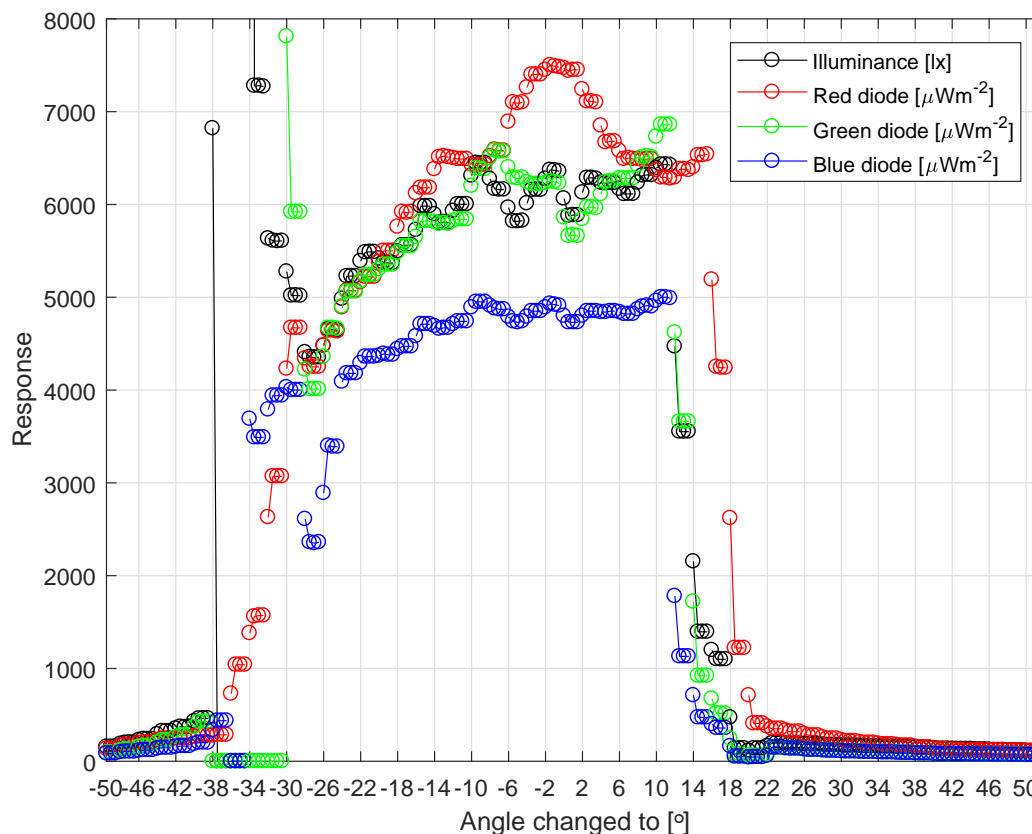

Figure 46: Measurement for vertical cosine response of ActiWatch. Measurements are made form $-50°$ to $50°$, with a step of $2°$. Data sets are plotted in sets of four; measured at same angle. First data point of an angle usually deviates, due to changing of angle over time influencing the measurement. One point is off scale, and was not included for aesthetic reasons: First measurement of illuminance at $32°$ was 75 klx.
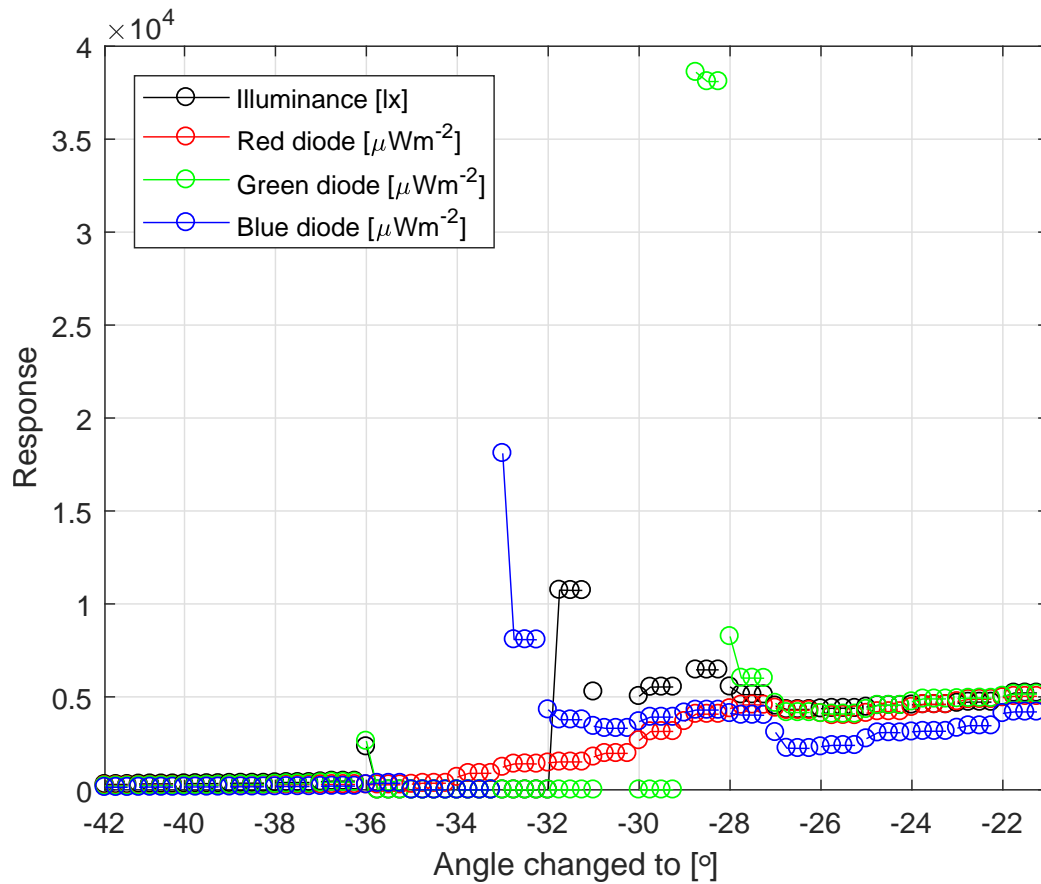
Figure 47: Measurements on vertical cosine response for ActiWatch. Measurements are made form $-42°$ to $-22°$, with a step of $1°$. Measurements are arranged in sets of four, each set measured at the same angle. First measurement usually deviates, due to the changing of angle over time. Some data sets have less than 4 point, due to ActiWatch measuring NaN.
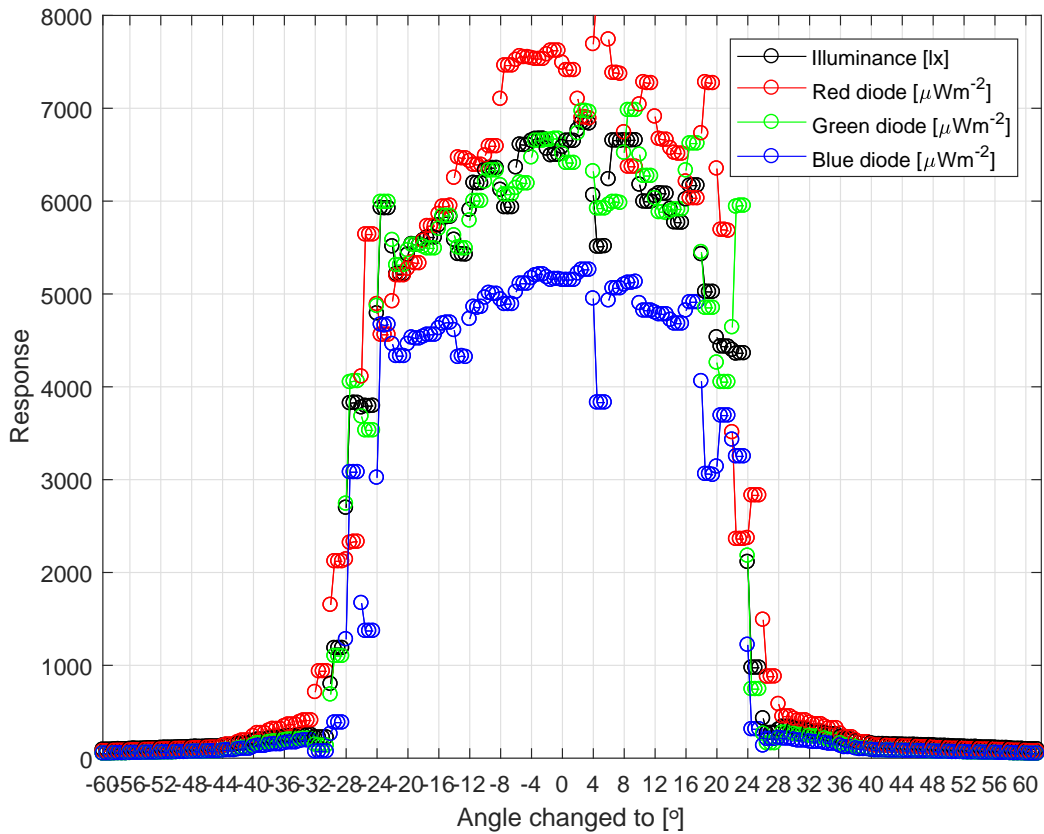
Figure 48: Measurements on horizontal cosine response for ActiWatch. Measurements are made form −60° to 60°, with a step of 2°. Measurements are arranged in sets of four, each set measured at the same angle. First measurement usually deviates, due to the changing of angle over time. Some data sets have less than 4 point, due to ActiWatch measuring NaN.

A.2 Filters

Table 19: Filters used for responsivity measurements, with OD, and serial numbers of the specific filters. Manufacturer: Newport Corporation

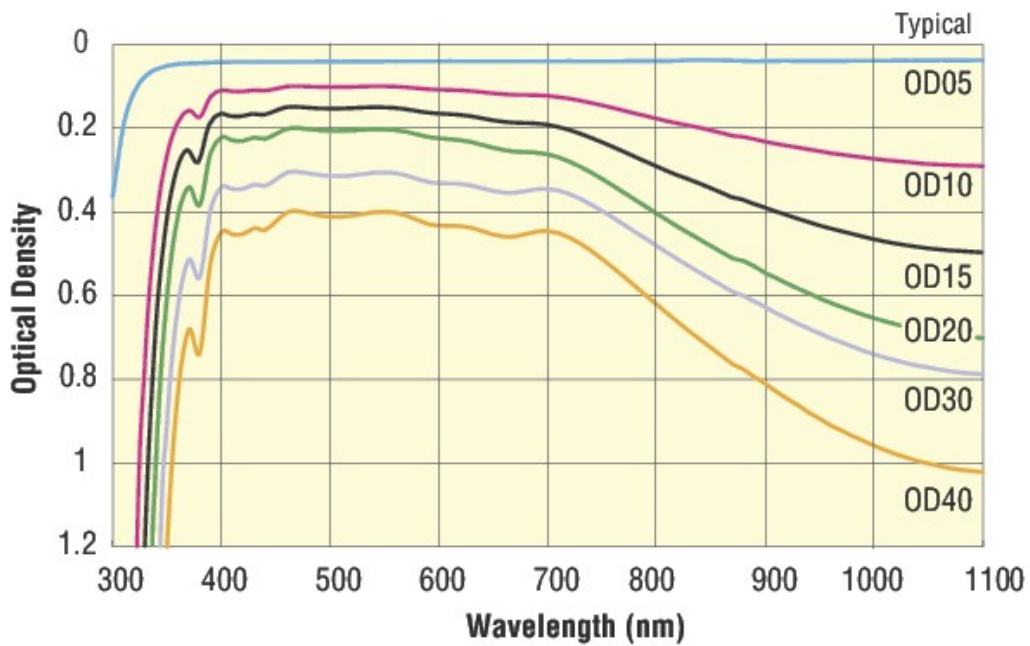| Filter name	Optical depth	Serial #
FSQ-OD05	0.05	1009346
FSQ-OD20	0.2	M3M0380
FSQ-OD40	0.4	PO44396
FSQ-OD60	0.6	M3M9220
FSQ-OD80	0.8	M3M0390
FSQ-OD100	1.0	M3M9810
FSQ-OD200	2.0	M3M9940
FSQ-OD300	3.0	M3M0900

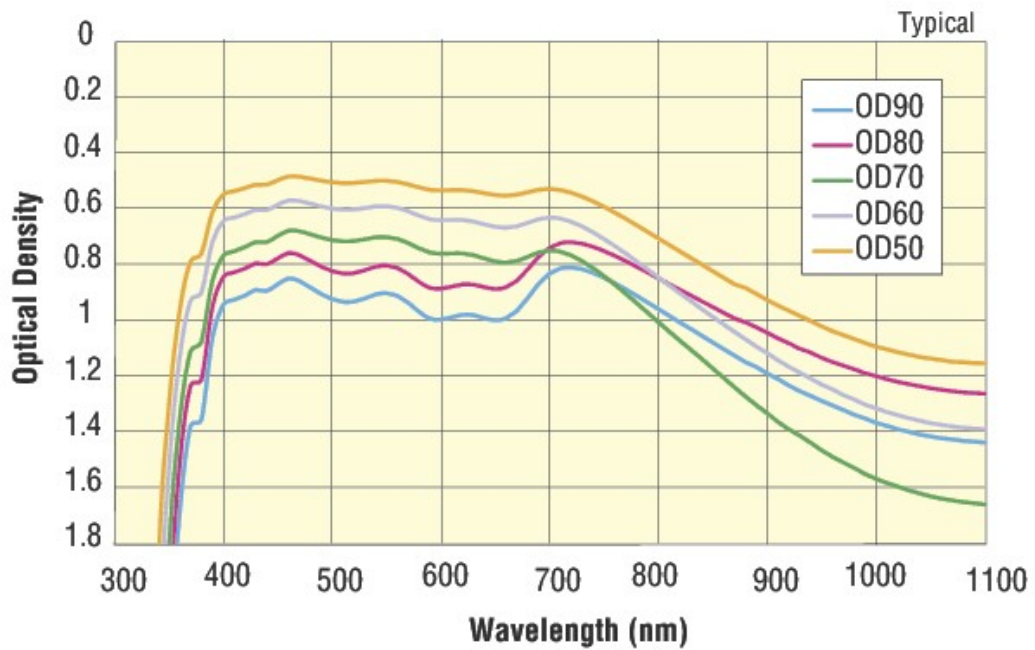Figure 49: OD variations with wavelength. From manufacturer (Newport Corporation).

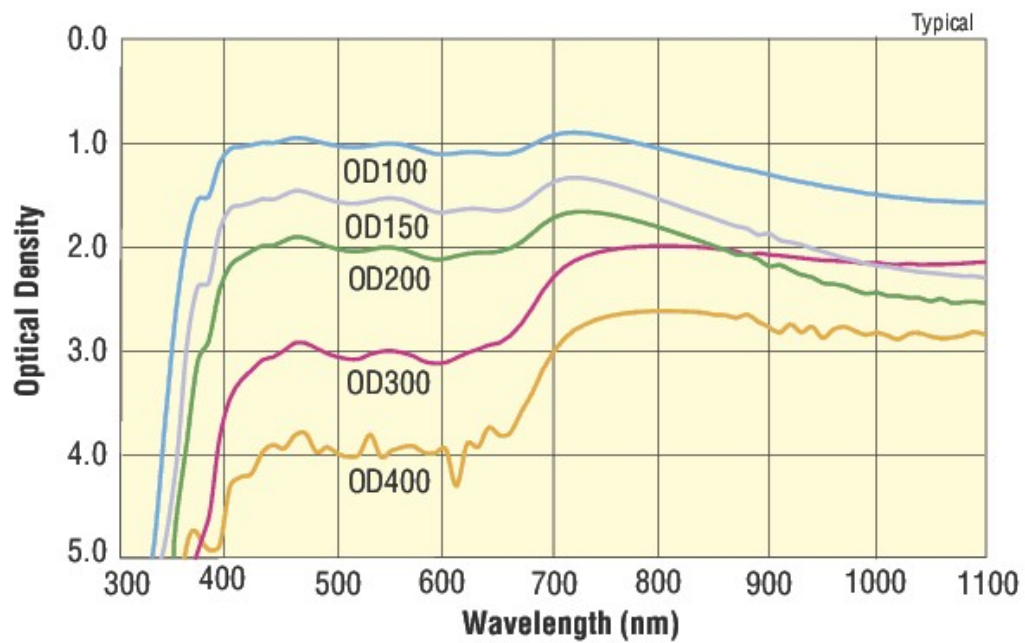Figure 50: OD variations with wavelength. From manufacturer (Newport Corporation).

Figure 51: OD variations with wavelength. From manufacturer(Newport Corporation).